

ADA 136910



DYNAMIC CHARACTERISTICS OF A JET ENGINE
TEST FACILITY AIR SUPPLY

THESIS

Mark L. Ross
Captain, USAF

AFIT/GAE/AA/83D-20

DTIC
ELECTED
S JAN 18 1984 D

DEPARTMENT OF THE AIR FORCE
AIR UNIVERSITY

AIR FORCE INSTITUTE OF TECHNOLOGY

Wright-Patterson Air Force Base, Ohio

This document has been approved
for public release and sale; its
distribution is unlimited.

84 01 17 069

DYNAMIC CHARACTERISTICS OF A JET ENGINE
TEST FACILITY AIR SUPPLY

THESIS

Mark L. Ross
Captain, USAF

AFIT/GAE/AA/83D-20

Approved for public release; distribution unlimited

①
DTIC
ELECTED
S JAN 18 1984 D
E

AFIT/GAE/AA/83D-20

DYNAMIC CHARACTERISTICS OF A JET ENGINE TEST
FACILITY AIR SUPPLY

THESIS

Presented to the Faculty of the School of Engineering
of the Air Force Institute of Technology
Air University
In Partial Fulfillment of the
Requirements for the Degree of
Master of Science in Aeronautical Engineering

Mark L. Ross, B.S.

Captain, USAF

December 1983

Accession For	
MAIN	NTIS GRA&I <input checked="" type="checkbox"/>
COPY	DTIC TAB <input type="checkbox"/>
INSPECTED	Unannounced <input type="checkbox"/>
Justification _____	
By _____	
Distribution/ _____	
Availability Codes	
Dist	Avail and/or Special
A1	

Approved for public release; distribution unlimited

Preface

This report applies existing pneumatic transmission line theory to predict the frequency response of a portion of the air supply ducting of the Aeropropulsion Systems Test Facility (ASTF) at Arnold Engineering Development Center (AEDC), Arnold AFS, Tennessee. The purpose of this thesis was to conduct an experimental investigation on a scale model of ASTF to verify theoretical results for frequency response of this large, complex system of fluid lines. The verified program was then run on representative ASTF configurations to determine typical ASTF frequency response.

To achieve this result, the computer program originated at AFIT by Miller and modified by several others was adapted to the dimensions of the scale model and the computer results verified by experiment. Computer results for the ASTF configurations were then obtained and analyzed.

I would like to express my appreciation to Dr. Milton E. Franke, who introduced me to fluidics and suggested this thesis topic. His assistance and guidance throughout were invaluable.

Mr. John A. Brohas has my undying gratitude for building and helping design my experimental model. This excellent machinist constantly kept me out of trouble with his helpful suggestions and timely work.

Lt. Mark S. Briski deserves my thanks for the help he gave me in day-to-day discussions of our work and his parallel effort. His assistance led to my better understanding of the theory and experimental apparatus.

I would also like to thank Messrs. Leroy Cannon, Harley Linville, and Steve Coates for the eager technical support they gave whenever needed.

Mrs. Pat Norton, who typed this thesis, was very professional, patient, and helpful during this critical phase. She remained unruffled even through the last-minute changes.

I owe a special debt to Capt. Kathleen Collins and Lt. Peter Axup for their love and support throughout my course of study at AFIT.

Table of Contents

	Page
Preface	ii
List of Figures	vi
List of Tables	x
List of Symbols	xi
Abstract	xii
I. Introduction	1
Background	1
Aeropropulsion Systems Test Facility (ASTF)	2
Objectives	3
Approach	4
II. Modeling	6
Lines	6
Pneumatic Signal Generator	12
Valves	12
Venturis	14
Flow Straightening Grids	18
Materials	18
III. Theory and Analysis	19
IV. Experimental Apparatus	22
Pneumatic Signal Source	22
Signal Analysis Equipment	22
V. Experimental Procedures	27
VI. Experimental Results and Discussion	29
Blocked Line Cases	29
Cases with Mean Flow	30
General	32

List of Figures

Figure	Page
1. ASTF Air Supply System with Modeled Portion Outlined	7
2. Modeled Portion of ASTF	8
3. Schematic Diagram of Experimental Model	9
4. Experimental Model	10
5. Experimental Model Including Experimental Apparatus	11
6. Close View of Dynamic Valves with AC Motor and Cam Arrangement	13
7. Close View of ASTF Test Cell	15
8. ASTF Venturis	16
9. Venturi Models	17
10. Schematic Diagram of Experimental Apparatus . . .	23
11. Pneumatic Signal Source	24
12. Signal Analysis Equipment	25
13. Case 1: P_{end}/P_{input} , Correlation of Experiment with Theory	35
14. Case 1: Phase Shift (P_{end}/P_{input}), Correlation of Experiment with Theory	36
15. Case 2: P_{end}/P_{input} , Correlation of Experiment with Theory	37
16. Case 2: Phase Shift (P_{end}/P_{input}), Correlation of Experiment with Theory	38

	Page
VII. ASTF Results and Discussion	63
Blocked Line Cases	63
Cases with Mean Flow	64
General	66
VIII. Conclusions	88
IX. Recommendations	90
Bibliography	92
Appendix A: Computer Program	A-1
Appendix B: Complete Line Dimensions	B-1
Appendix C: Signal Analysis Equipment Specifications .	C-1
Vita	V-1

Figure	Page
17. Case 3: $P_{\text{vent}}/P_{\text{input}}$, Correlation of Experiment with Theory	39
18. Case 3: Phase Shift ($P_{\text{vent}}/P_{\text{input}}$), Correlation of Experiment with Theory	40
19. Case 3: $P_{\text{end}}/P_{\text{input}}$, Correlation of Experiment with Theory	41
20. Case 3: Phase Shift ($P_{\text{end}}/P_{\text{input}}$), Correlation of Experiment with Theory	42
21. Case 4: $P_{\text{vent}}/P_{\text{input}}$, Correlation of Experiment with Theory	43
22. Case 4: Phase Shift ($P_{\text{vent}}/P_{\text{input}}$), Correlation of Experiment with Theory	44
23. Case 4: $P_{\text{end}}/P_{\text{input}}$, Correlation of Experiment with Theory	45
24. Case 4: Phase Shift ($P_{\text{end}}/P_{\text{input}}$), Correlation of Experiment with Theory	46
25. Case 7: $P_{\text{vent}}/P_{\text{input}}$, Correlation of Experiment with Theory	47
26. Case 7: Phase Shift ($P_{\text{vent}}/P_{\text{input}}$), Correlation of Experiment with Theory	48
27. Case 7: $P_{\text{end}}/P_{\text{input}}$, Correlation of Experiment with Theory	49
28. Case 7: Phase Shift ($P_{\text{end}}/P_{\text{input}}$), Correlation of Experiment with Theory	50
29. Case 6: $P_{\text{vent}}/P_{\text{input}}$, Correlation of Experiment with Theory	51
30. Case 6: Phase Shift ($P_{\text{vent}}/P_{\text{input}}$), Correlation of Experiment with Theory	52

Figure	Page
31. Case 6: P_{end}/P_{input} , Correlation of Experiment with Theory	53
32. Case 6: Phase Shift (P_{end}/P_{input}), Correlation of Experiment with Theory	54
33. Case 8: P_{vent}/P_{input} , Correlation of Experiment with Theory	55
34. Case 8: Phase Shift (P_{vent}/P_{input}), Correlation of Experiment with Theory	56
35. Case 8: P_{end}/P_{input} , Correlation of Experiment with Theory	57
36. Case 8: Phase Shift (P_{end}/P_{input}), Correlation of Experiment with Theory	58
37. Case 9: P_{vent}/P_{input} , Correlation of Experiment with Theory	59
38. Case 9: Phase Shift (P_{vent}/P_{input}), Correlation of Experiment with Theory	60
39. Case 9: P_{end}/P_{input} , Correlation of Experiment with Theory	61
40. Case 9: Phase Shift (P_{end}/P_{input}), Correlation of Experiment with Theory	62
41. ASTF Case 1	68
42. ASTF Case 1	69
43. ASTF Case 2	70
44. ASTF Case 2	71
45. ASTF Case 3	72
46. ASTF Case 3	73
47. ASTF Case 4	74

List of Tables

Table	Page
I. Test Configuration	33
II. Experimental Data	34
III. ASTF Configuration	67
IV. Case 1	B-6
V. Case 2	B-7
VI. Case 3	B-8
VII. Case 4	B-9
VIII. Case 6	B-10
IX. Case 7	B-11
X. Case 8	B-12
XI. Case 9	B-13
XII. ASTF Case 1	B-17
XIII. ASTF Case 2	B-18
XIV. ASTF Case 3	B-19
XV. ASTF Case 4	B-20
XVI. ASTF Case 5	B-21
XVII. ASTF Case 6-10	B-22
XVIII. Signal Analysis Equipment Specifications . . .	C-2

List of Symbols

<u>Symbol</u>	<u>Description</u>	<u>Units</u>
A	line cross-sectional area	in ²
c	speed of sound	ft/sec
C _d	discharge coefficient	dimensionless
f _{crit}	critical frequency	hertz
M	Mach number	dimensionless
m	mass flow rate	lb _m /sec
P	AC pressure	psi-rms
\bar{P}	DC (mean) pressure	psi
Δp	orifice pressure drop	psi
Q	volumetric flow rate	cis in - lb _f
R	gas constant for air	$\frac{lb_m}{lb_f \cdot R}$
T	temperature	°R
z	impedance/unit length	$\frac{psi}{cis}$ /in
λ _{crit}	critical wavelength	ft/cycle
ν	kinematic viscosity	in ² /sec
ρ	density	lb _f - sec ² /in ⁴
ω	angular frequency	rad/sec
ω _ν	viscous characteristic frequency	rad/sec

Subscripts

() _{end}	properties at the end of the lines
() _{input}	input end properties
() _{line}	properties of a given line
() _{vent}	properties just upstream of the venturi

Abstract

The dynamic response of a scale model of the Aeropropulsion Systems Test Facility (ASTF) air supply ducting was determined experimentally over a frequency range from 20-200 Hz. Blocked lines with no flow and orifice terminated lines with a mean flow were used. The experiments examined the effects of signal input on three different lines and of using different size venturis. Gain and phase were measured upstream of the venturi and at the end of the line.

The experimental results were compared with the results of a computer program based on Nichols' theory as modified by Krishnaiyer and Lechner. With few exceptions, the gains were predicted within ± 5 dB, and phase angles within $\pm 10^\circ$. This agreement between theory and experiment verified that the theory can be applied successfully to large, complex systems and that the computer program was running properly.

The verified program was then applied to the full-scale ASTF air supply and results analyzed. The ASTF results show higher gains at low frequencies and no reduction in the average gain with frequency. This was as expected for the large ASTF ducting, which ranges from 4-22 ft in diameter.

DYNAMIC CHARACTERISTICS OF A JET ENGINE
TEST FACILITY AIR SUPPLY

I. Introduction

Background

During the past 35 years, many investigators have attempted to model the dynamic response of fluid transmission lines to sinusoidal acoustic signals. The theory developed by Iberall (Ref. 3) and simplified by Nichols and Brown (Refs. 1, 10) employed a linearized theory analogous to electrical transmission line theory. These equations accurately predicted the frequency response of lines of constant circular cross-section by modeling the signal as a one-dimensional plane acoustic wave. Several studies employing this theory have shown good agreement with experimental results for blocked, cascaded transmission lines (Refs. 2, 4, 8, 9, and 11).

Subsequent approximations to Nichols' equations by Krishnaiyer and Lechner (Ref. 6) extended the accuracy of predictions to lower frequencies. Krishnaiyer and Lechner also obtained good agreement with experiment for fluid lines with mean flow by modeling the impedance at the end of the line as the DC resistance.

Miller (Ref. 9) developed a computer program based on Nichols' equations and Krishnaiyer and Lechner's modifications to predict frequency response. It has since been modified to accept a variable number of cascaded fluid lines, both series and parallel (branched).

Aeropropulsion Systems Test Facility (ASTF)

The Aeropropulsion Systems Test Facility is a revolutionary jet engine test facility being built at Arnold AFS, Tennessee. Rather than taking the conventional approach of testing jet engines by stabilizing on one test condition and taking data, ASTF will be able to run through a range of test conditions and simultaneously gather data without the need to allow the test conditions to stabilize. ASTF achieves this real-time control of test conditions via a feedback control system employing large butterfly-type valves. Using heaters, compressors, and turboexpanders, ASTF creates four separate flow legs with different pressures and temperatures in each leg. The control valves then mix these flows in varying amounts in a mixing plenum to create the desired temperature, pressure, and flow rate at the test cell. A steady-state flow analysis has been performed on the ASTF air supply, but no frequency response analysis has been done to date. No problems are anticipated, but due to the transient nature of the system, some significant disturbances could be generated by the

control valves or the rotating turbomachinery. Thus, there is a need to study the frequency response of ASTF to determine its dynamic characteristics.

Objectives

Since the previous experimental results obtained at AFIT were for small fluid lines, typically smaller than an inch in diameter and 20 ft in length, some data were needed on an intermediate size system of greater complexity in order to obtain confidence in predictions on an ASTF-size system. Toward this end, the following objectives were established:

1. Verify that the existing computer program could be used to accurately predict frequency response of more complicated systems by:
 - a. Building a physical scale model of the ASTF air supply.
 - b. Conducting experiments to determine the frequency response of the model.
 - c. Obtaining good correlation of experimental and computer program results for frequency response of the model.
2. Adapt the verified computer program to predict frequency response for the full-scale ASTF system by:

- a. Studying the scaling effects to determine the applicability of the one-dimensional theory to the large ASTF lines.
- b. Running the computer program using typical ASTF conditions and summarizing results.

Approach

To accomplish these objectives, the model will be scaled differently relative to diameter and length of the ASTF air supply because of material availability, cost, and laboratory space limitations. The lines will be made of flexible plastic tubing and coiled to conserve space. The diameters will be scaled 236:1 down from the ASTF line diameters so that available plastic tubing can be used. The ASTF lengths will be halved to conserve space and fit available tubing lengths. Only three of the ASTF flow legs will be modeled because Leg 4 is seldom used.

The computer program as modified by Malanowski (Ref. 7) will be adapted to the more complicated set of series and parallel lines in the experimental model. Tests will be run to determine experimental frequency response and the program will be run to plot these experimental results vs theory.

The verified program will then be used to predict results for the ASTF dimensions and several runs will be

made under typical ASTF test conditions. These results will be analyzed and recommendations will be made concerning their applicability.

II. Modeling

The ASTF air supply and test cells are shown in Fig.

1. The physical scale model was designed to represent the outlined portion of the ASTF air supply including three of the air supply legs which feed the mixing plenum, the mixing valves, the mixing plenum, and one of the test cells. A close-up of this portion of the system is shown schematically in Fig. 2. The dimensions are shown here and in detail in Appendix B.

Figure 3 is a schematic of the physical scale model, and Figs. 4 and 5 are photographs of the actual model. The three input lines on the model correspond to legs 1, 2, and 3 on the ASTF.

Lines

The lines in the model were scaled to half the length of the ASTF lines and were coiled as shown in Figs. 4 and 5 to fit in a reasonable amount of laboratory space. Preliminary computer runs with full and half-length lines showed the frequency response curves to be similar, with the harmonic frequencies doubled in the half-length case. Thus, half-length lines could be used to model full-length lines if this factor were accounted for.

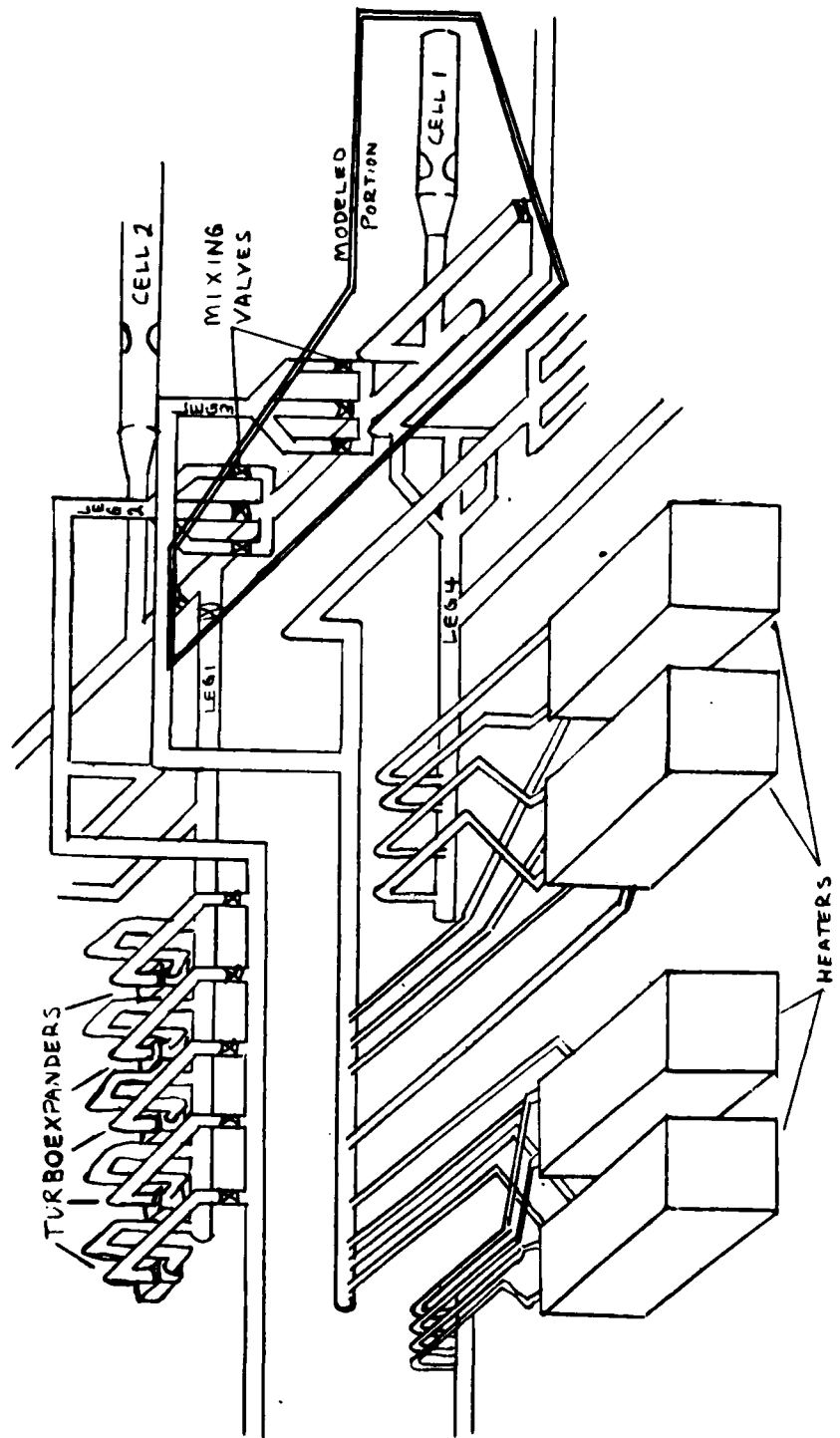


Fig. 1: ASTF Air Supply System with Modeled Portion Outlined

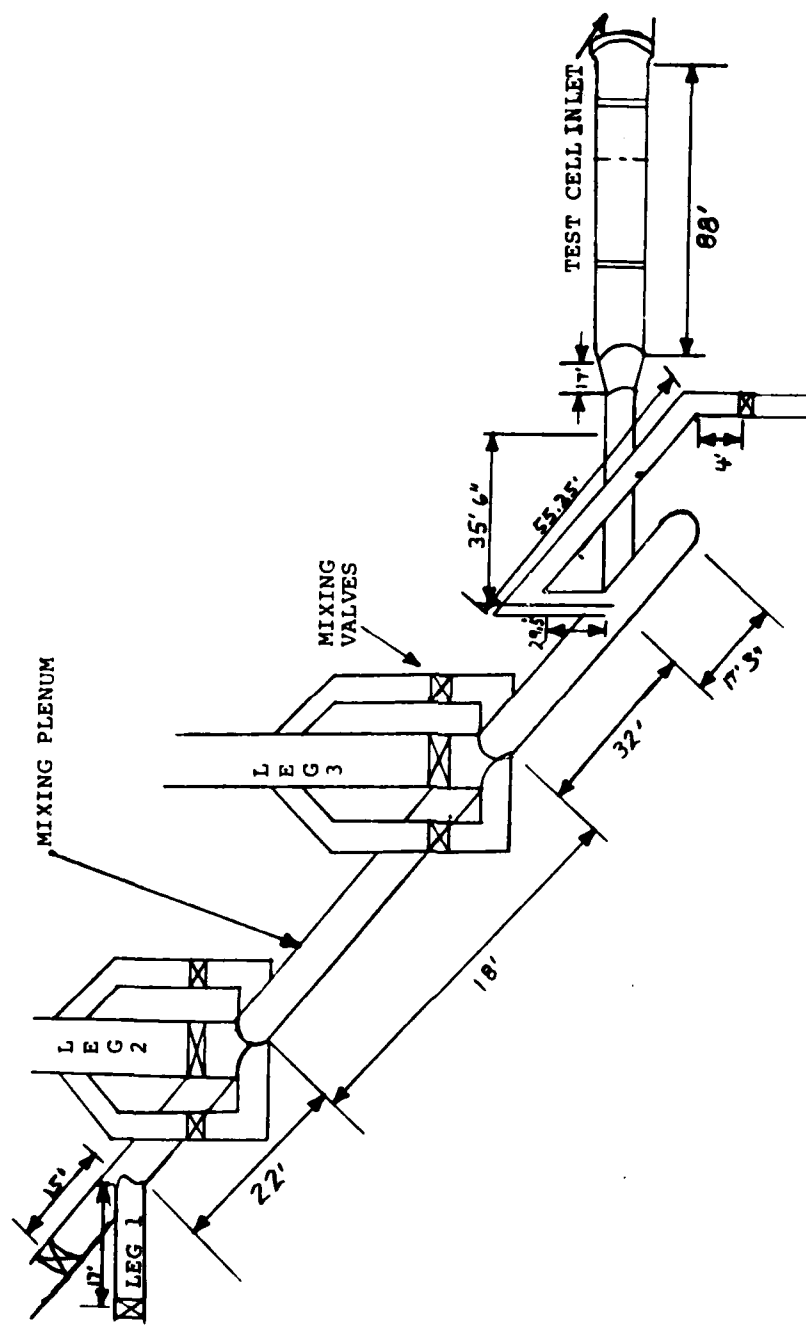


Fig. 2: Modeled Portion of ASTF

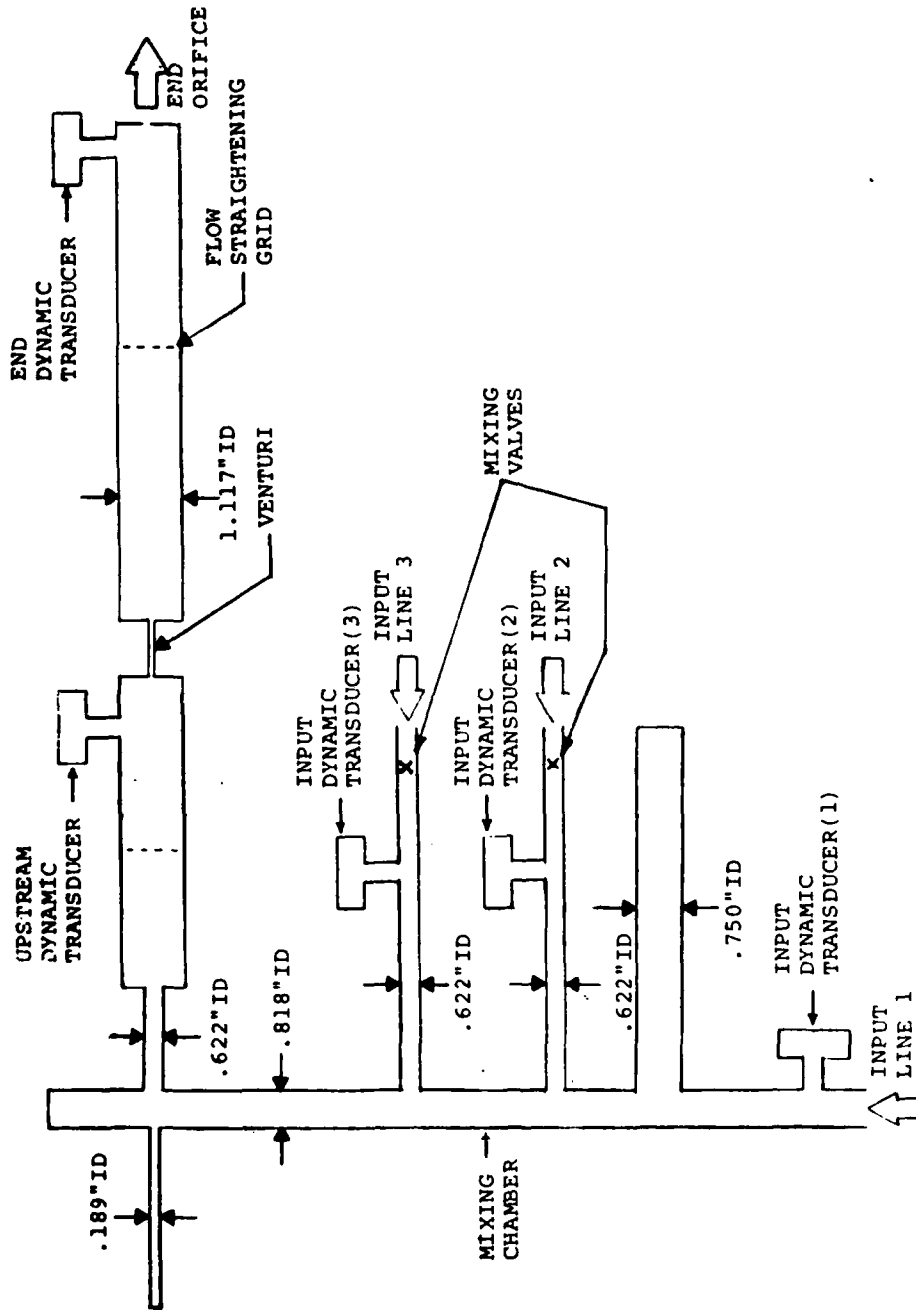
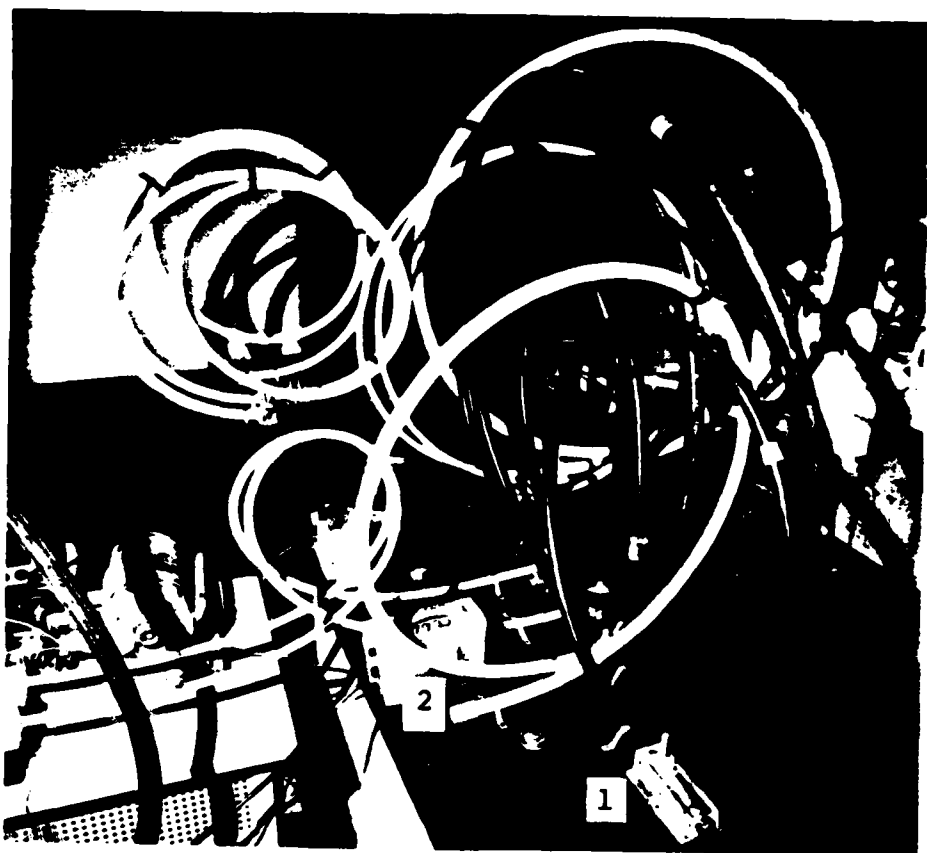
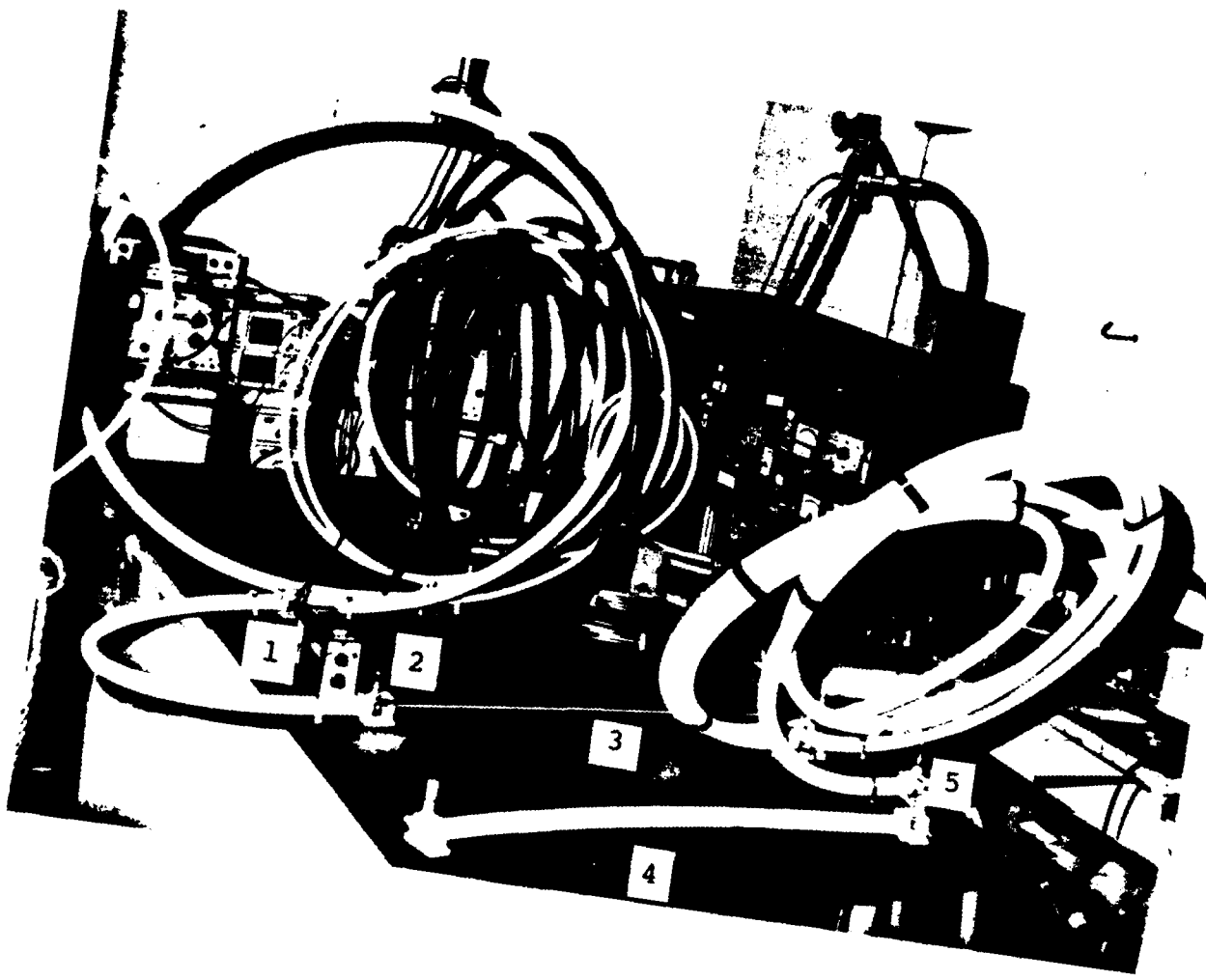


Fig. 3: Schematic Diagram of Experimental Model



1. Leg 1 Input Fixture
2. Charge Amplifier

Fig. 4: Experimental Model



1. Change Amplifier
2. Dynamic Transducer Upstream of Venturi
3. Venturi 2 in Place
4. Venturi 1
5. Dynamic Transducer at End of Line

Fig. 5: Experimental Model Including
Experimental Apparatus

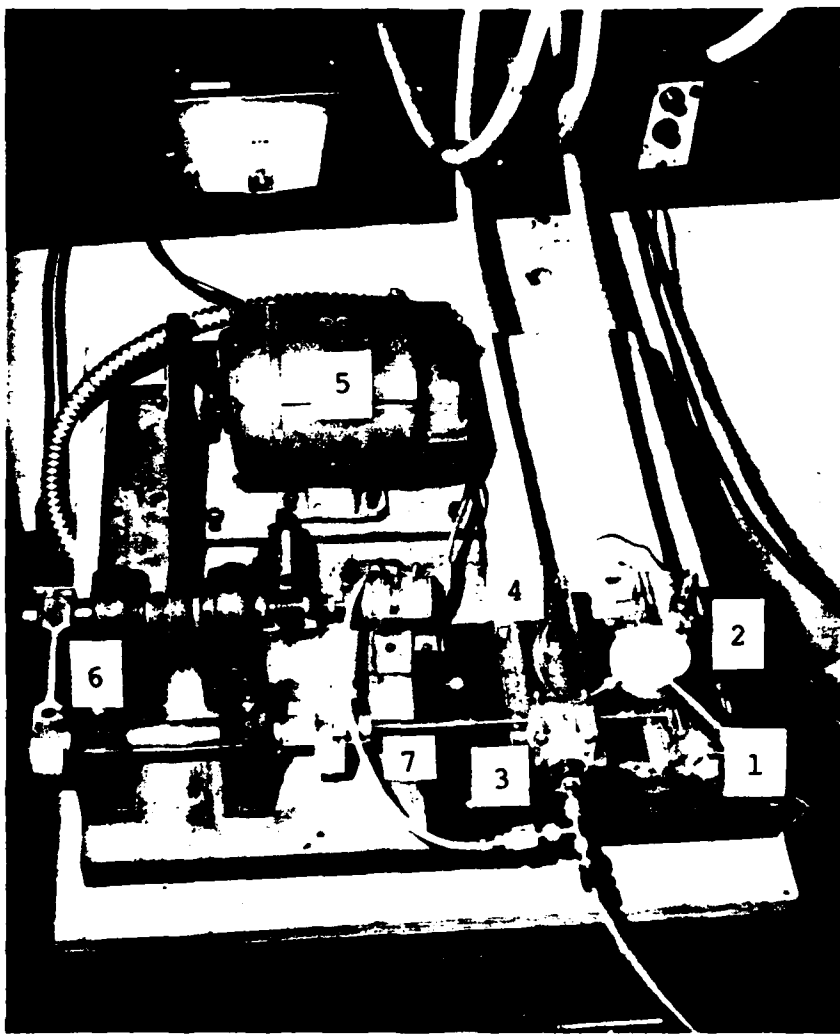
The diameters of the model lines were scaled down roughly 236:1 from the ASTF lines, with the 1.117 in diameter model lines corresponding to the 22 ft diameter ASTF lines. These diameters were chosen based on available tubing.

Pneumatic Signal Generator

A pneumatic signal generator was used to input sinusoidal pressure signals to determine frequency response. This generator employs a piezoelectric flapper valve which, when driven by an AC voltage, oscillates at the AC frequency of the input voltage. The valve superimposes a sinusoidal pressure signal on the flow through the valve. This pressure signal was then input to the model through lines 1, 2, or 3 (Fig. 3).

Valves

An alternate method of simulating disturbances introduced by the mixing valves was a simulated valve arrangement consisting of an AC motor and adjustable cam driving two 0.62 in diameter butterfly valves (Fig. 6). This arrangement allowed the valves to oscillate from 0° to $\pm 24^\circ$. The valve frequency was 1/30th of the motor RPM. As flow entered line 2 or 3, the valve, oscillating back and forth, provided the appropriate area change to create a pressure signal on the mean flow. The signal created by



1. Mean Pressure Transducer
2. Leg 2 Input Fixture
3. Leg 3 Input Fixture
4. Dynamic Pressure Transducer
5. AC Motor
6. Cam
7. Oscillating Shaft with Valves in Legs 2 and 3 Input Fixtures

Fig. 6: Close View of Dynamic Valves with AC Motor and Cam Arrangement

the valves was unsatisfactory for determining frequency response, and these valves were abandoned in favor of a pneumatic signal generator. Chapter VII reports the results of measurements made on these valves.

Venturis

The venturis in the ASTF test cell are shown schematically in Figs. 7 and 8. Any number of the venturis can be closed off at any time, but the cell normally operates with either two or nine open.

The open venturis were modelled experimentally as a single opening with a diameter corresponding to the open area. The area ratio between the venturi and the 22 ft diameter duct was matched in the model. Since the area change through each ASTF venturi is small relative to the 22 ft duct, the use of a straight tube to model the converging-diverging venturi was considered justified. The throat diameter of Venturi 1 corresponded to the ASTF case with two venturis open, while Venturis 2 and 3 represent nine open venturis in the ASTF case.

Since the model venturi was to be half the length of the ASTF venturis, but only 1/236th of the diameter, it was impossible to model it exactly. The two venturi models used are shown in Fig. 9. Venturi 2 is at the throat diameter

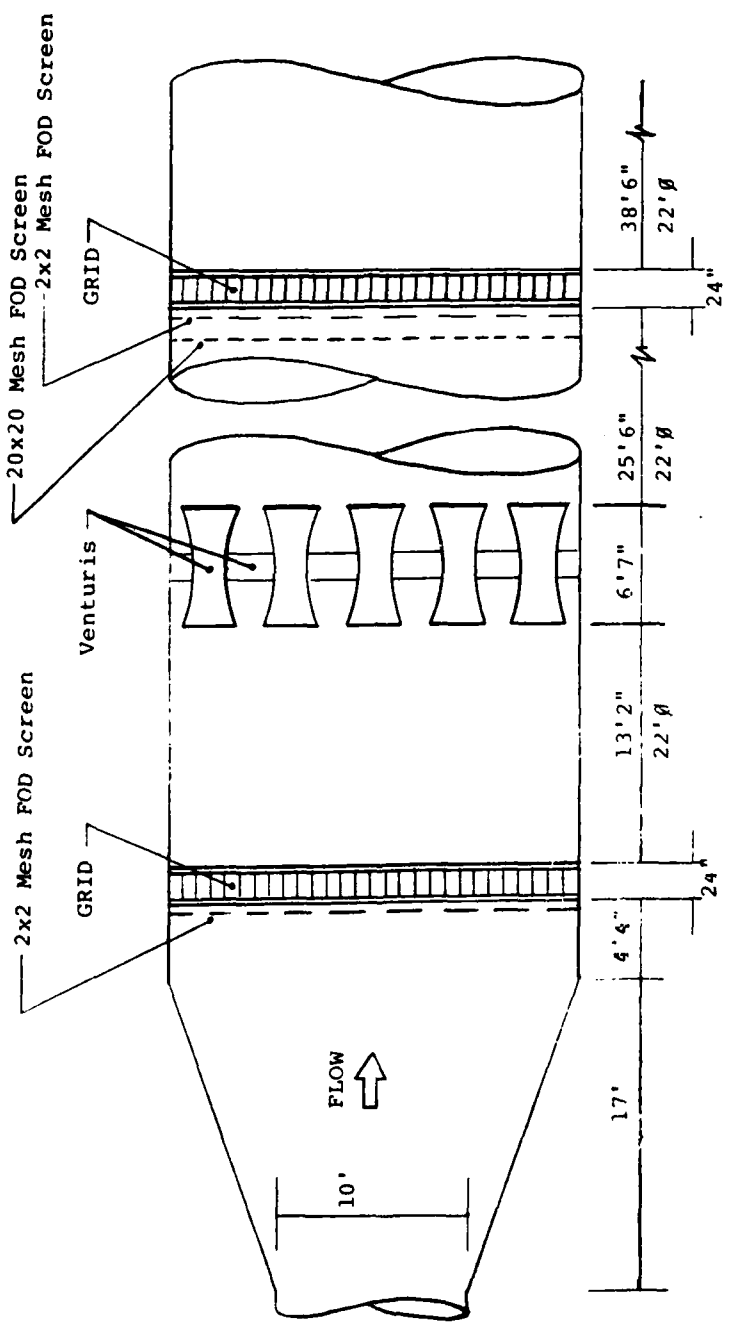


Fig. 7: Close View of ASTF Test Cell

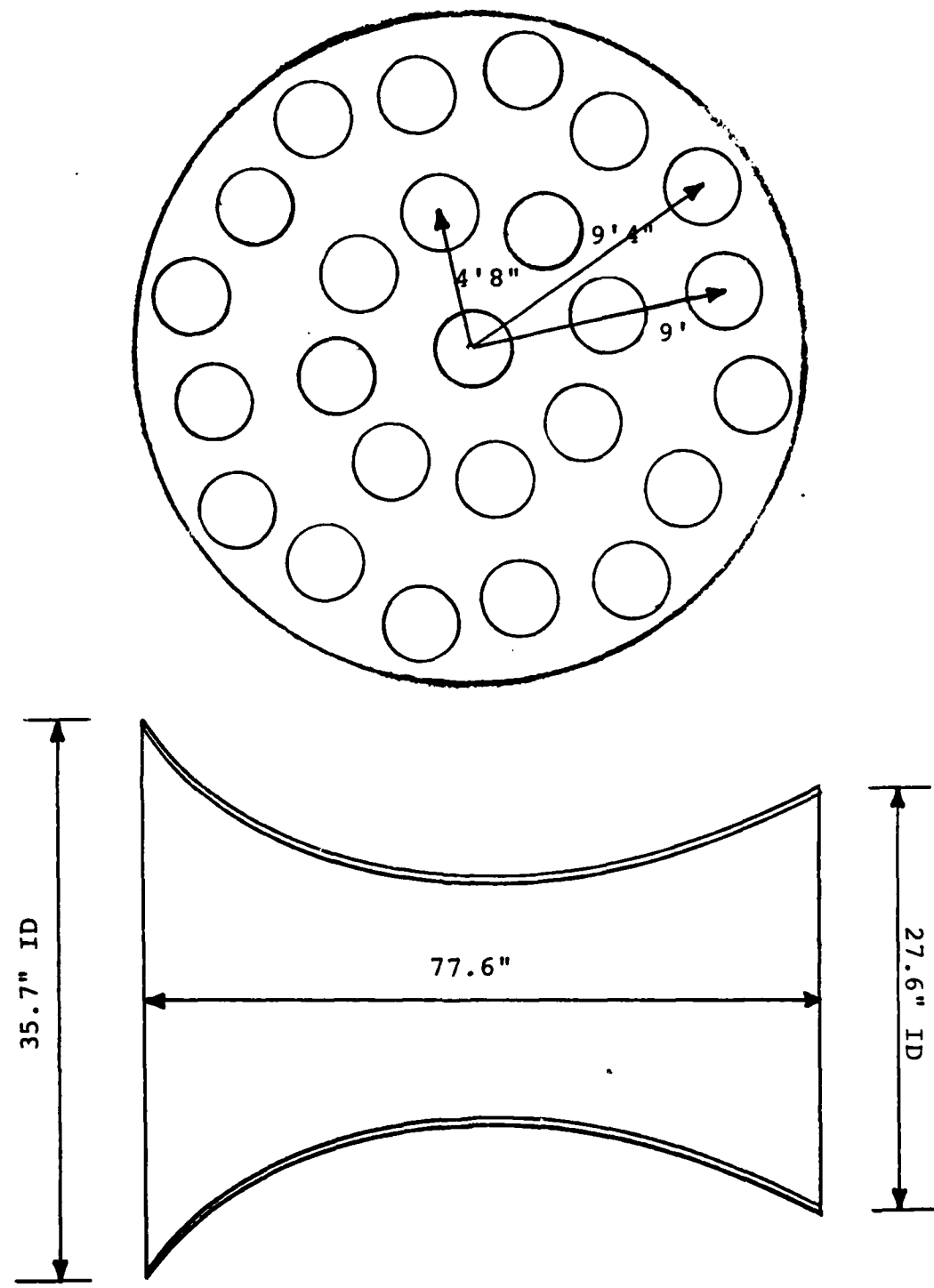


Fig. 8: ASTF Venturis

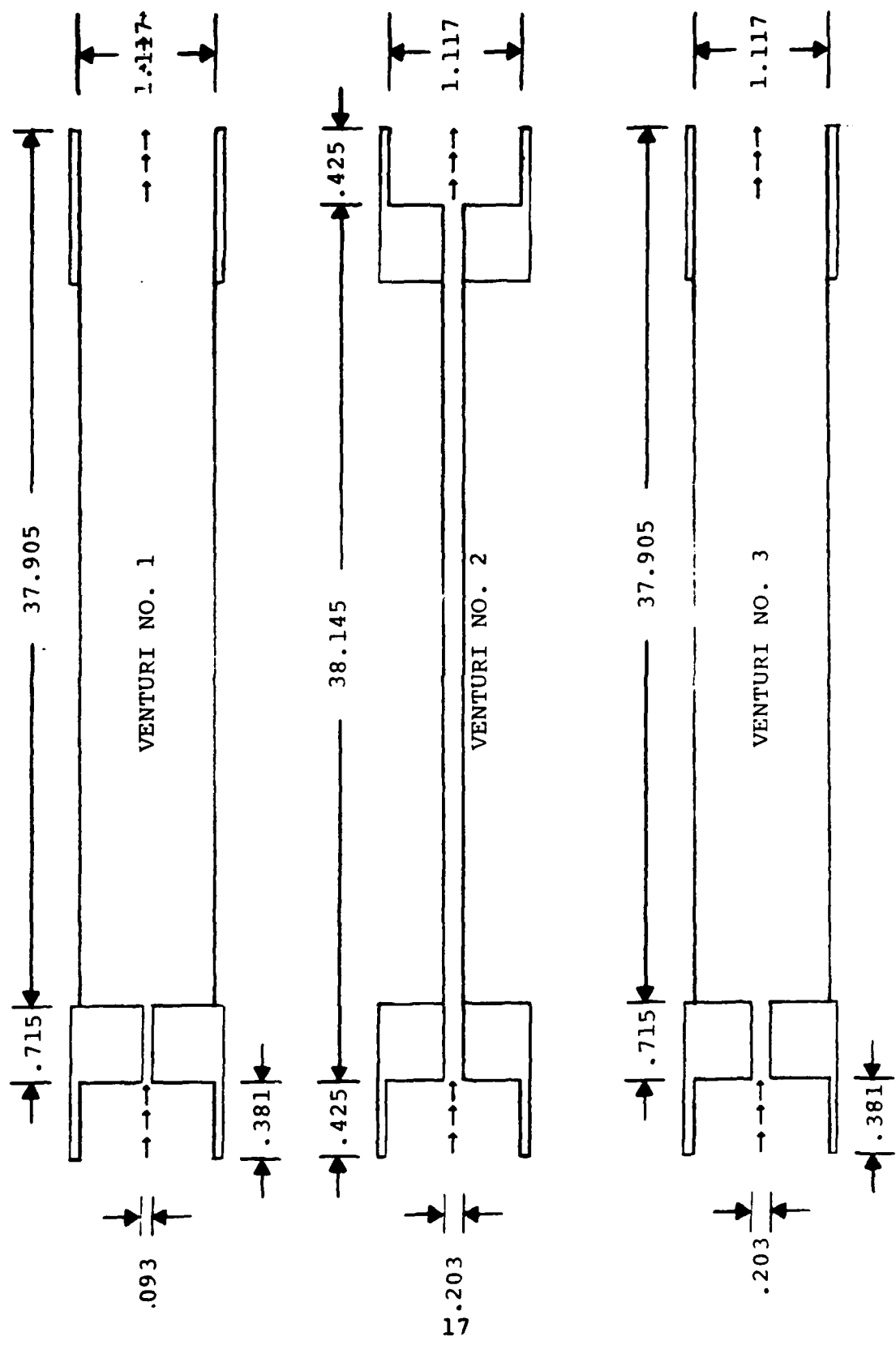


Fig. 9: Venturi Models

for most of its length while Venturis 1 and 3 have only a short throat. These two venturi models also appear in Fig. 5.

Flow Straightening Grids

The ASTF flow straightening grids and Foreign Object Damage (FOD) screens shown in Fig. 7 are honeycomb-shaped passages made of thin sheet metal which serve to create one-dimensional flow into the engine and prevent engine damage. The model uses 1/16 in thick perforated metal plates to simulate the flow straightening grids. The diameter of each of the 31 holes is 0.125 in. If the perforations are considered as a single hole, the corresponding diameter is 0.696 in. The percentage area reduction through the model grids is 61% for each grid. The ASTF grids with all FOD screens in place represent a 48% area reduction in the first (upstream) grid and 52% in the second.

Materials

The tubes used in the model were of high-density polyethylene and polypropylene. These tubes were flexible enough to be coiled, but stiff enough that the walls could be considered rigid. The junctions were machined of clear plexiglass and the tubes were joined to the junctions with either PVC cement or five-minute epoxy.

III. Theory and Analysis

The computer program is the same as that used by Malanowski. His thesis (Ref. 7) contains the necessary background analysis. The theory, based on the assumption of one-dimensional plane waves, is good for larger lines, but is restricted in its application.

As discussed in Kinsler (Ref. 5), the one dimensional assumption is only valid when the wavelength of the signal is longer than the radius of the tube. Assuming a sonic velocity of 1100 ft/sec and a wavelength equal to the radius of the largest ASTF line,

$$f_{crit} = \frac{c}{\lambda_{crit}} = 100 \frac{\text{cycles}}{\text{sec}}$$

the critical frequency for the largest ASTF line is 100 Hz. Thus, the one-dimensional assumption is valid for the ASTF system at frequencies below 100 Hz.

As Malanowski reports, the computer program calculates the end impedance as

$$z_{end} = \frac{P_{end}}{Q_{end}}$$

For the predictions on the experimental model, the pressure drop across the end orifice was used to calculate Q_{end} :

$$Q_{end} = C_d A \sqrt{\frac{2 \Delta P}{\rho}}$$

and the flow rates upstream were calculated using the continuity equation:

$$Q_{line} = Q_{end} \frac{\rho_{end}}{\rho_{line}}$$

The pressures were measured at several points upstream to obtain the densities assuming an isothermal pressure drop and using the ideal gas law.

The F-100 engine will be the first engine tested in ASTF, and its operating envelope provided typical ASTF operating conditions. The DC resistance, also used to model the ASTF end impedance, was calculated as follows using P_{end} and Q_{end} obtained from the F-100 envelope:

$$\frac{P_{end}}{Q_{end}} = \frac{P_{end}}{(\dot{m}/\rho)_{end}} = \frac{P_{end}^2}{(\dot{m}RT)_{end}}$$

The pressures and temperatures upstream were then determined from the isentropic flow tables using area ratios. The steady-flow pressure drops across the upstream lines were assumed to be negligible because of the large diameters. The venturi pressures were assumed to be the same as P_{end} .

Krishnaiyer and Lechner (Ref. 6) found their approximations to be valid from $0.1\omega_v < \omega < \infty$, where ω_v is the characteristic frequency defined as:

$$\omega_v = \frac{8\pi\nu}{A}$$

The value of $0.1\omega_v$ for the smallest diameter ASTF line is 1.2×10^{-4} Hz, so the theory should be valid between 1.2×10^{-4} Hz and 100 Hz.

IV. Experimental Apparatus

Figure 10 is a schematic of the major system components and Figs. 11 and 12 show the arrangement of the apparatus in the laboratory. The test apparatus consisted of two major subsystems: the pneumatic signal source and the signal analysis equipment.

Pneumatic Signal Source

The pneumatic signal source included an electronic signal generator, a linear amplifier, a push-pull amplifier, and a pneumatic driver. Appendix C contains the equipment specifications.

An electronic signal generator in one of the wave analyzers provided a sinusoidal voltage which was amplified first by the linear amplifier and then by the push-pull amplifier. This amplified signal drove a piezoelectric flapper valve in the pneumatic driver. The flapper valve oscillated at the signal frequency and superimposed a sinusoidal pressure signal on the mean flow through the driver.

Signal Analysis Equipment

The signal analysis equipment, shown in Figs. 4, 5, 6, 11, and 12, included three quartz dynamic pressure transducers, three charge amplifiers, three wave analyzers, a

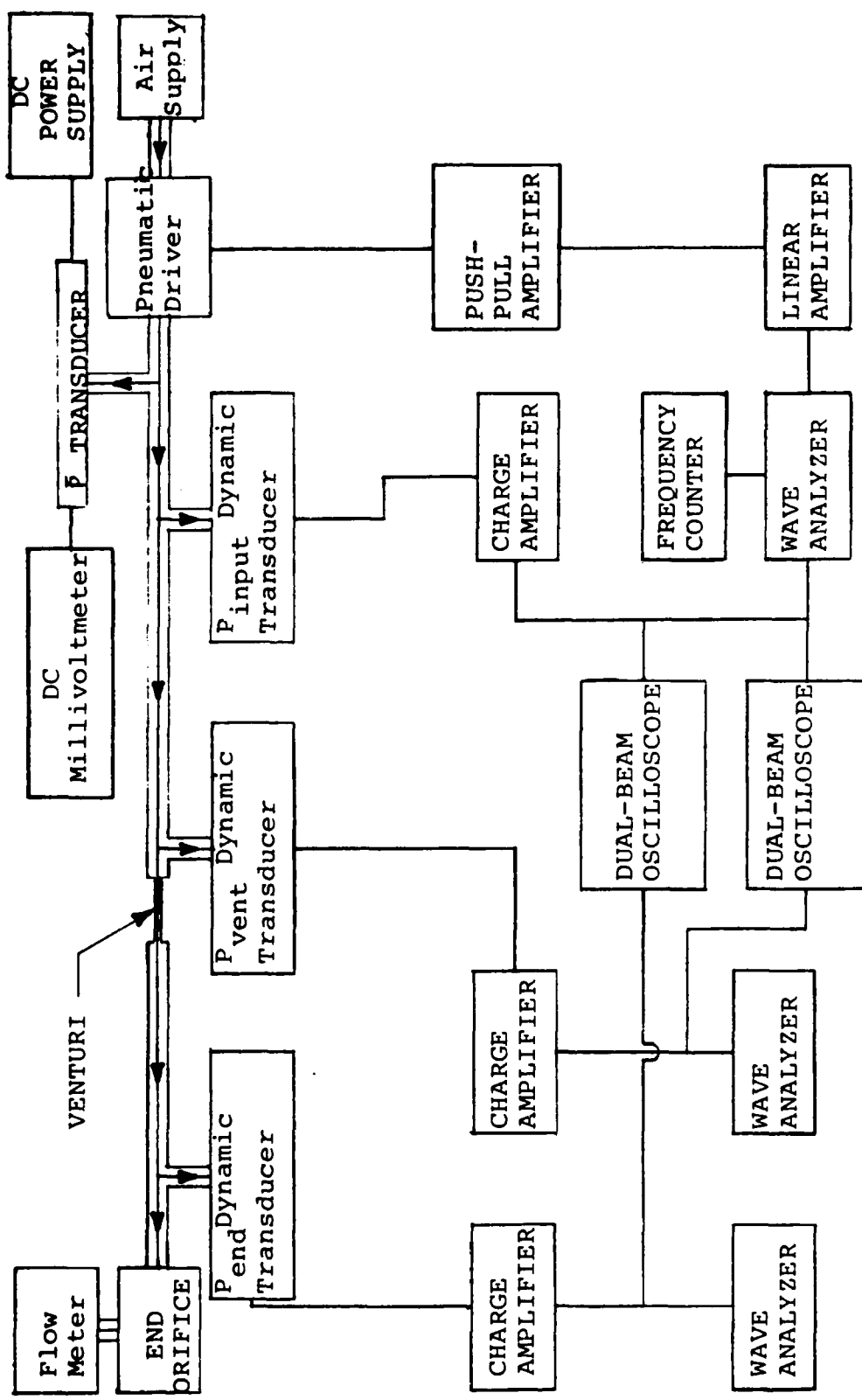
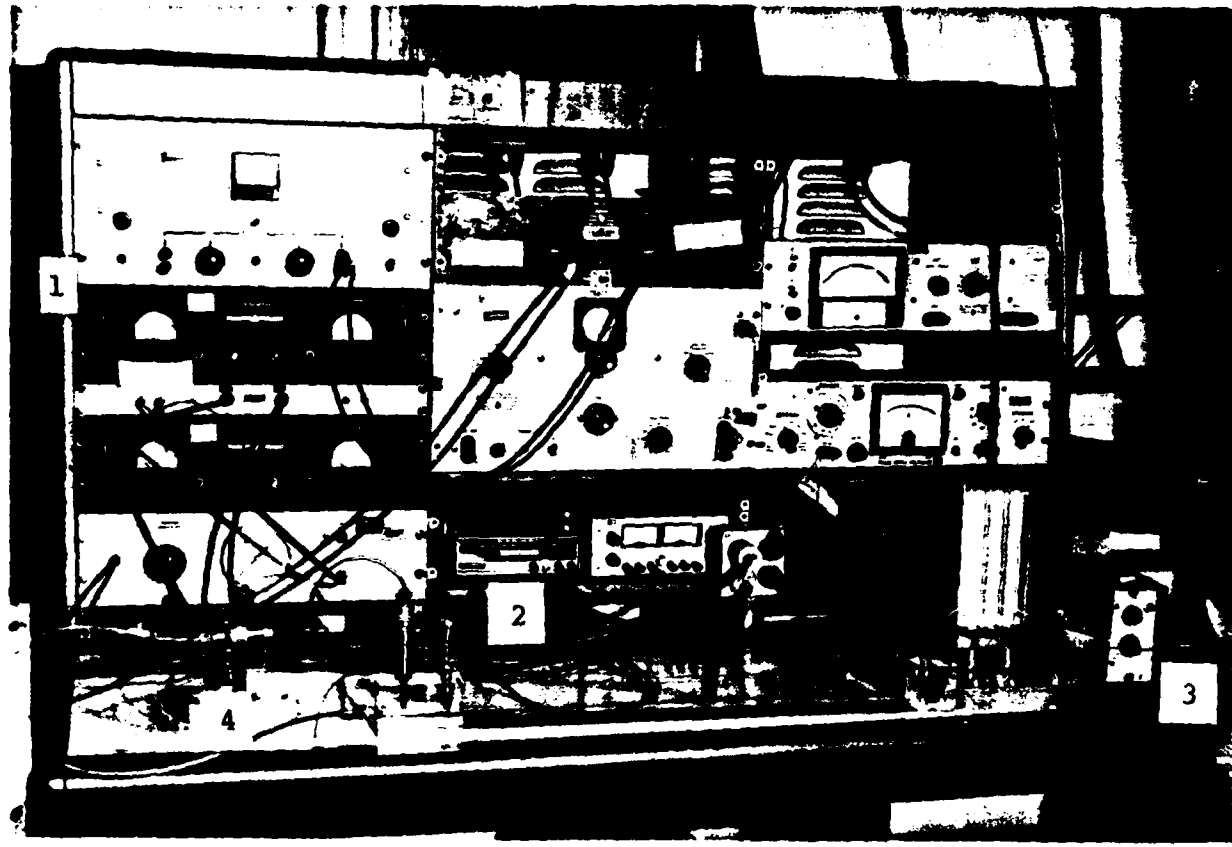
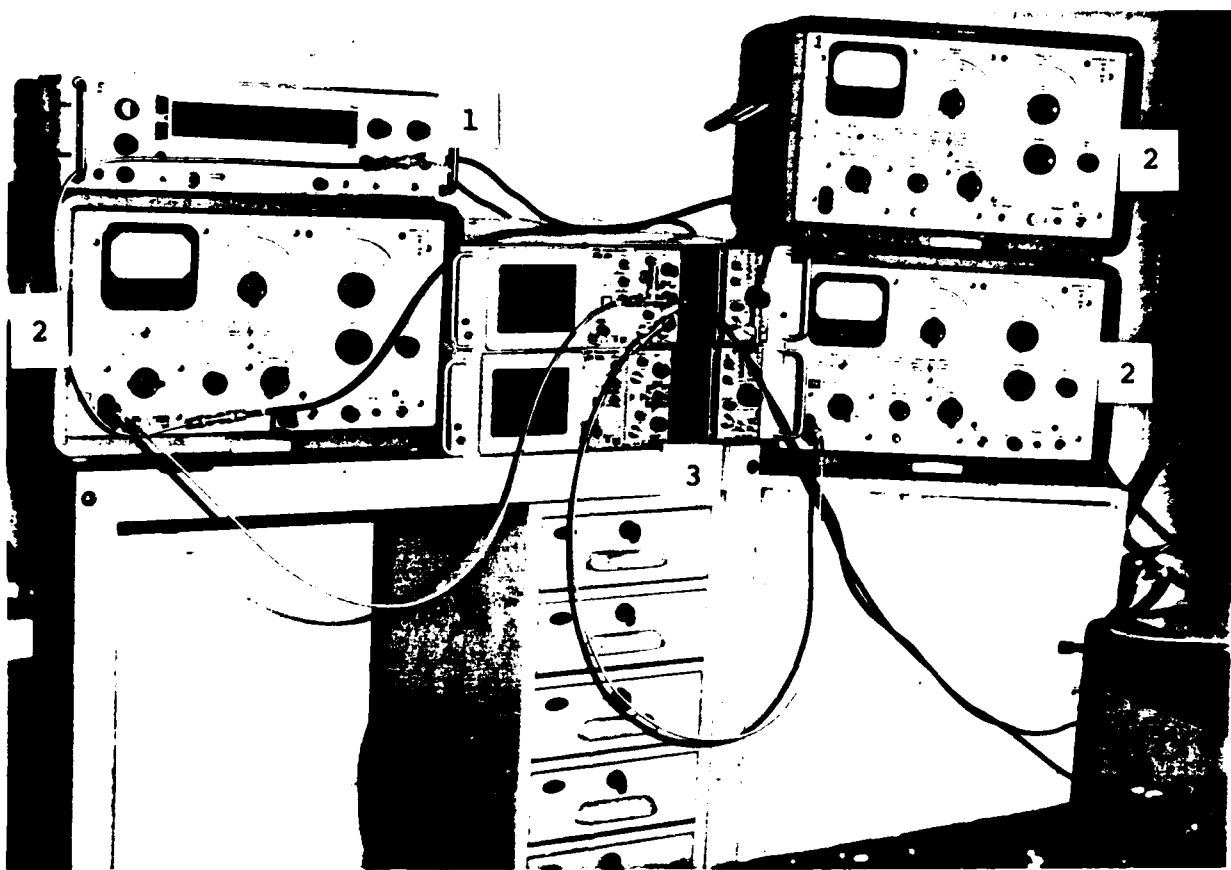


Fig. 10: Schematic Diagram of Experimental Apparatus



1. Pneumatic Signal Generator
2. Digital DC Millivoltmeter
3. Charge Amplifier
4. Pneumatic Driver

Fig. 11: Pneumatic Signal Source



1. Frequency Counter
2. Wave Analyzers
3. Dual-Beam Oscilloscopes

Fig. 12: Signal Analysis Equipment

frequency counter, a strain-gage mean pressure transducer, a DC digital millivoltmeter, two dual-beam storage oscilloscopes, a mercury-in glass thermometer, a precision mercury barometer, and a rotameter type flowmeter. See Appendix C for specifications.

The dynamic pressure transducers measured the input signal, the signal at the end of the line, and the signal just upstream of the venturi. The transducer outputs were fed into the charge amplifiers and the amplified signals were then input to the RMS voltmeters in the wave analyzers for gain measurements and to the dual-beam oscilloscopes for phase angle measurements. The RMS voltmeters measured only at the signal frequency, and filtered all other frequencies. The frequency counter provided better resolution of the signal frequency than was available from the wave analyzer dial.

The strain-gage pressure transducer and millivoltmeter were used to monitor mean line pressure and measure pressure drop across the end orifice to calculate flow rates. The flowmeter was used to measure volumetric flow rate for comparison.

A thermometer and barometer were used to measure ambient temperature and pressure. Wilda (Ref. 11) provides a more detailed description of the signal analysis equipment.

V. Experimental Procedures

All equipment required a warmup period of approximately an hour. The procedure began with recordings of the ambient temperature and pressure. For cases involving blocked lines, the mean pressure transducer provided the mean pressure. For cases involving flow in the lines, this same transducer was used to measure the pressure upstream of the end orifice and at various points in the lines.

The desired frequency was set on the input signal wave analyzer and verified on the frequency counter. The receiving wave analyzers were then locked on the output signals. The RMS values of P_{input} , P_{end} , and P_{vent} from the three wave analyzers were then recorded. Phase measurements between P_{input} and P_{vent} and between P_{input} and P_{end} were made by positioning the oscilloscope cursor on the point at which the input wave crossed the axis on the positive slope and recording the dial reading. The cursor was then moved to the point at which the output signal crossed the axis on its positive slope and the new dial reading was recorded. Finally, the display factor (milliseconds/centimeter) and the mean line pressure were recorded.

Phase information was impossible to obtain at some frequencies because of noise and small signal size. The RMS voltmeter in the wave analyzers were difficult to read at some frequencies because of noise. At these frequencies, an average signal size was recorded.

The computer program processed the data for comparison with theory and the results were plotted by the Calcomp plotter on the same set of axes.

VI. Experimental Results and Discussion

Schematic diagrams showing how the lines in the experimental model were input to the computer program are included in Appendix B (Figs. 61-63). Tables I and II show which input line, venturi, end orifice, flow rate, and atmospheric conditions were used in each case.

Blocked Line Cases

The series of tests with blocked lines was run to demonstrate agreement with the well established theory for blocked lines on this complex model. A comparison of cases 1, 2, and 3 (Figs. 13-20) shows the effects of inputting signals at the three different lines corresponding to legs 1, 2, and 3 in ASTF. Comparison of cases 3, 4, and 7 (Figs. 17-28) shows the effect of different venturis (see Fig. 9 and Table I for venturi dimensions). The "mean gains" were obtained from a visual interpretation of the figures.

The data show generally good agreement with theory over the entire range 20-200 Hz. Large disagreements occur in some ranges, especially at low gains. The signals at the end of the lines (P_{end}) at these points were too low to be measured accurately by the wave analyzers. The mean gain at the end of the lines in cases 1-3 is about the same (-30

dB), which is to be expected. The curves for cases 1-3 show the same general shape and show little effect of different input lines. The mean gain at the end of the lines in case 4 is about -40 dB. This is as expected, because of the larger resistance of Venturi 2. The mean gain at the end in case 7 is about -18 dB, which is higher than the other case because of lower resistance through the venturi. The mean gains upstream of the venturi (P_{vent}/P_{input}) are about -16 dB in cases 3, 4, and 7. This is higher than the gains at the ends of the lines (P_{end}/P_{input}), again because of the venturi resistance.

In general, the gains agreed with theory within ± 5 dB with exceptions noted above. Due to the small and noisy output signals, phase information was more difficult to obtain accurately. Phase angles generally agree within $\pm 10\%$, with few exceptions.

Cases with Mean Flow

Cases with mean flow in the lines were run to determine correlation with theory and to show the effect of mean flow on results. Cases 6 and 8 (Figs. 29-36) compare the effects of two different venturis. Comparing case 9 (Figs. 37-40) with case 8 shows the effect of a lower volumetric flow rate and a smaller end orifice. The flow velocities ranged from 0.1 to 160 ft/sec.

With the exception of the gain at the end of the line (P_{end}/P_{input}), in case 6, the data show good agreement with theory. The gains at the end of the lines did not agree as well with theory as the gains measured upstream of the venturis (P_{vent}/P_{input}), again because of noise and small signal size. These signal sizes ranged from 2 to 110 mV in cases 8 and 9, and from 0.3 to 10.5 mV in case 6. The mean gain at the end of the line in case 6 was about -30 dB compared to -20 dB in case 8, because of the larger venturi throat in case 8. The mean gain upstream was about -15 dB in case 6 and -18 dB in case 8, showing that the venturi looks more like a blocked line (less attenuation) in case 6. The mean gains in case 9 show little difference from those in case 8.

An overlay of cases 6 and 3 (same geometry) shows about 3 dB less calculated gain in case 6 due to the open line, and about 15 dB less in measured data at the end of the line. The gain upstream in cases 3 and 6 shows almost no change due to flow. Comparison of cases 7 and 8 shows less gain in case 8 at most frequencies due to flow, but the venturi has less effect on differences between gains measured upstream and at the end. Case 9 shows about 1.5 dB less gain upstream and 2.5 dB less gain at the end due to flow. The curves are virtually identical in shape.

Agreement between theory and experiment in the cases with

mean flow was within ± 2 dB measured upstream of the venturi and ± 5 dB measured at the end of the line, with the notable exception of case 6. Two possible reasons for the disagreement in case 6 are low signal size and the fact that the venturi diameter (.093 in.) was less than the diameter of the end orifice (0.120 in.). The venturi would thus act as an orifice and cause larger attenuation downstream than predicted by the computer program, which models the venturi as a line. The phase measurements in case 6 were extremely difficult because of noise and small signals. The phase measurements agree within $\pm 10\%$, with few exceptions.

General

The data show quite good agreement with theory over a range of geometries and conditions. The gains are generally about 3 dB less due to flow. The phase angles also show excellent agreement where good measurements were obtainable. The frequency of the first harmonic in all cases was 2 Hz.

Table I
Test Configuration

Case #	Input Line	Venturi Diam., in	Venturi Throat Length, in	Line Dimensions	Orifice Diameter	Results
1	L1	0.093	0.715	Table IV	0.0	Figs. 13 & 14
2	L2	0.093	0.715	Table V	0.0	Figs. 15 & 16
3	L3	0.093	0.715	Table VI	0.0	Figs. 17 - 20
4	L3	0.203	38.0145	Table VII	0.0	Figs. 21 - 24
6	L3	0.093	0.715	Table VIII	0.120	Figs. 29 - 32
7	L3	0.203	0.715	Table IX	0.0	Figs. 25 - 28
8	L3	0.203	0.715	Table X	0.120	Figs. 33 - 36
9	L3	0.203	0.715	Table XI	0.043	Figs. 37 - 40

Table II
Experimental Data

Case #	Mean Pressure psig	Orifice Pressure Drop, psig	Q cfm	Ambient Pressure psia	Ambient Temperature °F
1	1.013	N/A	0.0	14.196	71.6
2	1.056	N/A	0.0	14.196	74.3
3	1.051	N/A	0.0	14.338	76.1
4	1.145	N/A	0.0	14.309	76.1
6	N/A	0.142	0.45	14.188	81.5
7	1.077	N/A	0.0	14.054	77.9
8	N/A	N/A	0.45	14.054	78.8
9	N/A	0.160	0.40	14.243	72.5

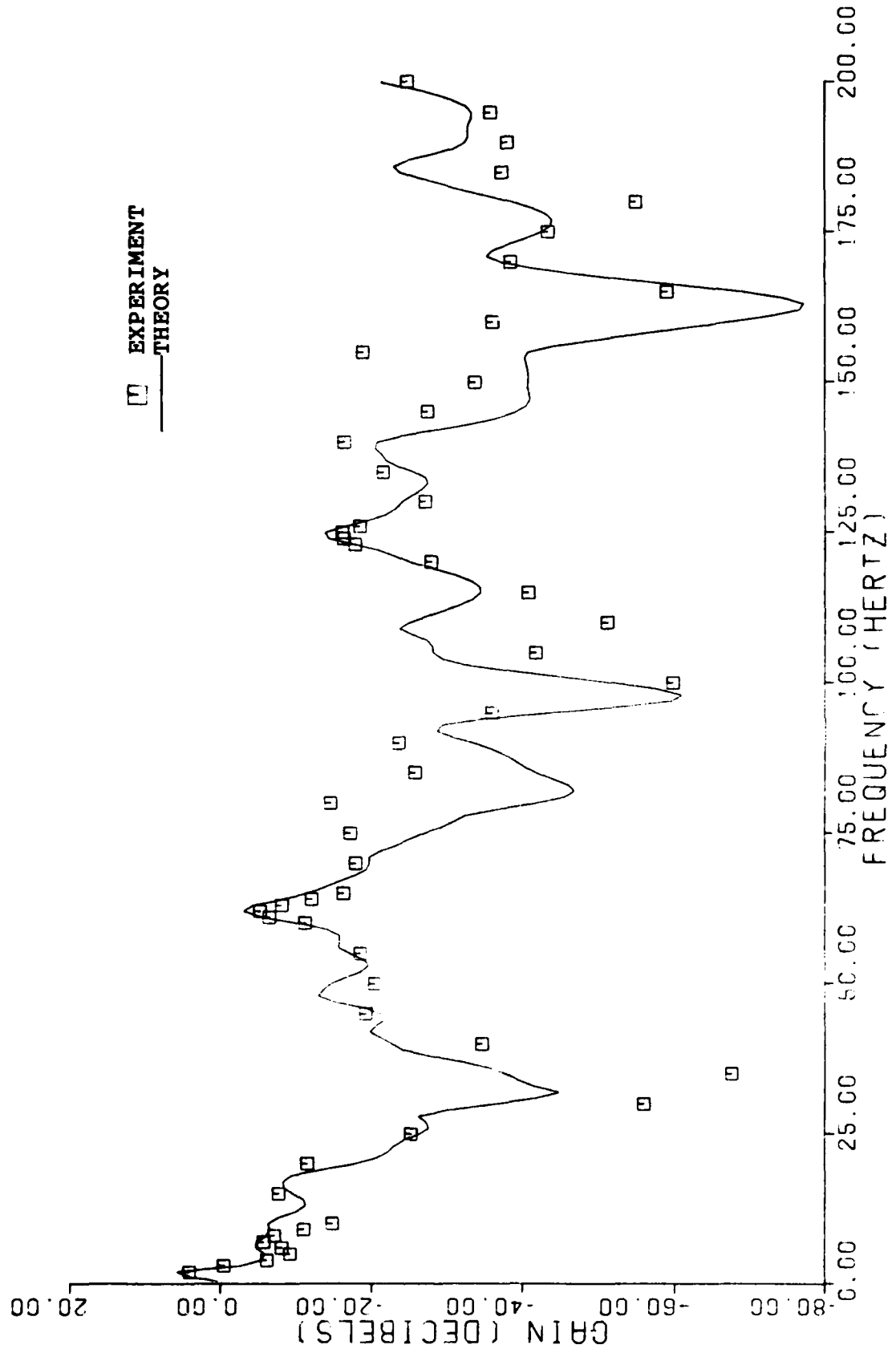


Fig. 13: Case 1: $P_{\text{end}}/P_{\text{input}}$ Correlation of Experiment with Theory

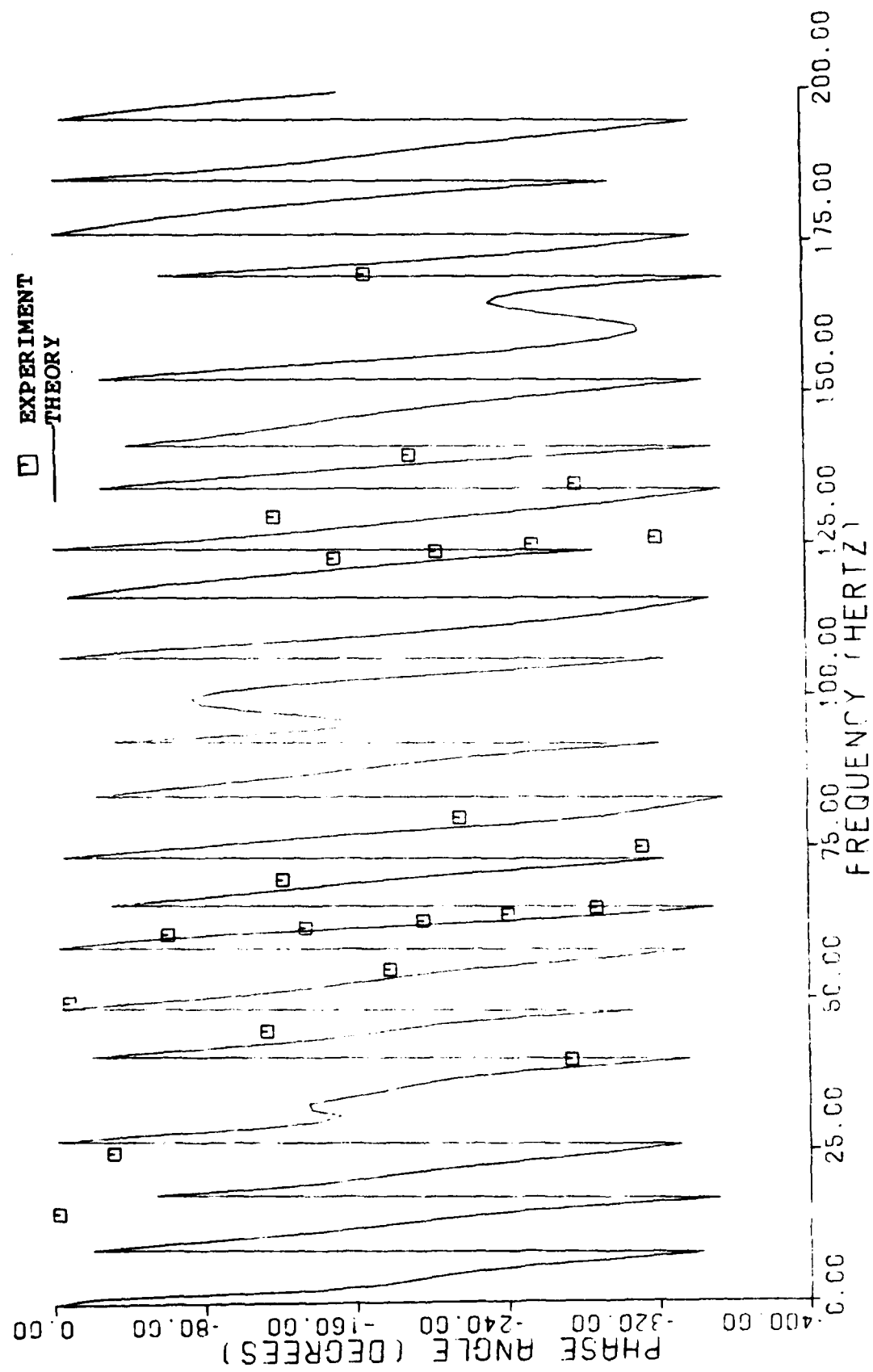


Fig. 14: Case 1: Phase Shift (P_{end}/P_{input}), Correlation of Experiment with Theory

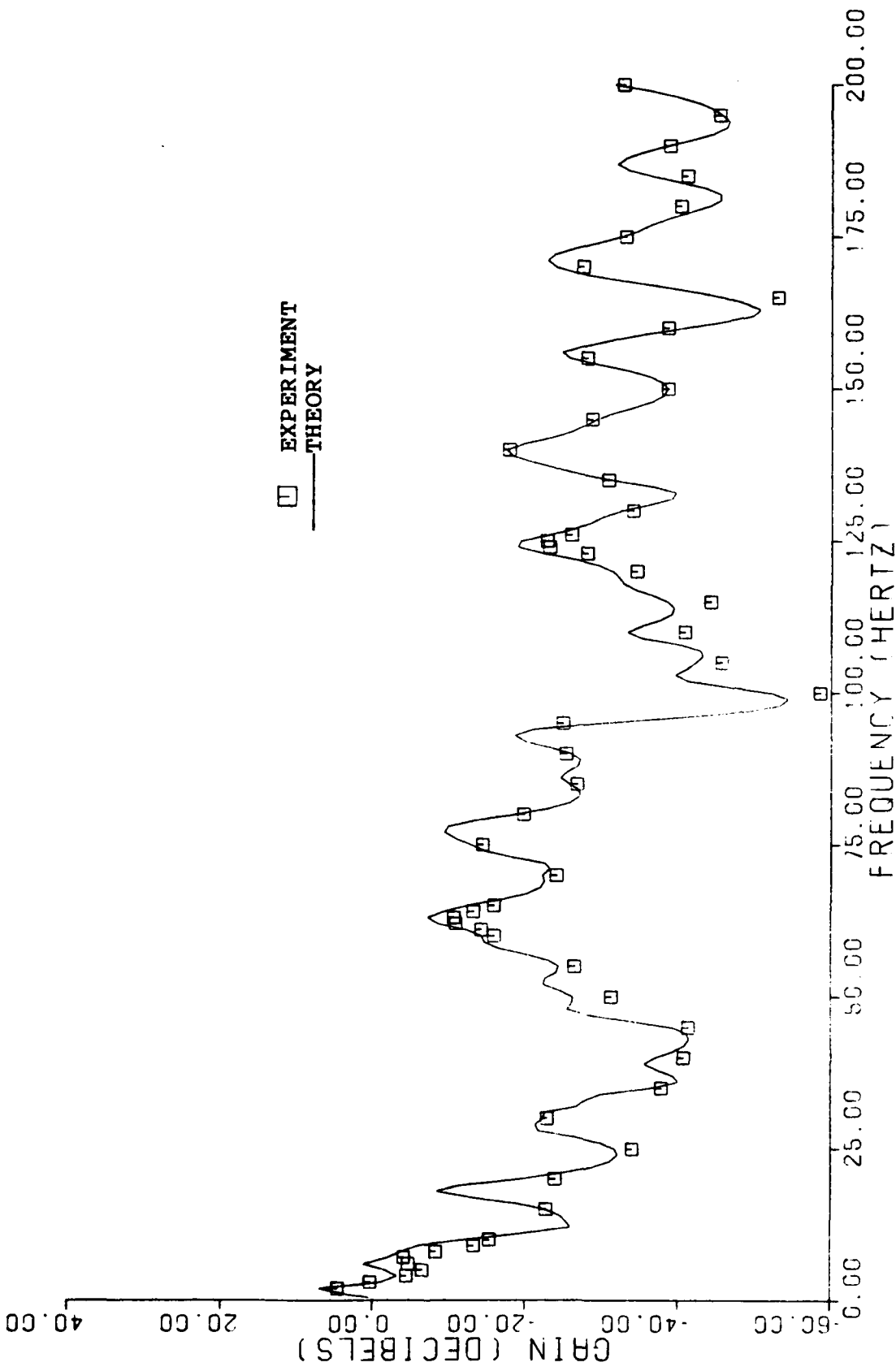


Fig. 15: Case 2: P_{end}/P_{input} , Correlation of Experiment with Theory

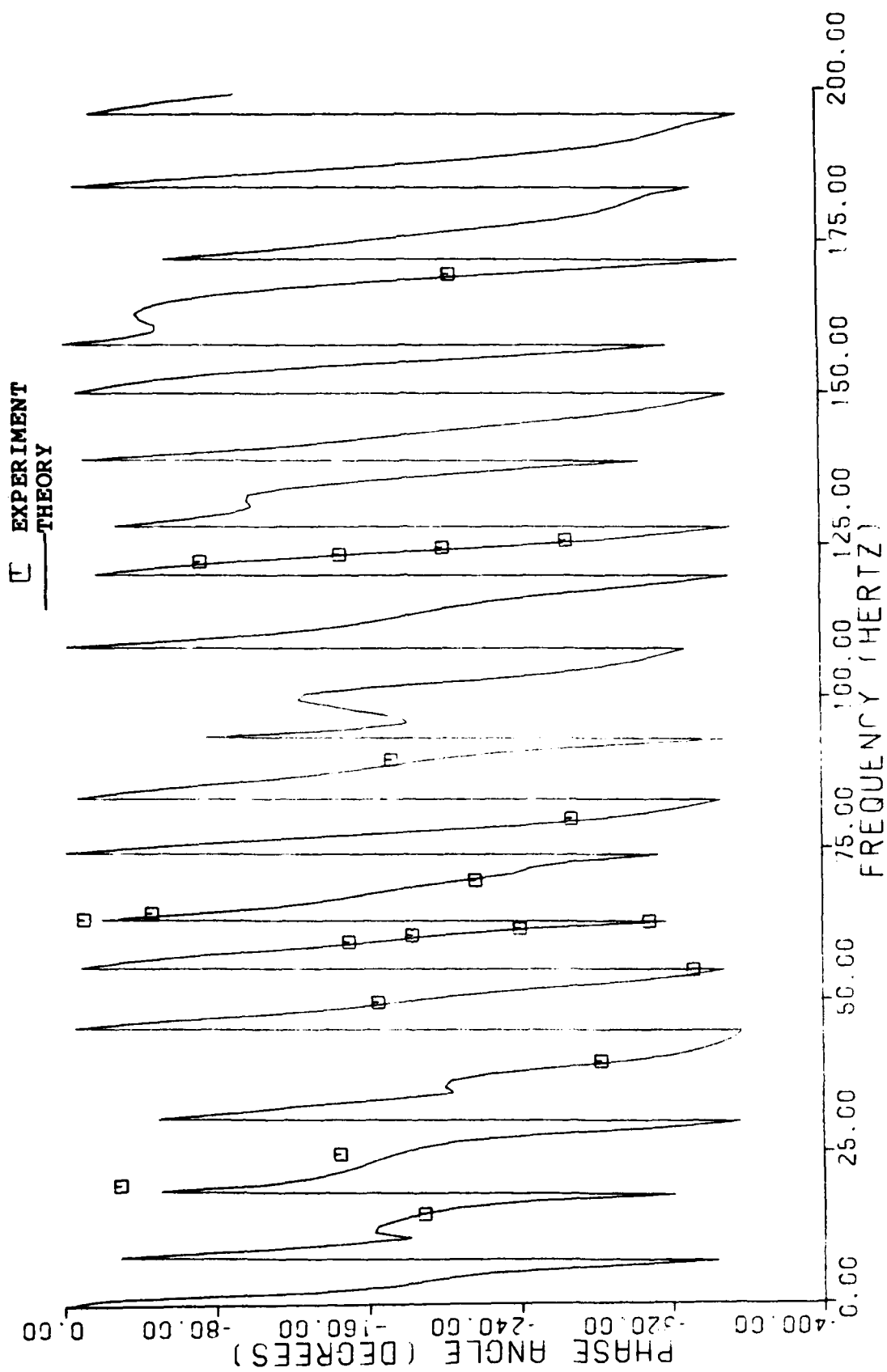


Fig. 16: Case 2: Phase Shift ($P_{\text{end}}/P_{\text{input}}$), Correlation of Experiment with Theory

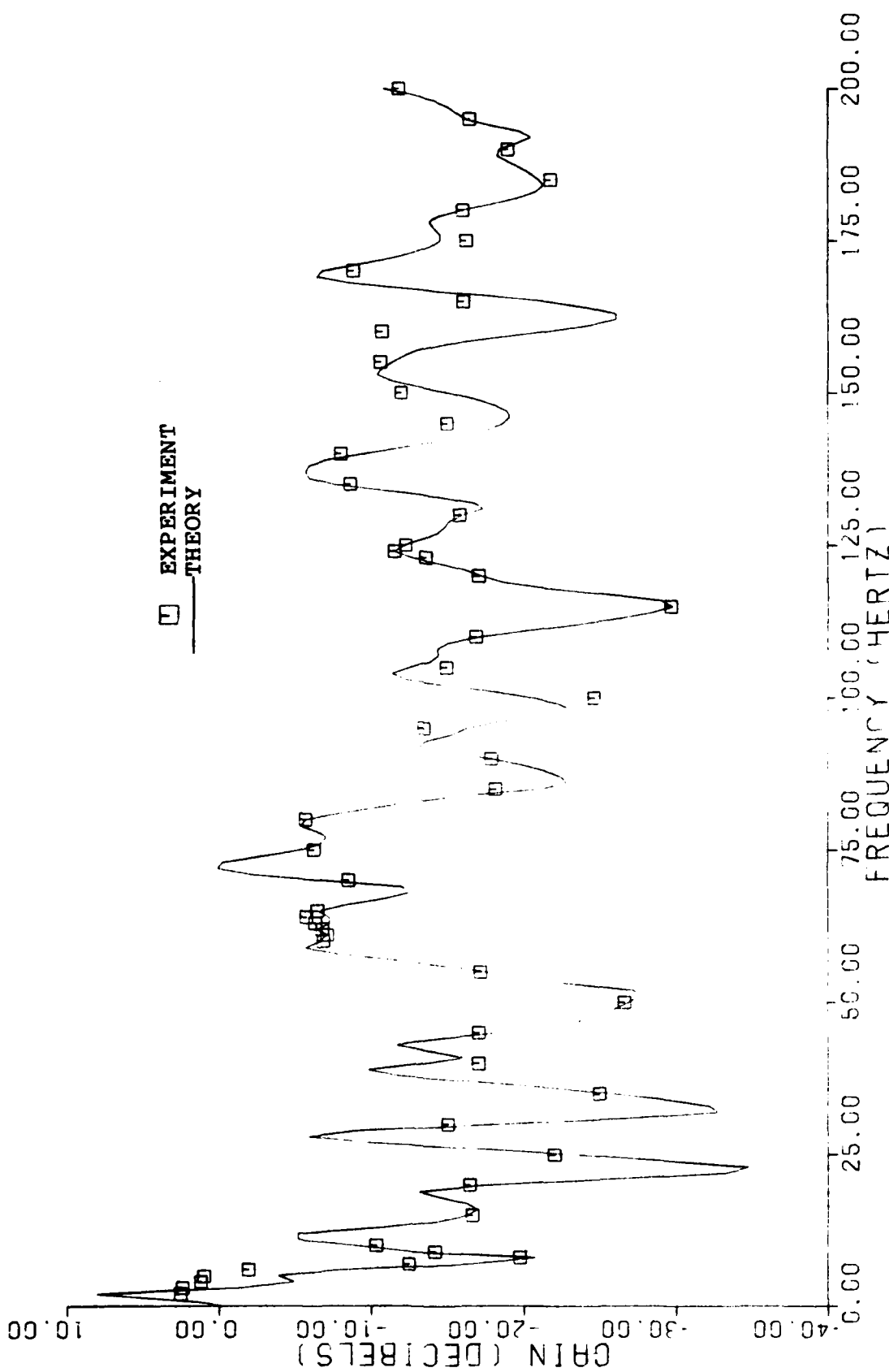


Fig. 17: Case 3: P_{vent}/P_{input} Correlation of Experiment with Theory

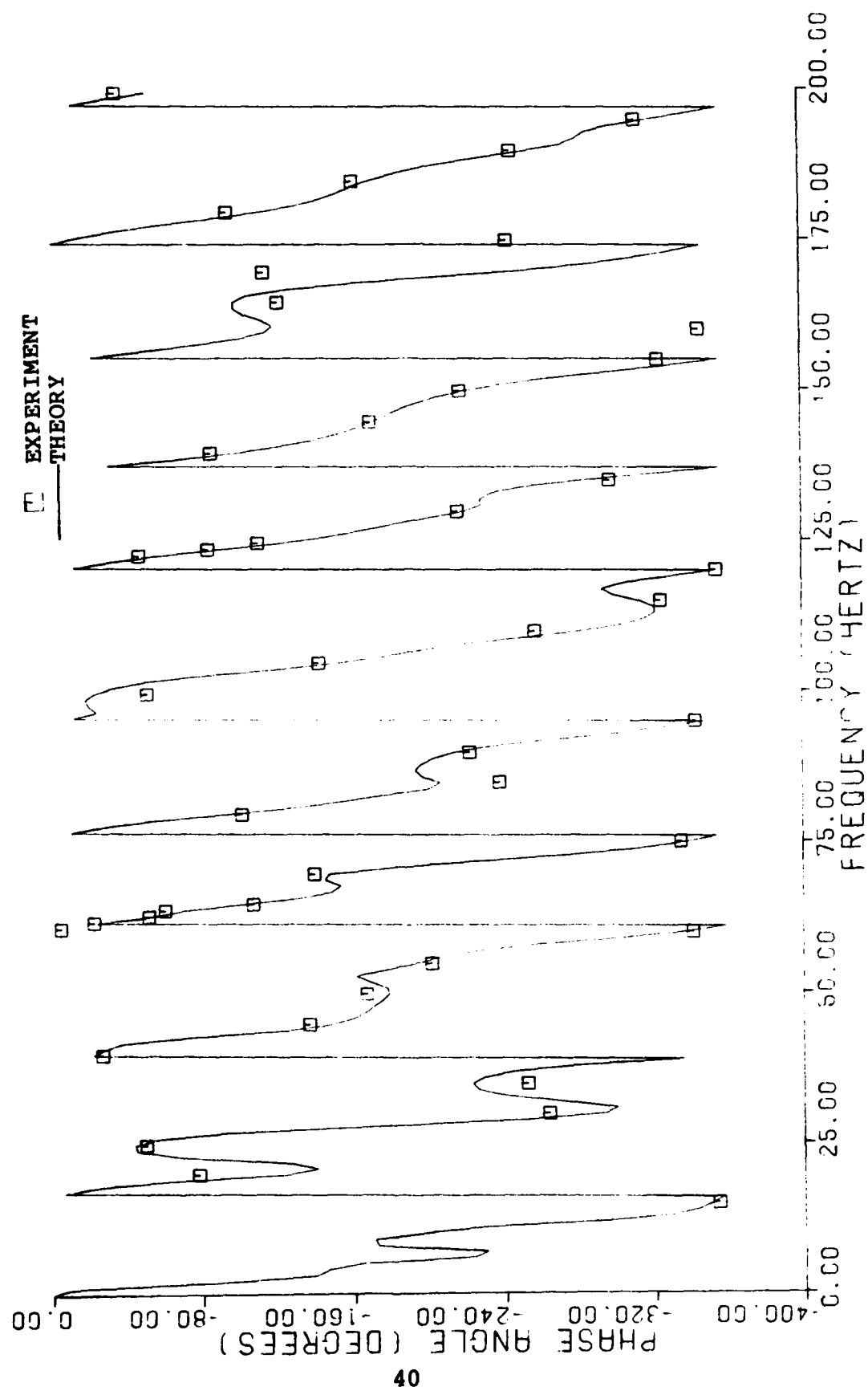


Fig. 18: Case 3: Phase Shift (P_{vent}/P_{input}), Correlation of Experiment with Theory

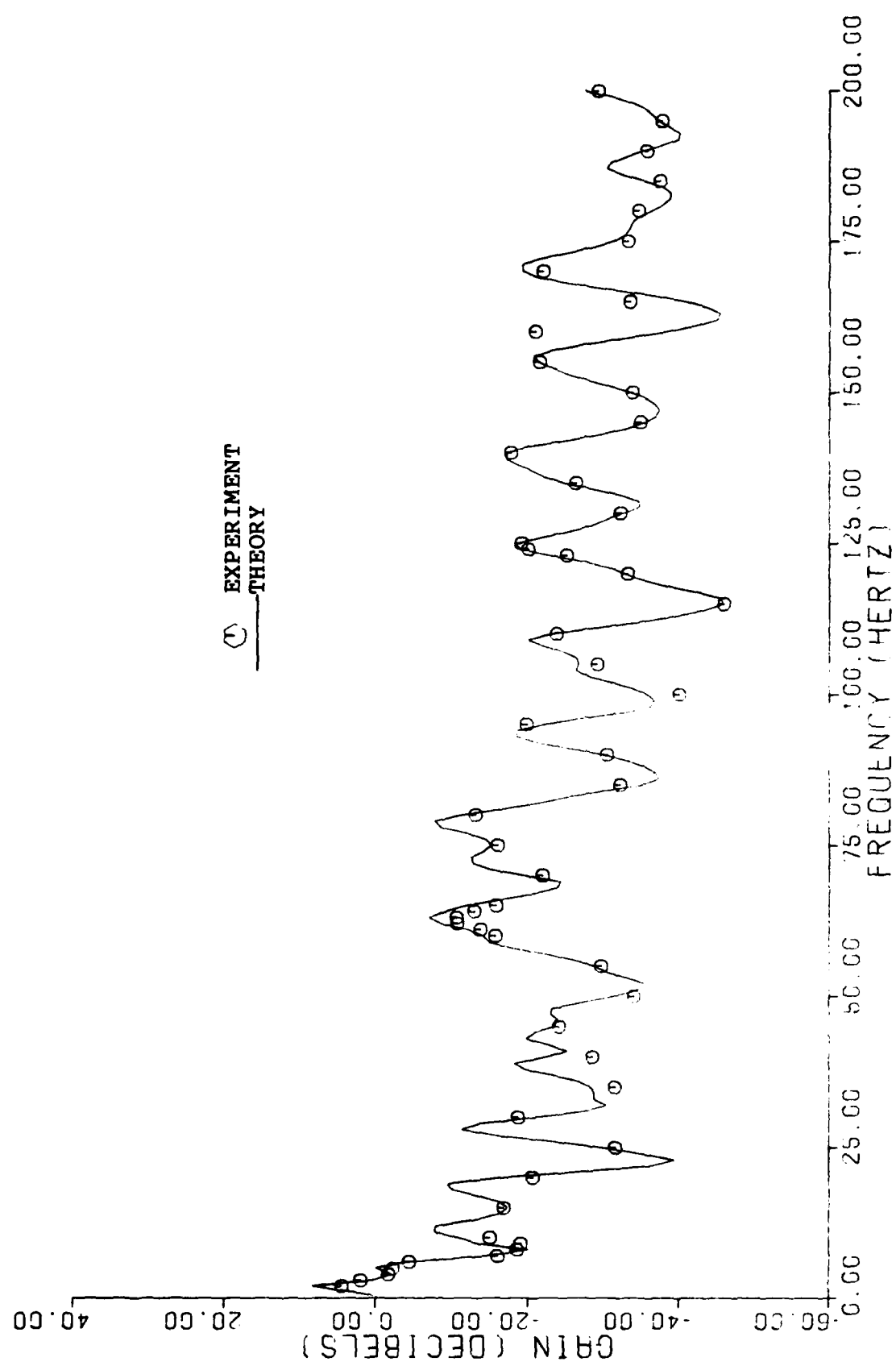


Fig. 19: Case 3: P_{end}/P_{input} , Correlation of Experiment with Theory

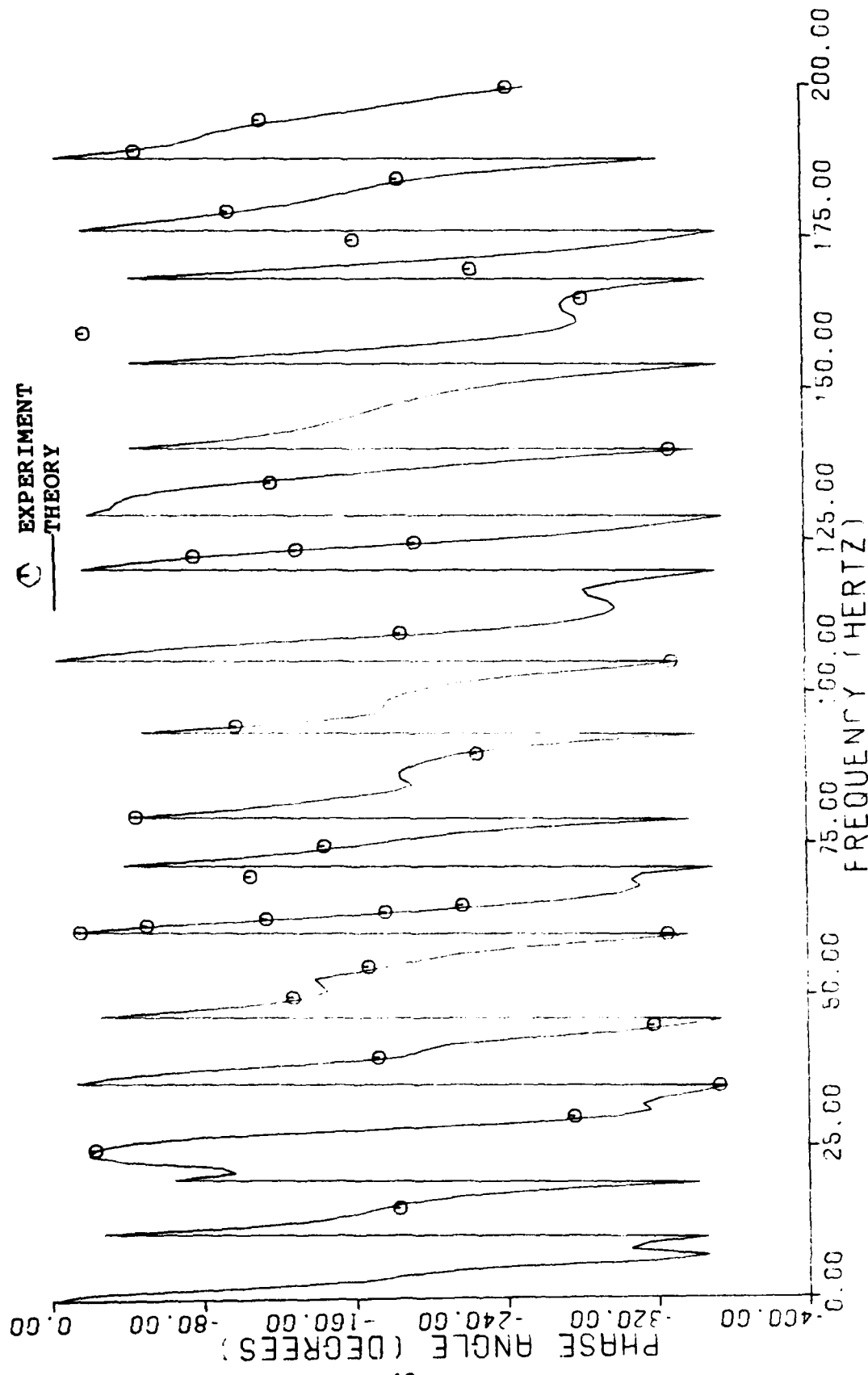


Fig. 20: Case 3: Phase Shift ($P_{\text{end}}/P_{\text{input}}$), Correlation of Experiment with Theory

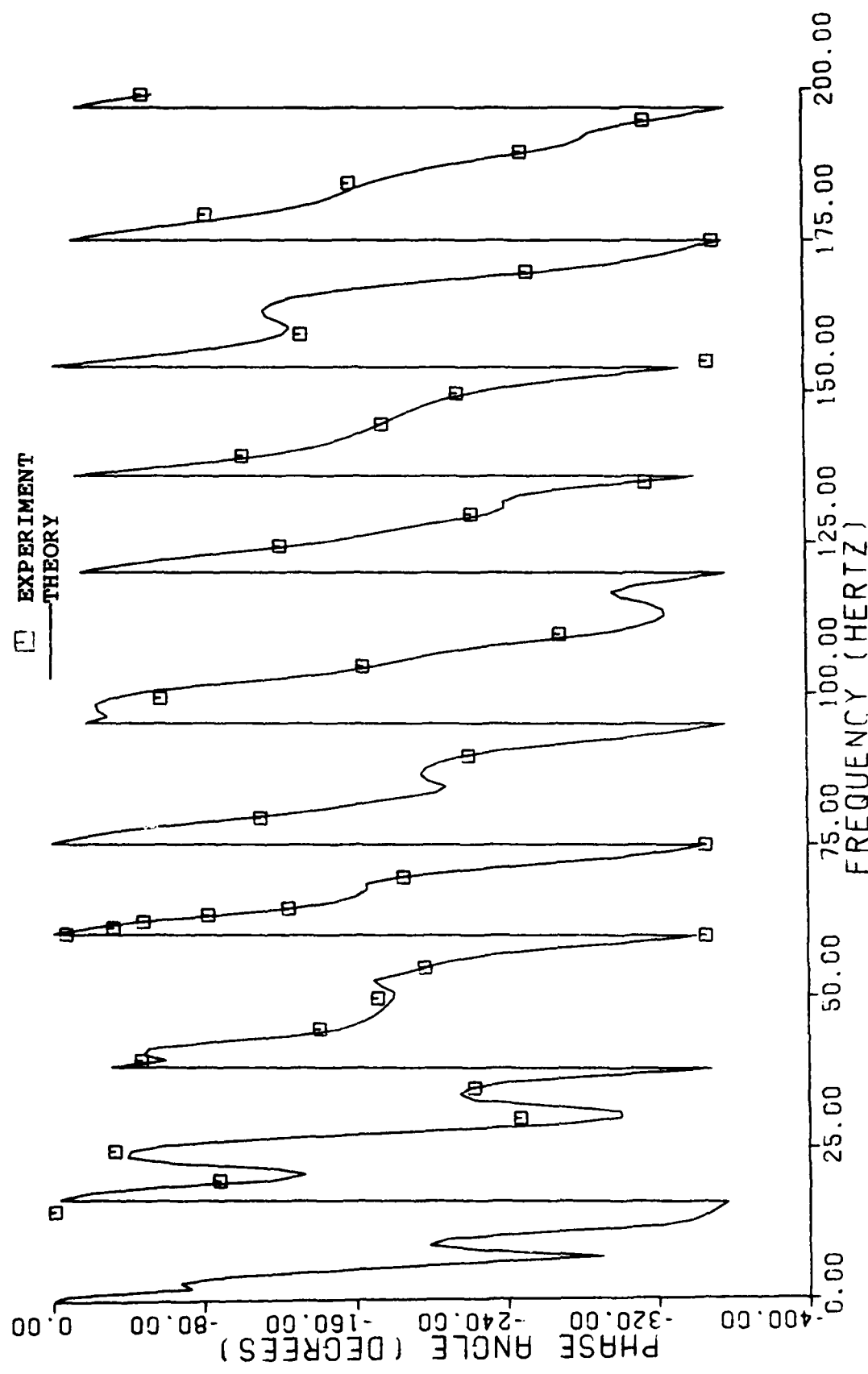


Fig. 22: Case 4: Phase Shift ($P_{\text{vent}}/P_{\text{input}}$), Correlation of Experiment with Theory

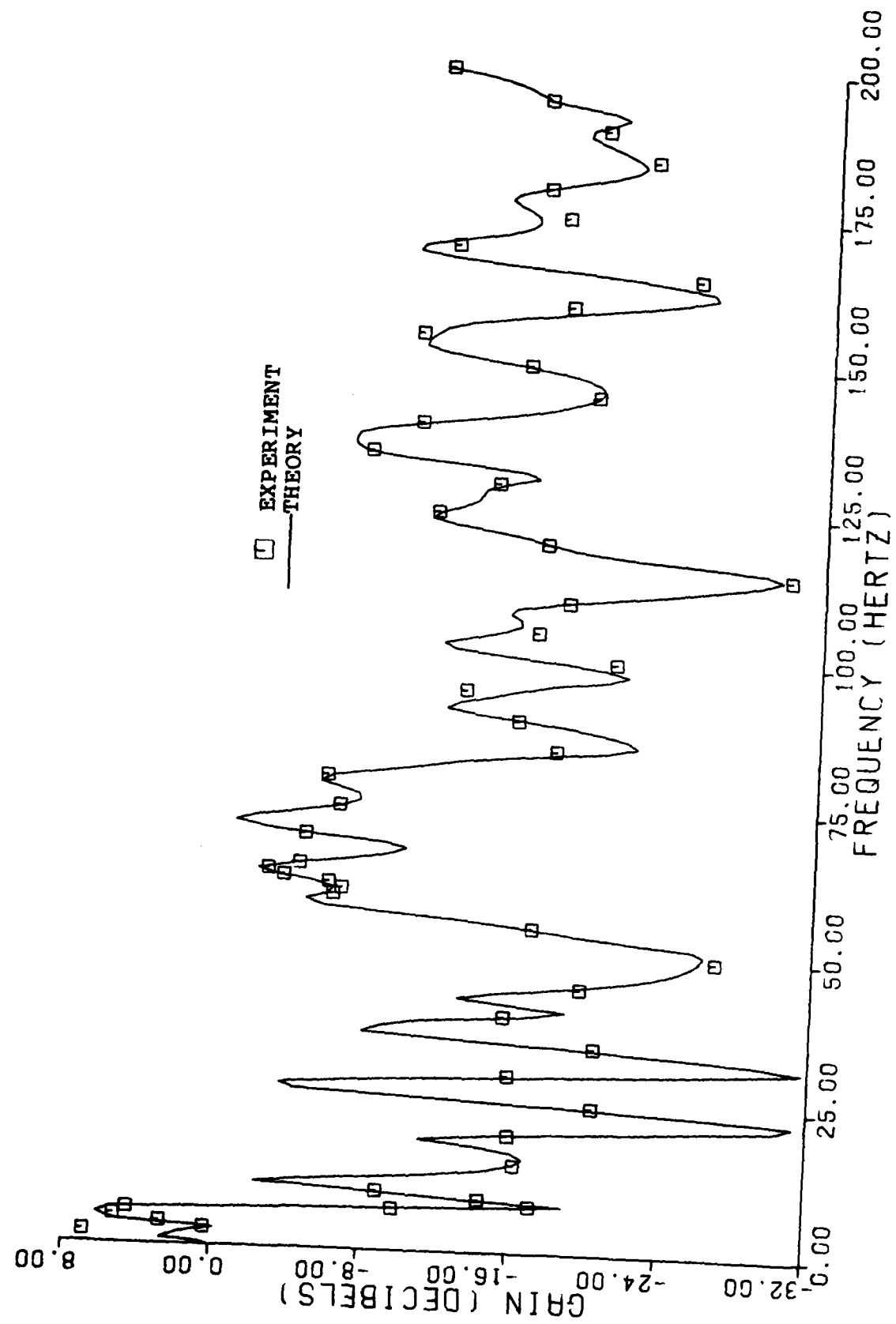


Fig. 21: Case 4: $P_{\text{vent}}/P_{\text{input}}$, Correlation of Experiment with Theory

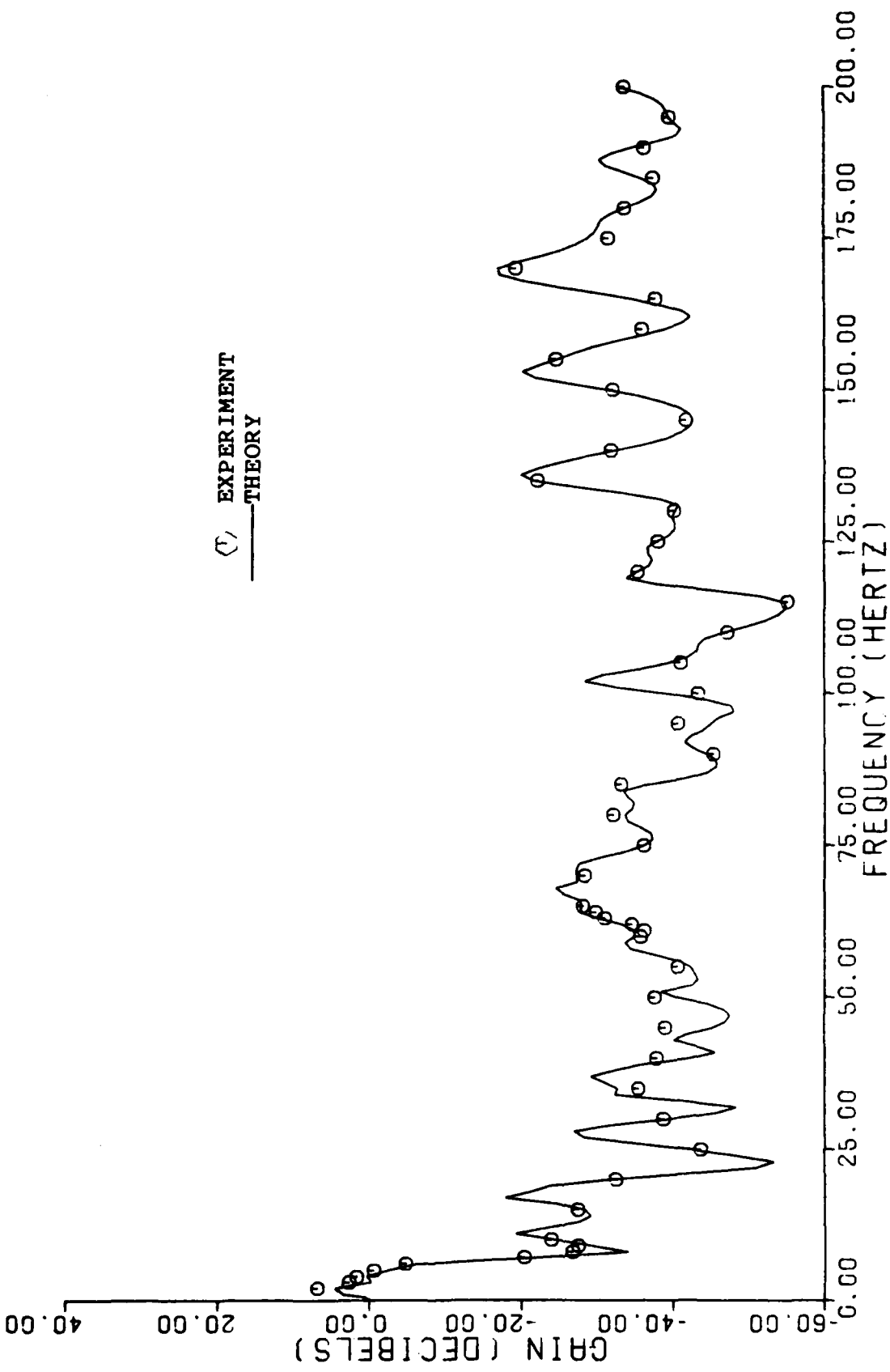


Fig. 23: Case 4: P_{end}/P_{input} Correlation of Experiment with Theory

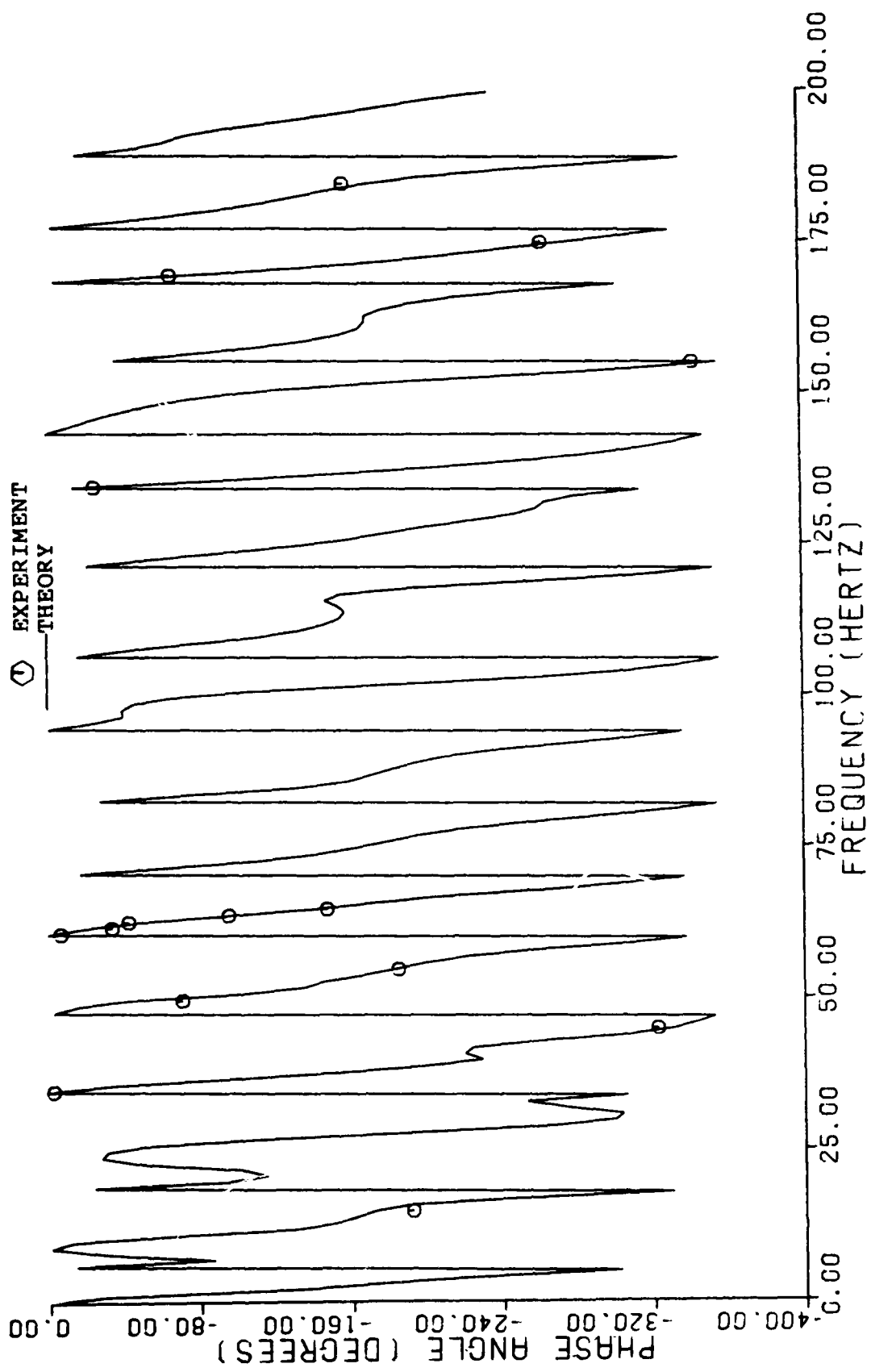


Fig. 24: Case 4: Phase Shift ($P_{\text{end}}/P_{\text{input}}$), Correlation of Experiment with Theory

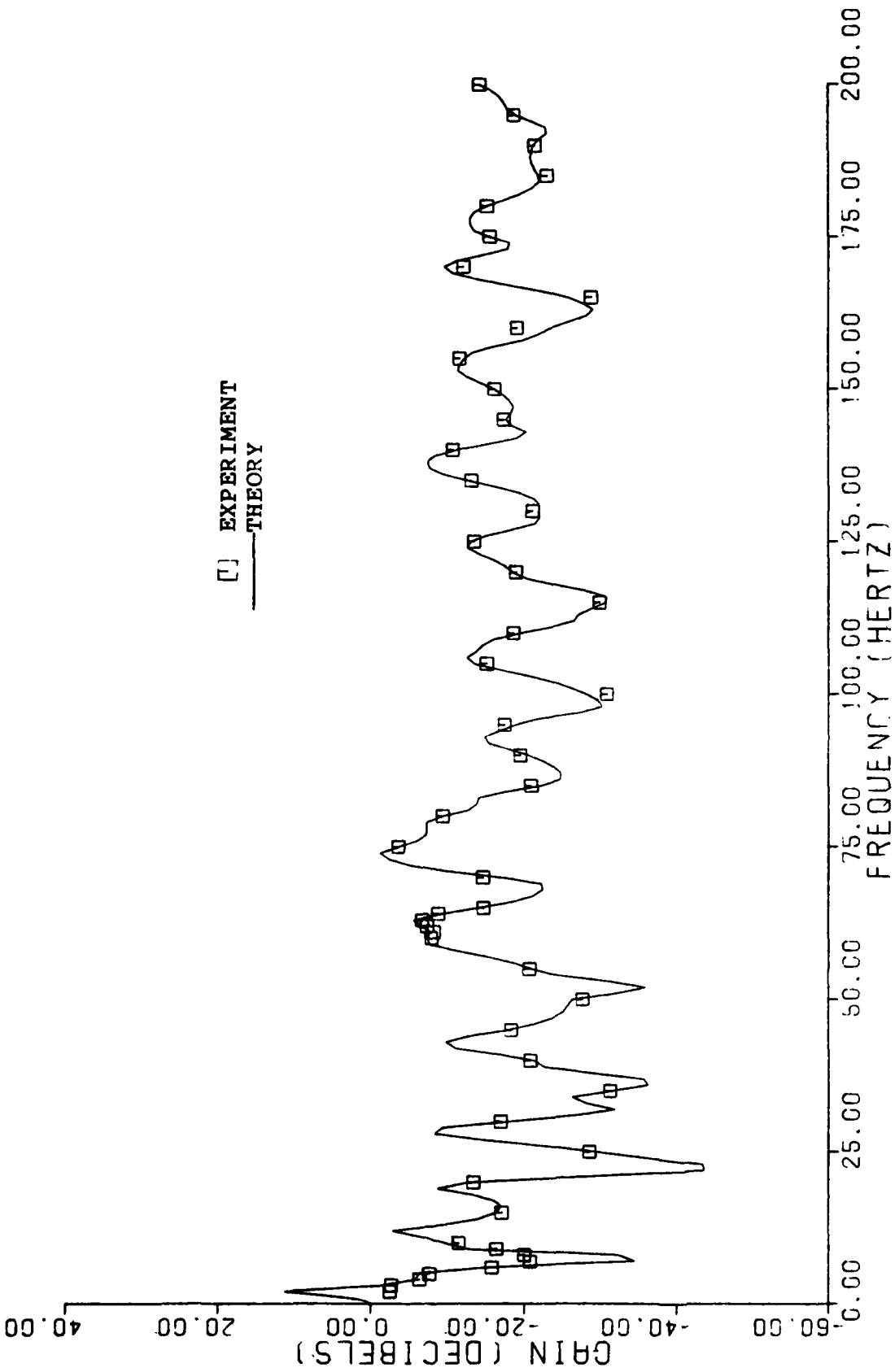


Fig. 25: Case 7: P_{event}/P_{input} 'Correlation of Experiment with Theory

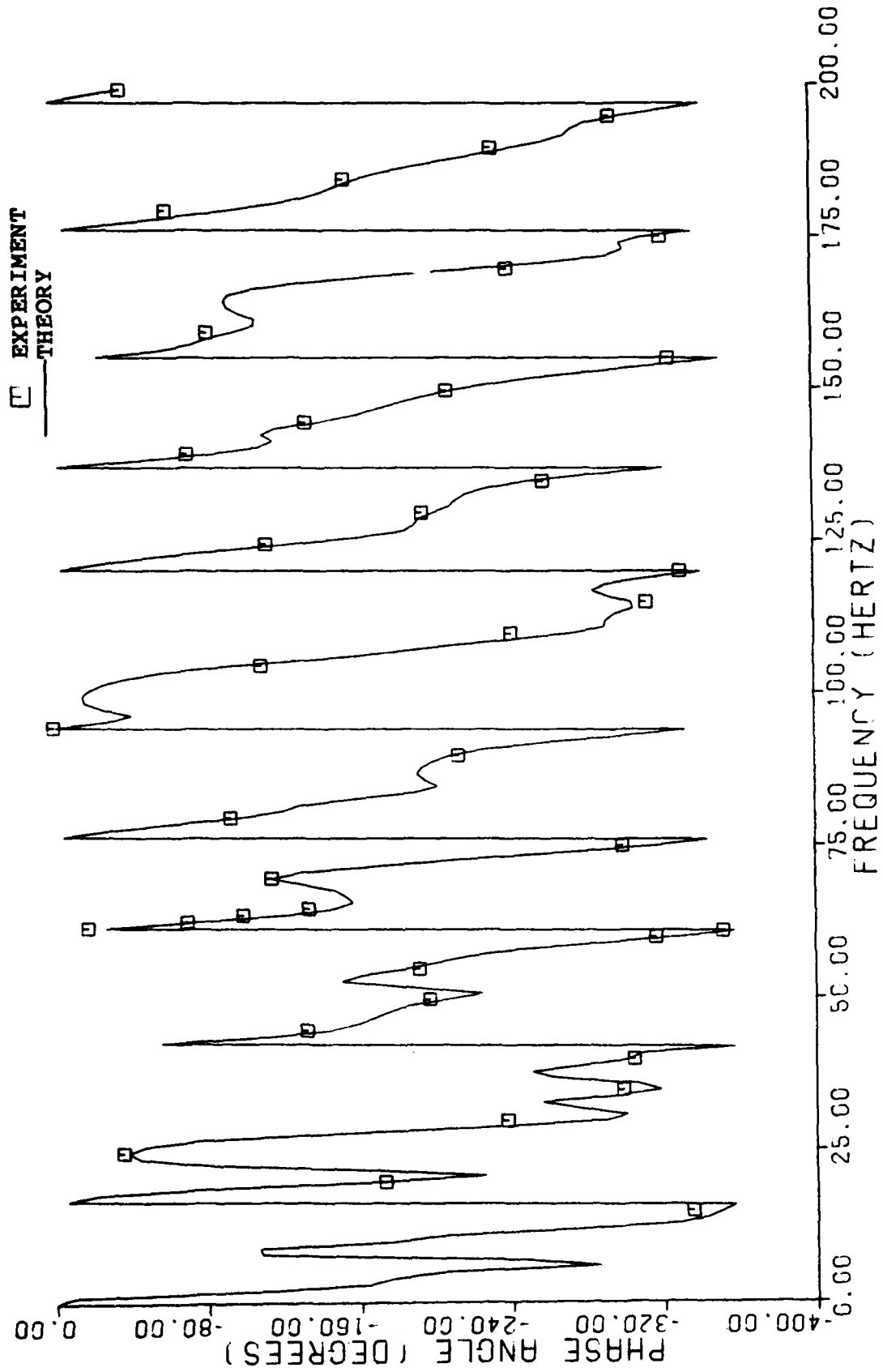


Fig. 26: Case 7: Phase Shift ($P_{\text{vent}}/P_{\text{input}}$), Correlation of Experiment with Theory

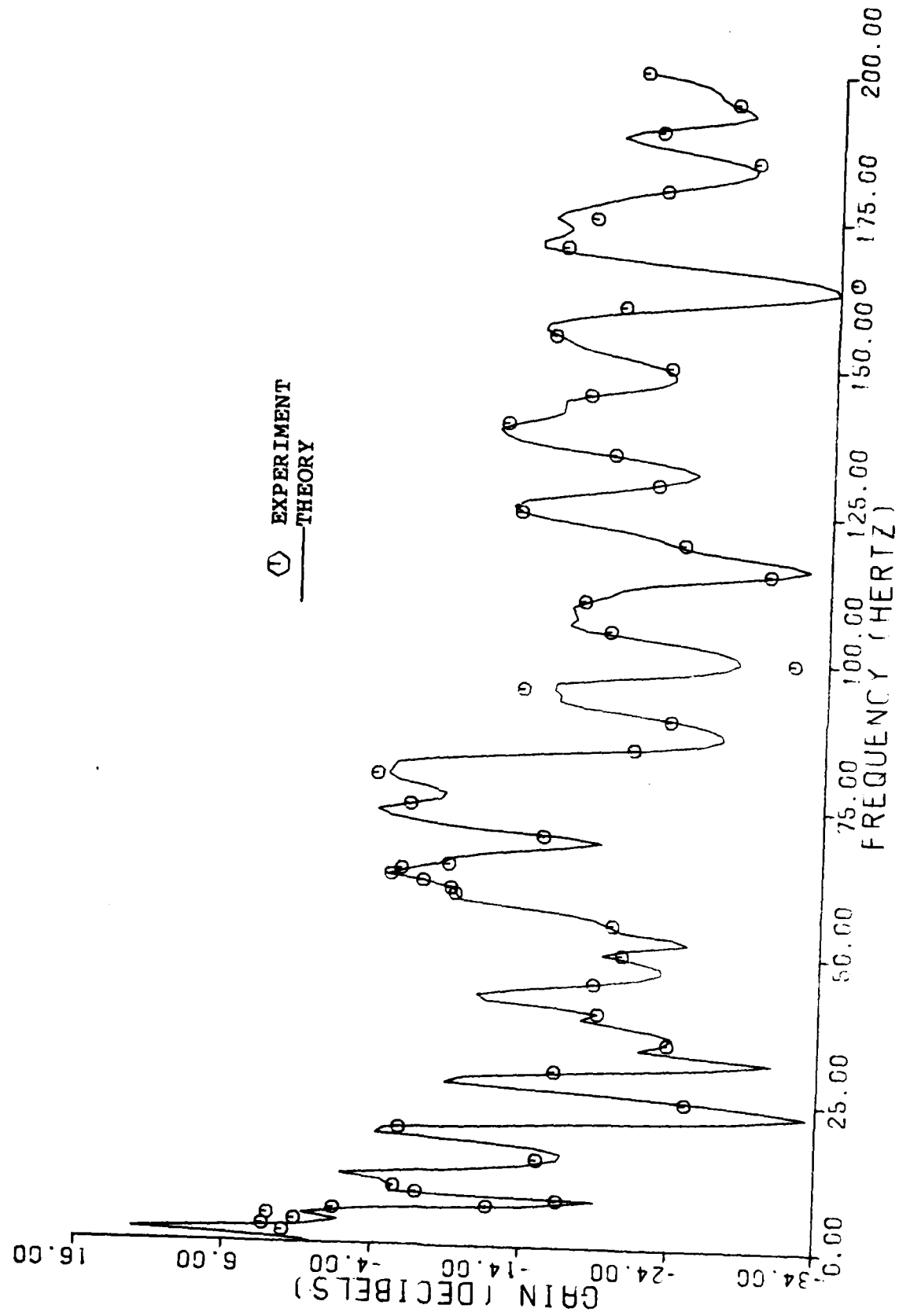


Fig. 27: Case 7: $P_{\text{end}}/P_{\text{input}}$, Correlation of Experiment with Theory

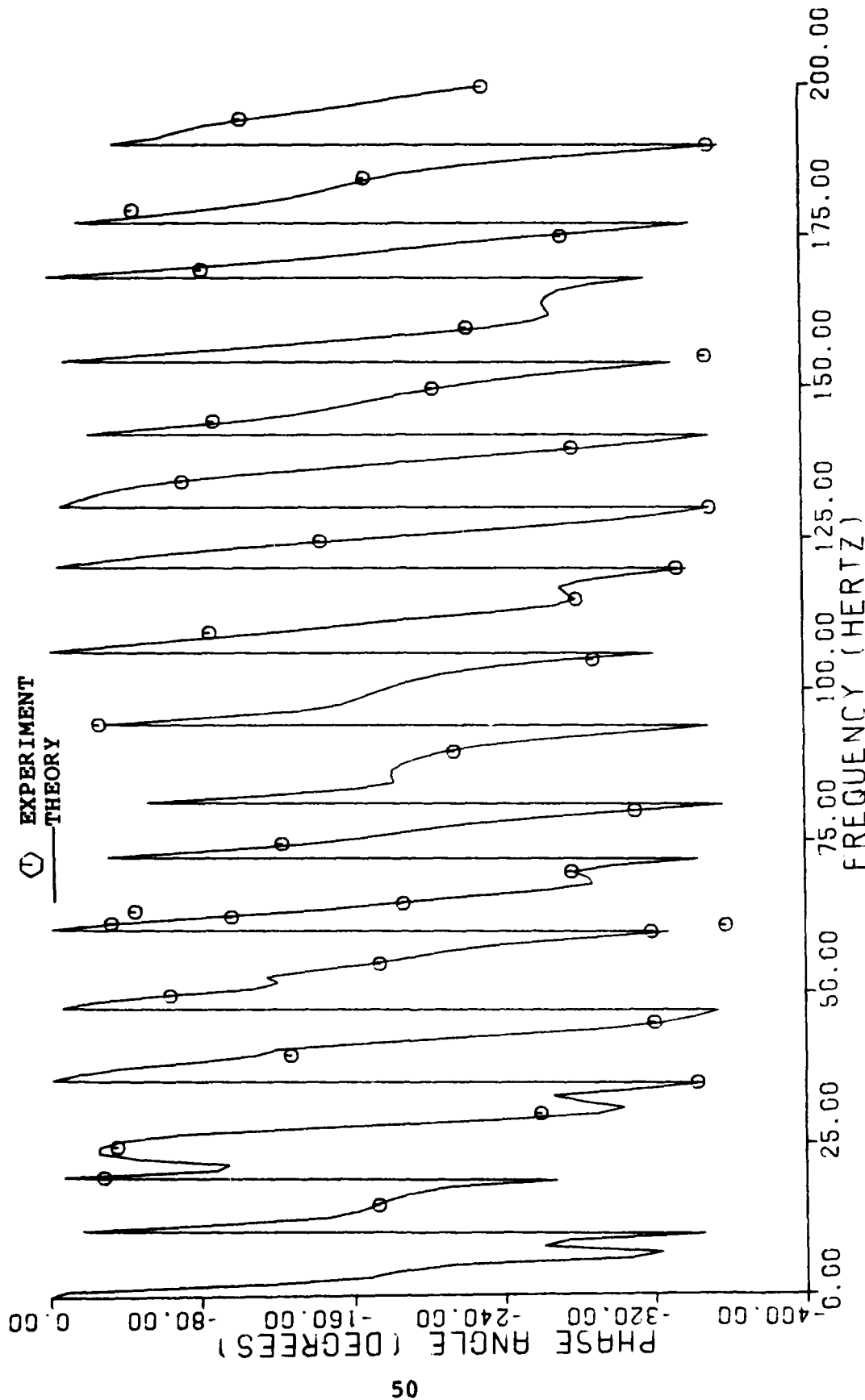


Fig. 28: Case 7: Phase Shift (P_{end}/P_{input}), Correlation of Experiment with Theory

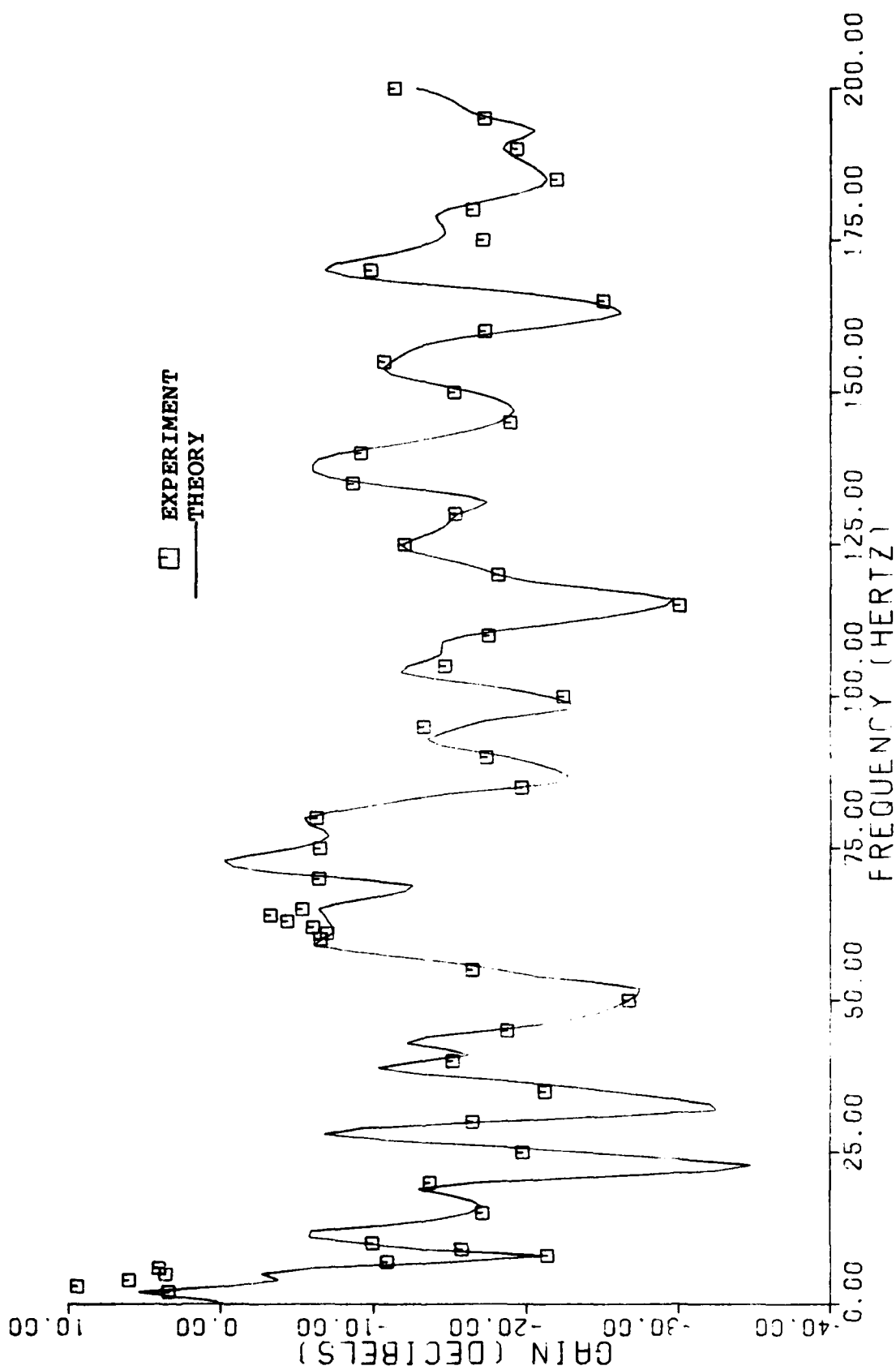


Fig. 29: Case 6: P_{vent}/P_{input} Correlation of Experiment with Theory

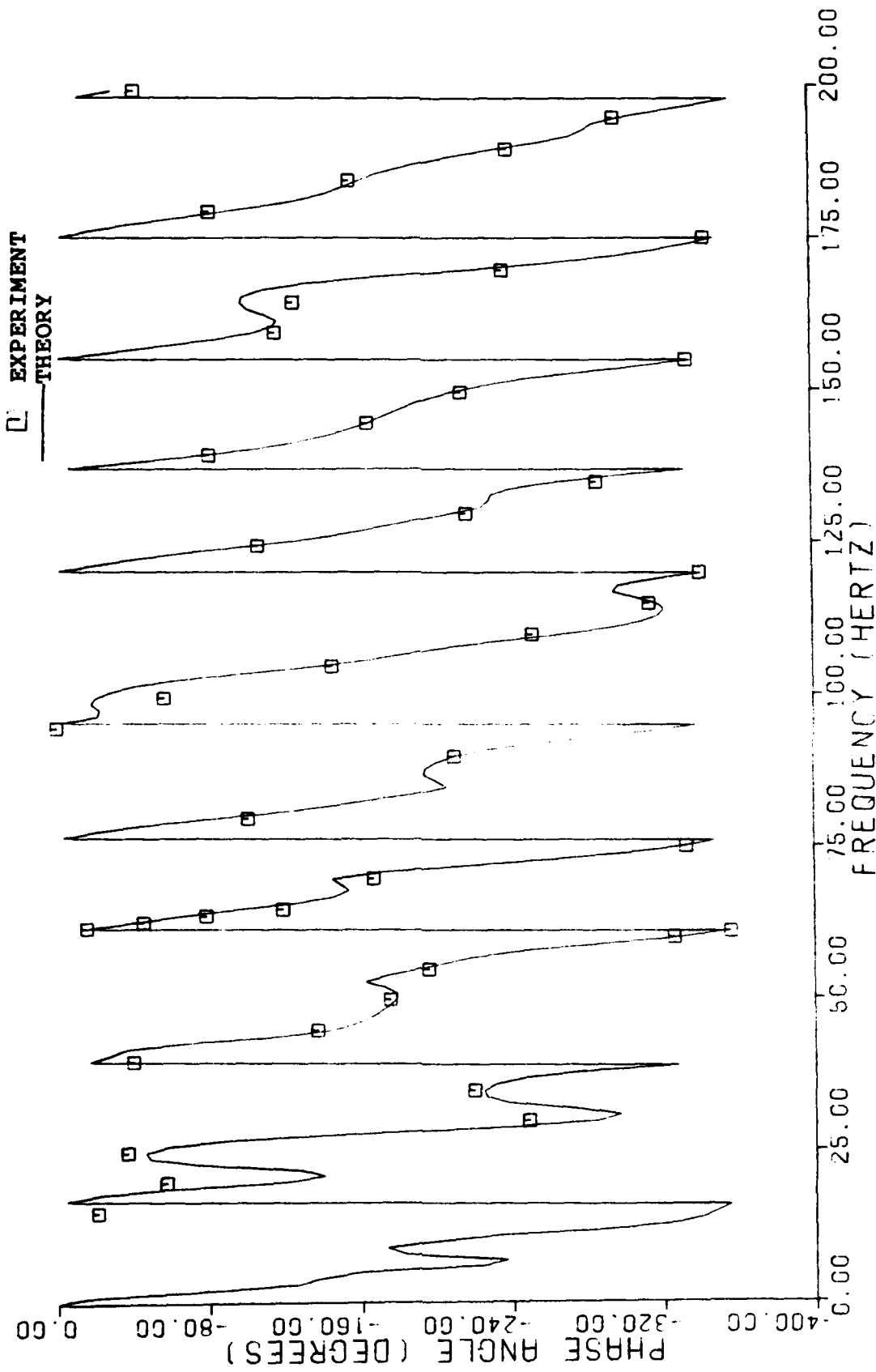


Fig. 30: Case 6: Phase Shift (P_{vent}/P_{input}), Correlation of Experiment with Theory

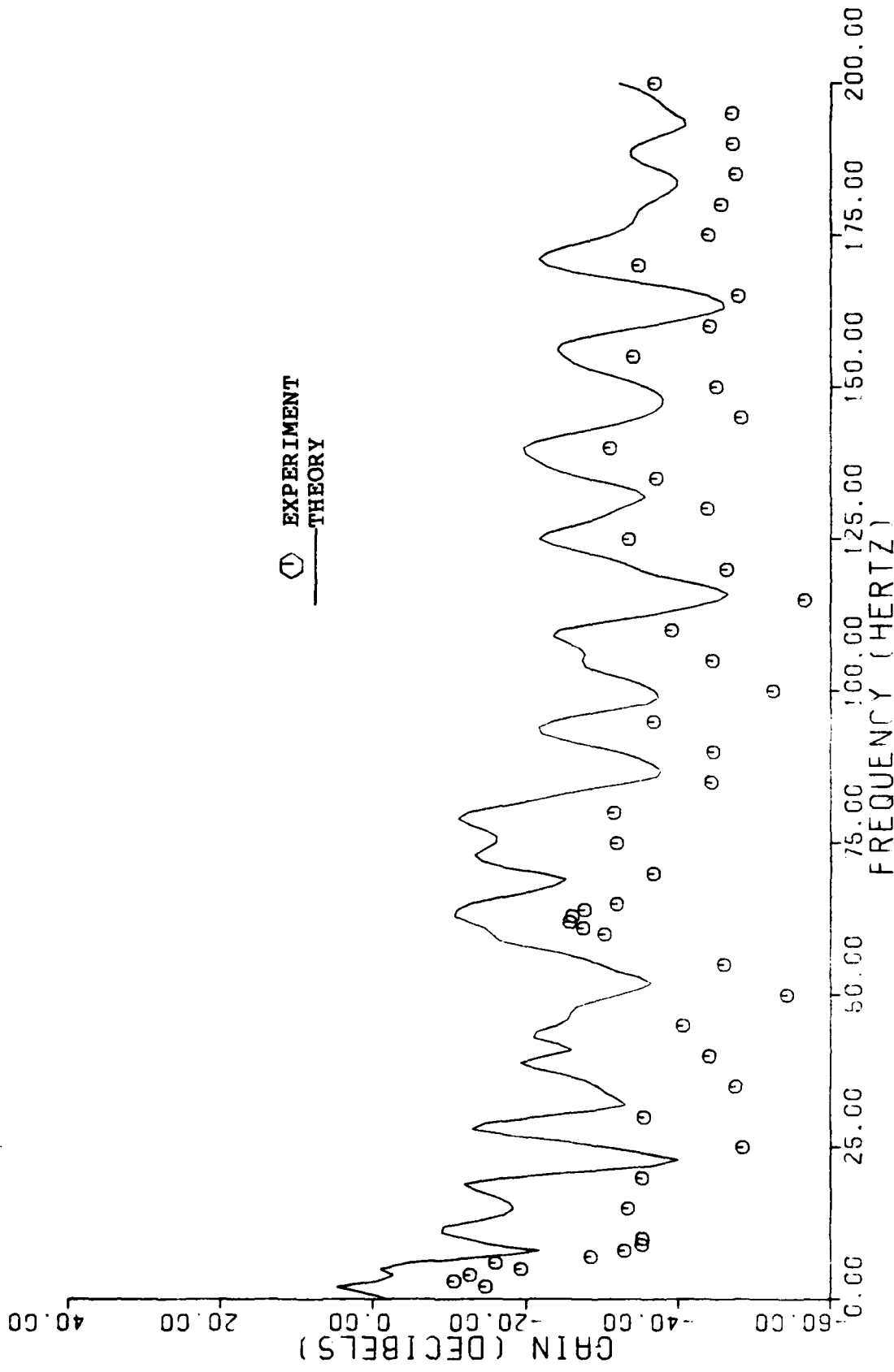


Fig. 31: Case 6: P_{end}/P_{input}, Correlation of Experiment with Theory

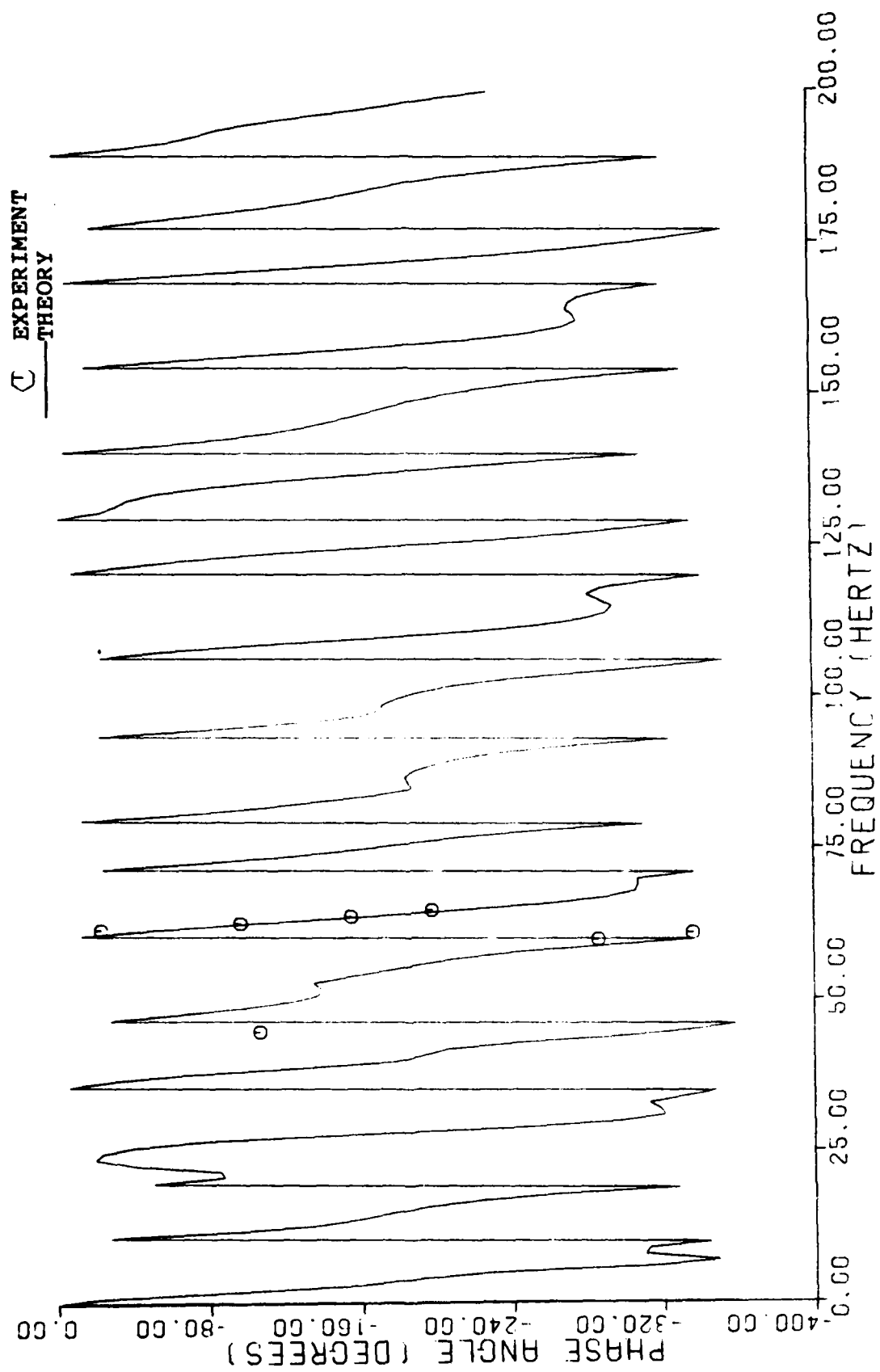


Fig. 32: Case 6: Phase Shift ($P_{\text{end}}/P_{\text{input}}$), Correlation of Experiment with Theory

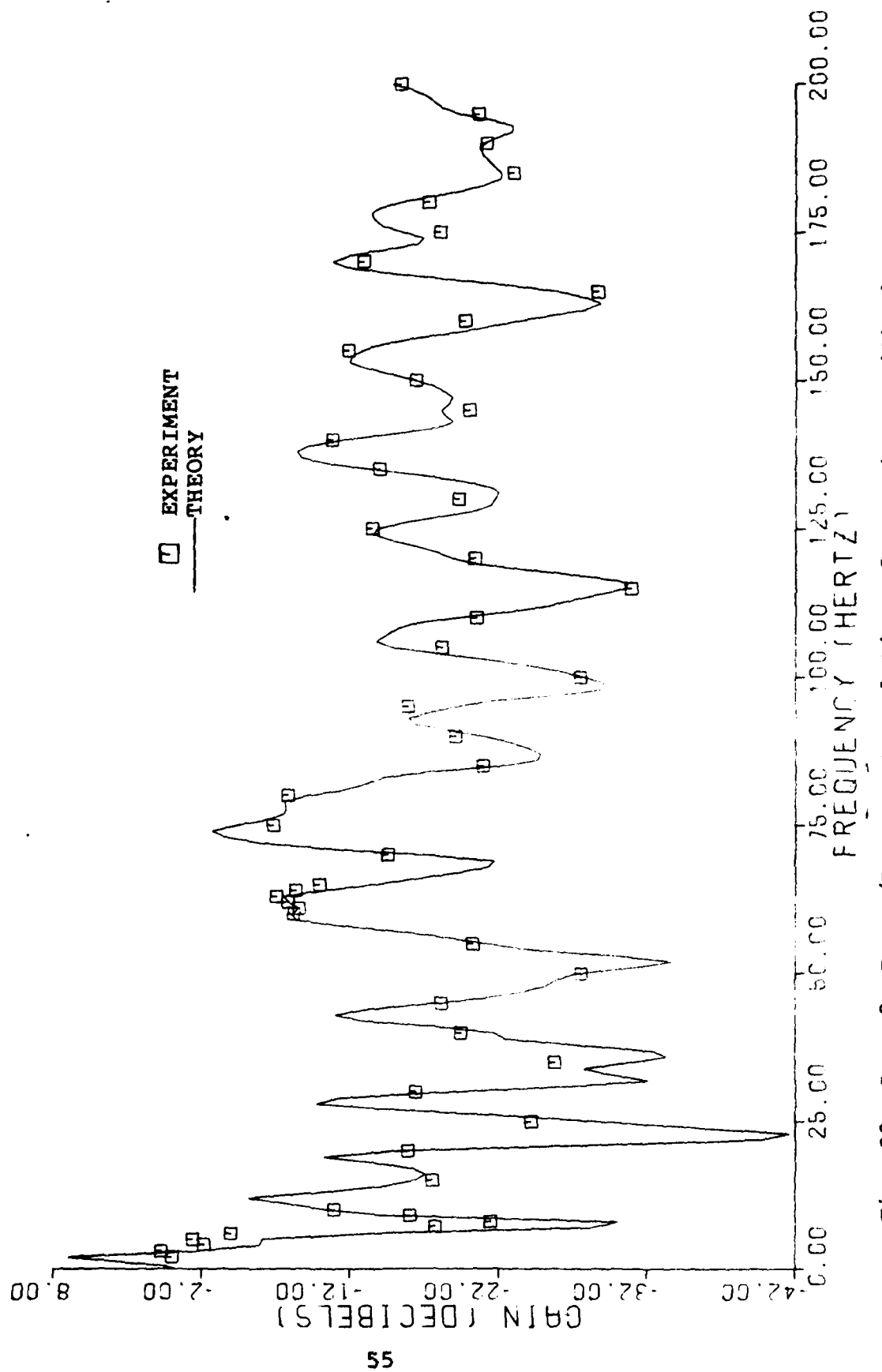


Fig. 33: Case 8: $P_{\text{vent}}/P_{\text{input}}$, Correlation of Experiment with Theory

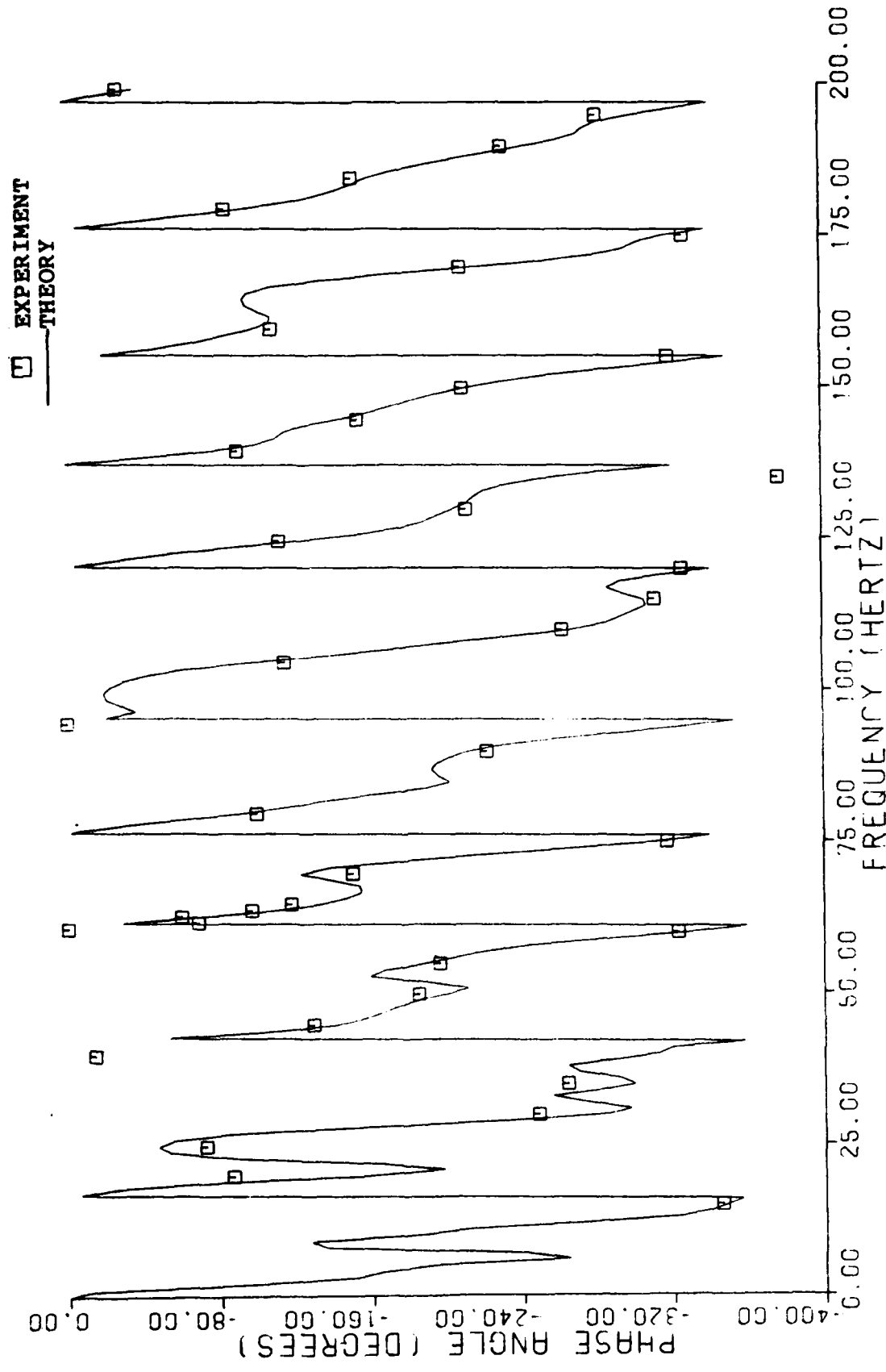


Fig. 34: Case 8: Phase Shift ($P_{\text{vent}}/P_{\text{input}}$), correlation of Experiment with Theory

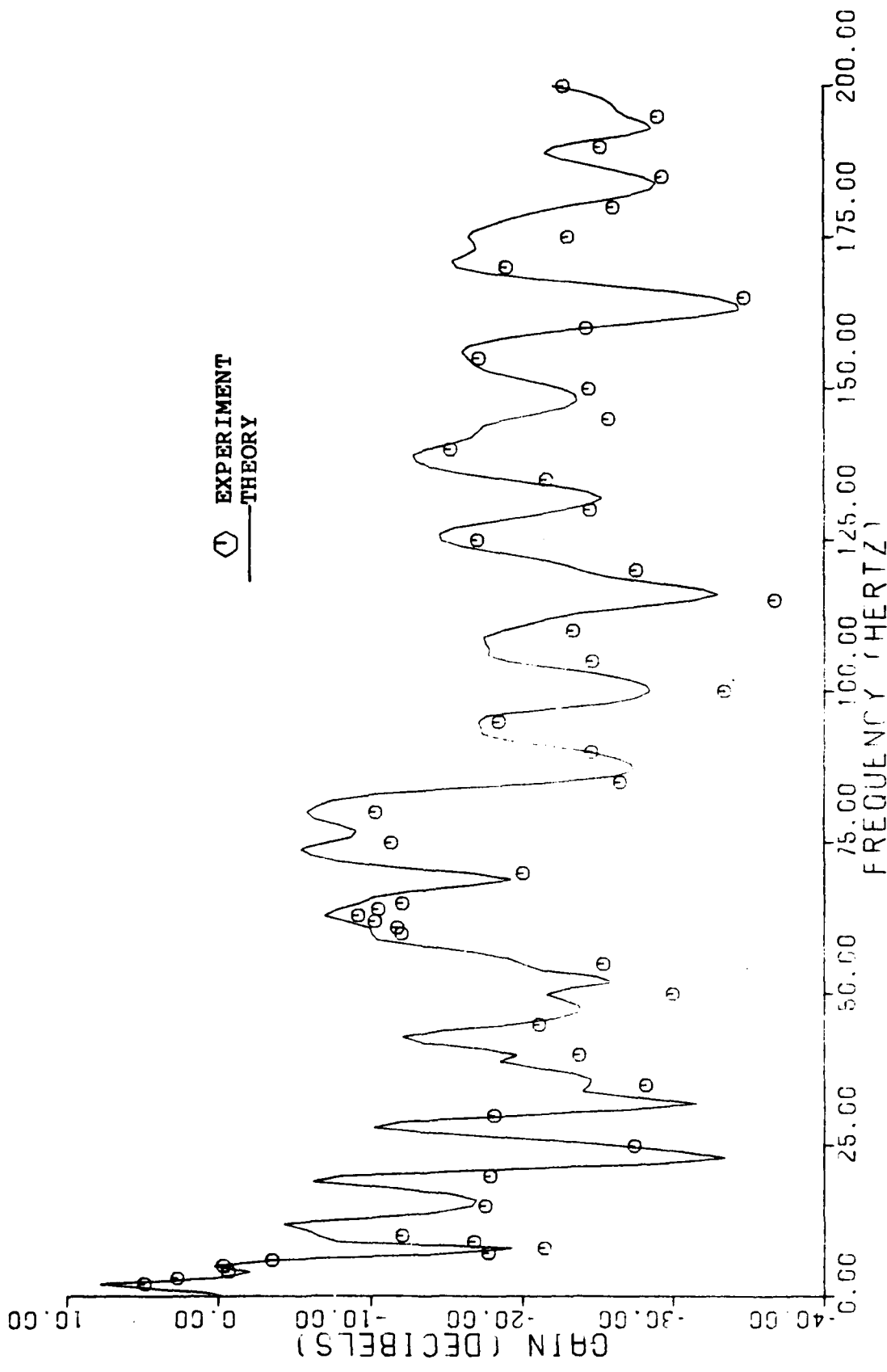


Fig. 35: Case 8: $P_{\text{end}}/P_{\text{input}}$, Correlation of Experiment with Theory

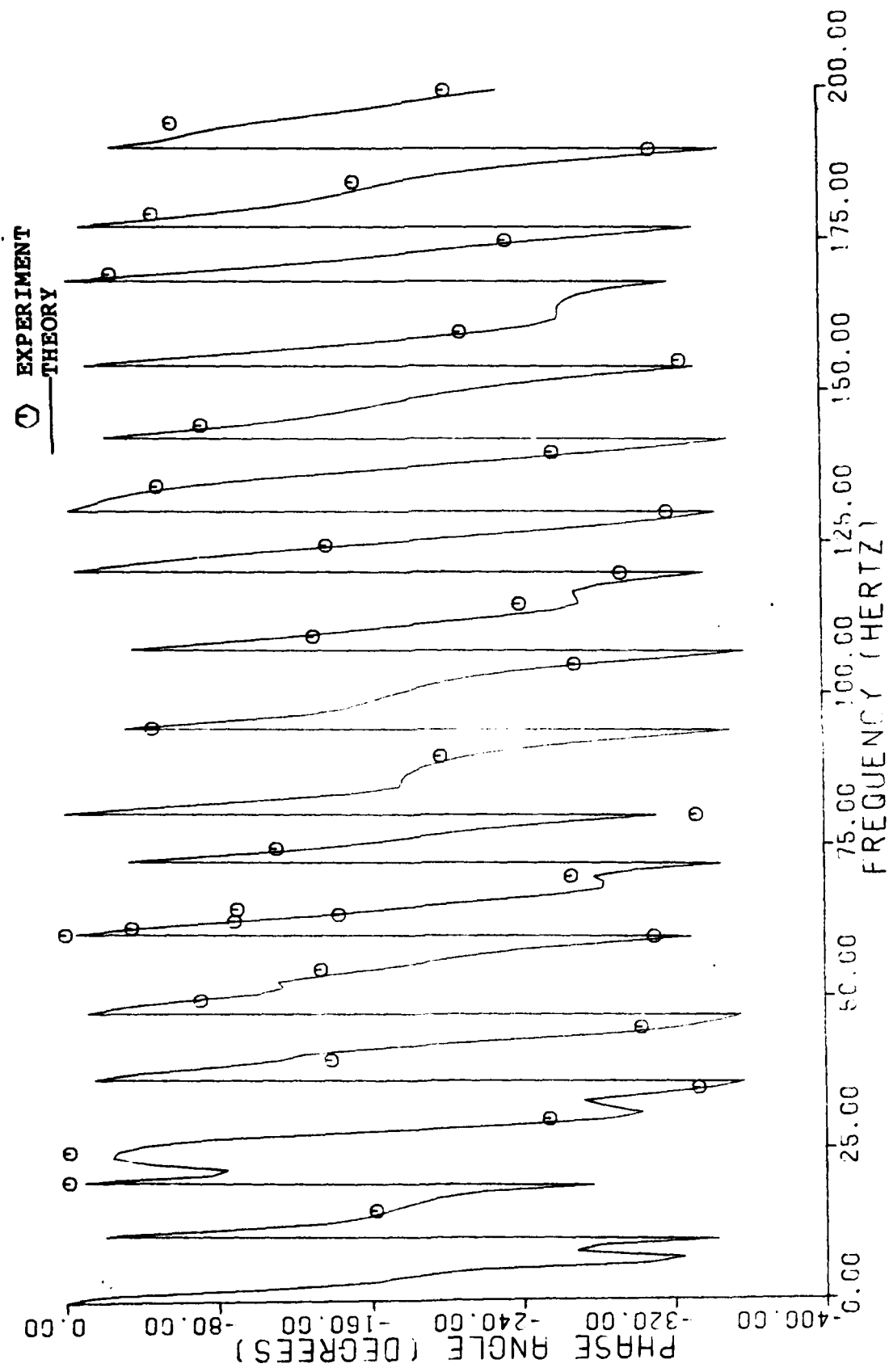


Fig. 36: Case 8: Phase Shift (P_{end}/P_{input}), Correlation of Experiment with Theory

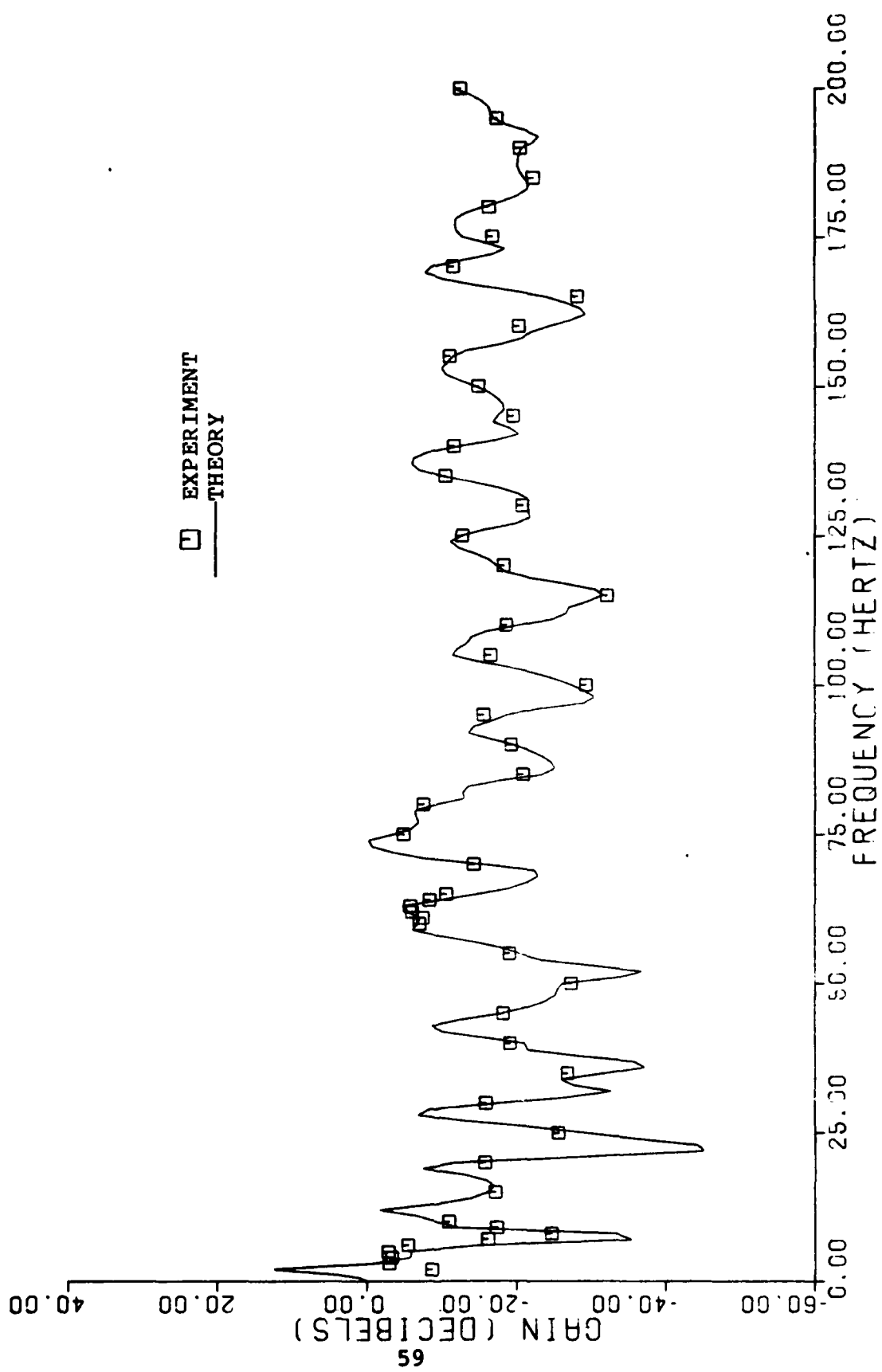


Fig. 37: Case 9: $P_{\text{vent}}/P_{\text{input}}$ Correlation of Experiment with Theory

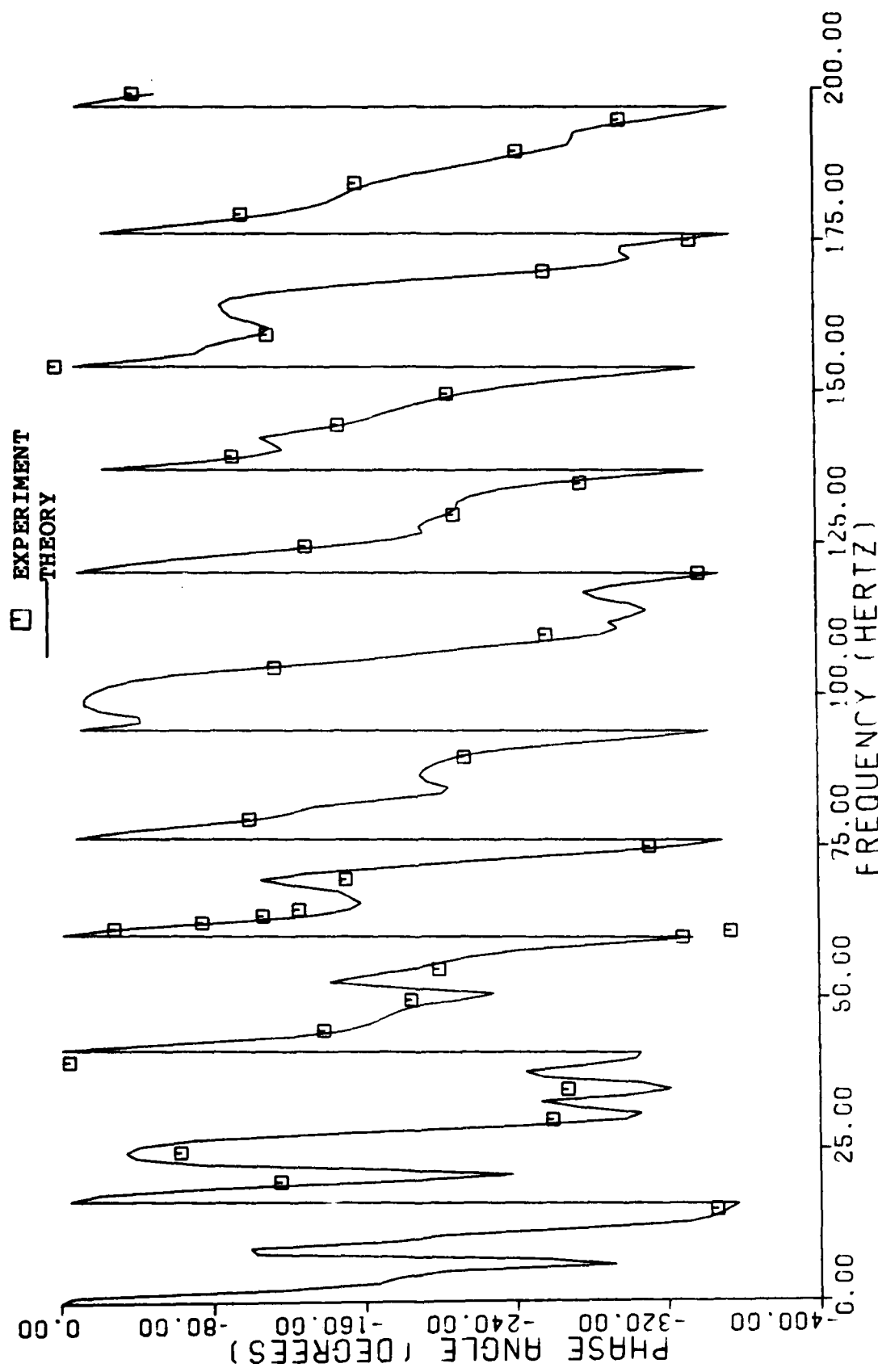


Fig. 38: Case 9: Phase Shift (P_{vent}/P_{input}), Correlation of Experiment with Theory

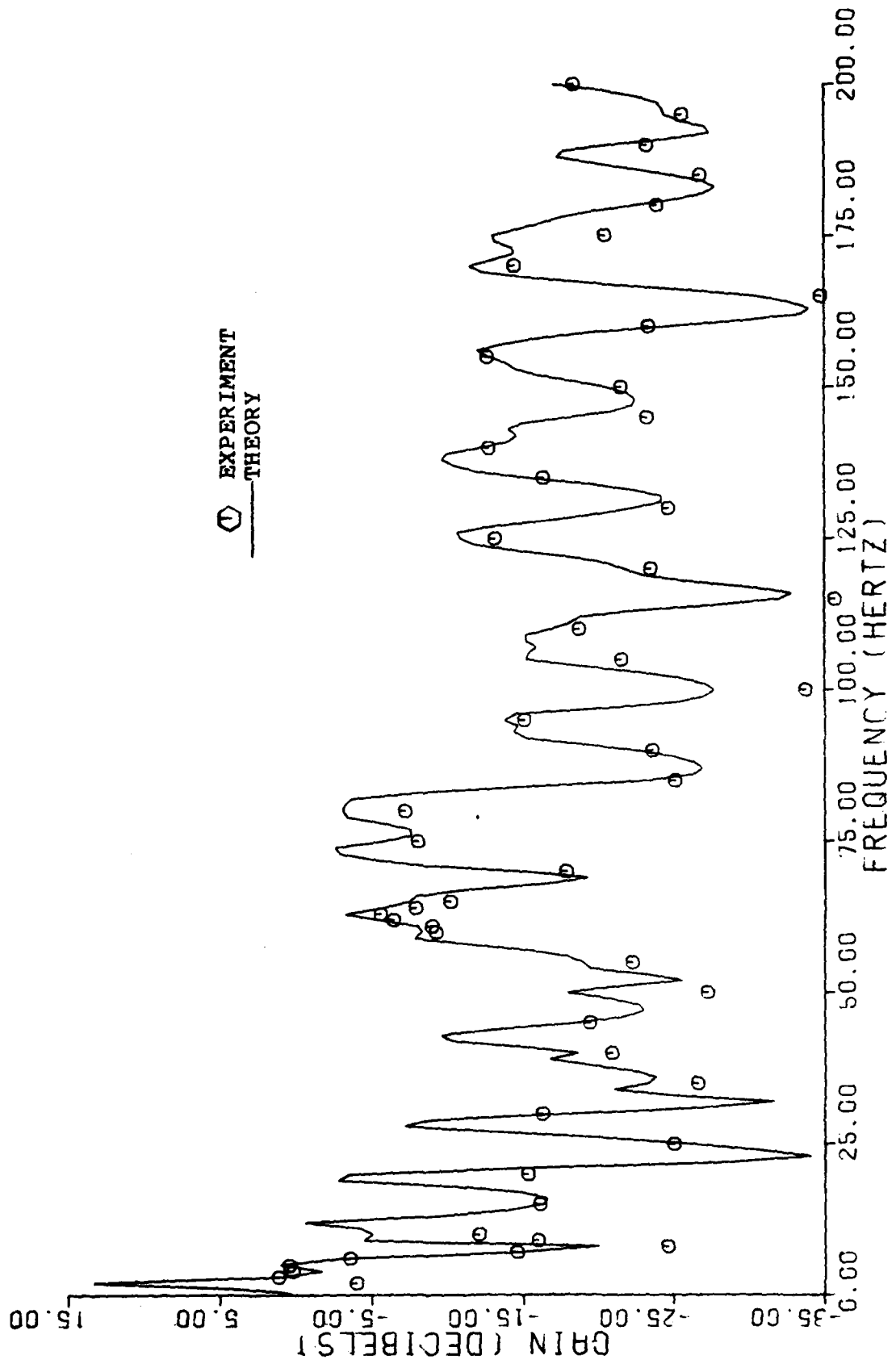


Fig. 39: Case 9: $P_{\text{end}}/P_{\text{input}}$, Correlation of Experiment with Theory

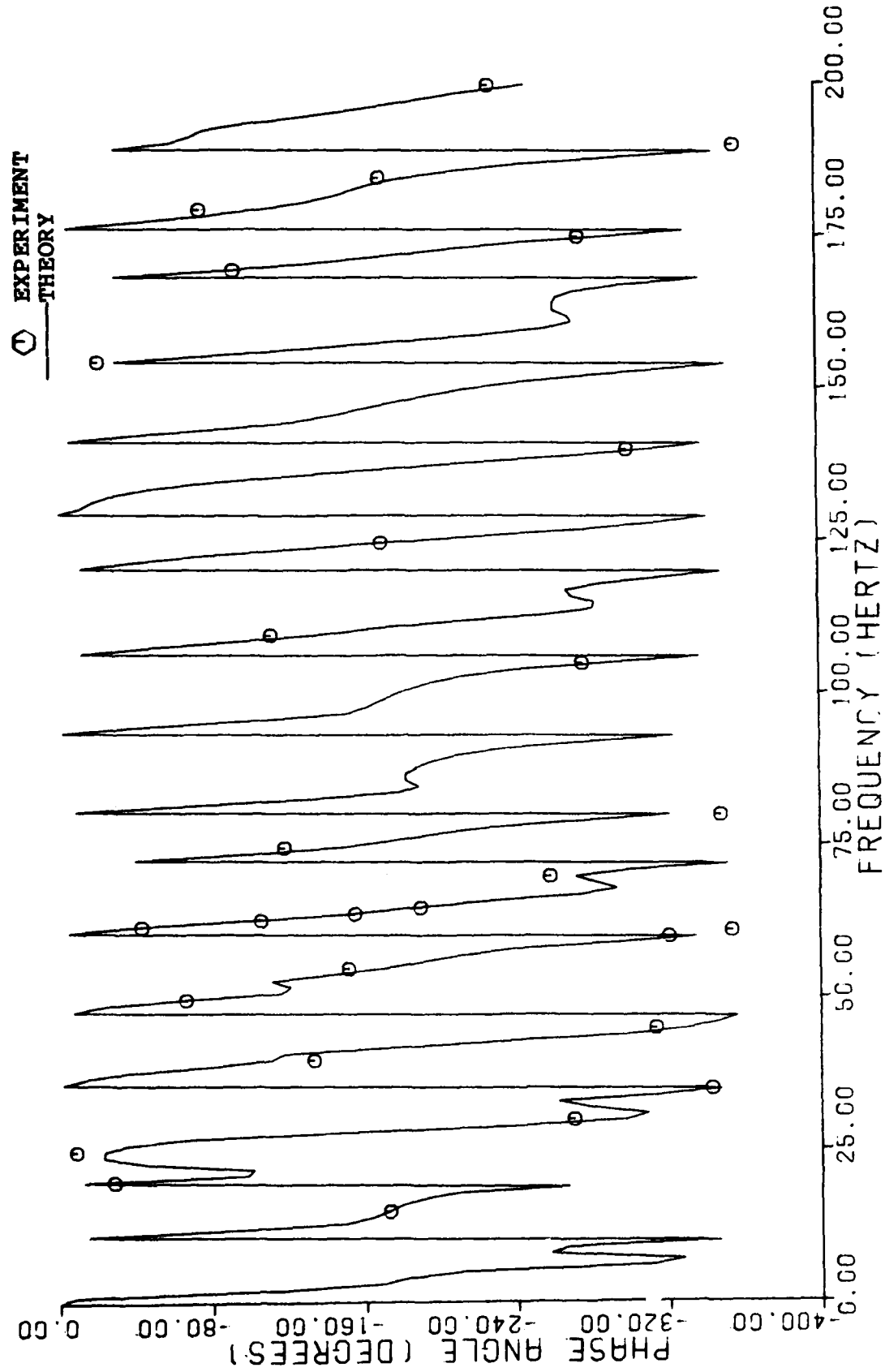


Fig. 40: Case 9: Phase Shift (P_{end}/P_{input}), Correlation of Experiment with Theory

VII. ASTF Results and Discussion

Schematics of the ASTF lines showing how they were input to the computer program are included in Appendix B (Figs. 64-66). Table III contains the system configuration for each case.

Blocked Line Cases

Although a blocked line represents an unrealistic case for ASTF, it represents an upper limit on results because the end impedance is infinite. Blocked lines also allow comparison of the effects of different input legs (cases 1-3) and the effect of FOD screens added to the flow straightening grids (cases 4 and 5).

The results from cases 1-3 (Figs. 41-46) show the same general trends, but there were larger gains in case 2 compared with case 1 and larger peaks and valleys in case 3 compared with the other two. All cases show greater attenuation at higher frequencies. The highest gain occurs consistently at 0.8 Hz in all three cases, and the gain values are:

Case 1	28.8 dB
Case 2	36.3 dB
Case 3	24.8 dB

The results from cases 4 and 5 (Figs. 47-50) show the same trends as those in case 3, with greater attenuation at most frequencies as the percentage of blockage at the flow straightening grids due to the FOD screens increases. Exceptions occur around 90, 131, and 174 Hz, where the gain with FOD screens is much greater.

As expected, the first harmonic occurs at approximately half the frequency (0.8 Hz vs 2 Hz) in the ASTF cases compared to the model. This occurs because ASTF lines are twice as long as the model lines.

Cases with Mean Flow

Table III shows the mass flow rates, pressures, and temperatures used in each case. These conditions were derived from the F-100 engine operating envelope as described in Chapter III. Cases 6-9 (Figs. 51-58) were taken from the supersonic regime and Case 10 (Figs. 59 and 60) was taken from the subsonic regime. Flow velocities in the largest ASTF ducts were about 12 ft/sec in all cases.

The frequency at which the first harmonic occurs is affected by temperature and impedance. Generally, this frequency is shifted upward by increasing temperature and by decreased end impedance. The decreased end impedance of open lines vs blocked lines would generally shift the harmonic upward in frequency. The ASTF results show no effect of open lines on this harmonic frequency because the

small engine diameter and large engine flow restriction create a very high end impedance. Thus, the cases with flow look very much like the blocked line cases.

The first peaks of each of the curves occurs at 0.8 Hz in cases 8-10, primarily because they are at nearly the same test cell temperature. In cases 6 and 7, the first peaks occur at 1.0 and 0.9 Hz, respectively. This increase in frequency is due to the higher speed of sound at the higher temperature in these cases. A comparison of all flow cases to case 3 shows the effect of temperature in that corresponding peaks occur at frequencies higher than in case 3 in cases 6 and 7, and at lower frequencies in case 8-10. The gains at the fundamental frequencies (0.8-1.0 Hz) for cases 6-10 are:

Case 6	23.63 dB
Case 7	21.49 dB
Case 8	21.60 dB
Case 9	24.75 dB
Case 10	30.99 dB

The mean gains in all the flow cases are about the same, and match those of the blocked line cases. The data show no trends indicating effects of flow rate.

General

The ASTF results show large gains (21-36 dB) at the fundamental frequency (0.8-1.0 Hz) and somewhat lower gains at all other frequencies investigated. The bandwidth of the peak at the fundamental frequency is narrow (3 Hz) and the gains fall off sharply either side of this peak.

Preliminary results of experiments with the mixing valves in the model indicate that butterfly valves oscillating at a given frequency do not generate significant signals at that frequency. Most of the output is of very high frequency, probably from vortices and turbulence.

Table III
ASTF Configuration

Case #	Input Leg #	Straightening Grids and FOD Screens		\dot{M}_{end} lbm/sec	P _{end} / P _{line} psia	T _{end} / T _{line} °R	Results
		1	2				
1	L1	4	4	0	24.7/ 24.7	539/ 539	Figs. 41, 42
2	L2	4	4	0	24.7/ 24.7	539/ 539	Figs. 43, 44
3	L3	4	4	0	24.7/ 24.7	539/ 539	Figs. 45, 46
4	L3	4	4	0	24.7/ 24.7	539/ 539	Figs. 47, 48
5	L3	48	48	0	24.7/ 24.7	539/ 539	Figs. 49, 50
6	L3	48	52	164	1.92/ 24.7	389/ 539	Figs. 51, 52
7	L3	4	4	200	5.32/ 12.9	427/ 550	Figs. 53, 54
8	L3	4	4	100	2.68/ 6.25	393/ 500	Figs. 55, 56
9	L3	4	4	50	1.41/ 3.0	391/ 485	Figs. 57, 58
10	L3	4	4	160	10.33/ 12.25	476/ 500	Figs. 59, 60

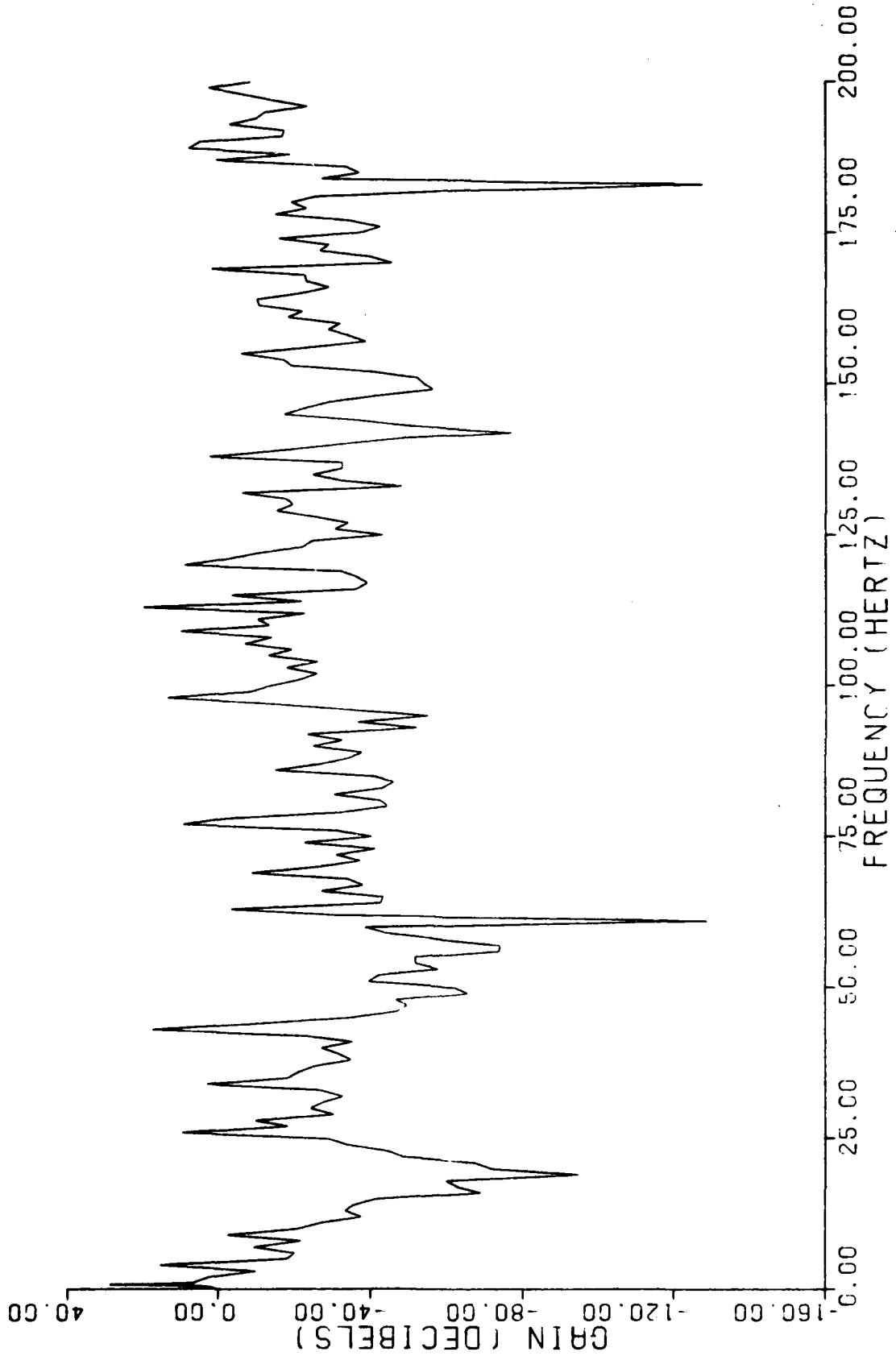


Fig. 41: ASTF Case 1

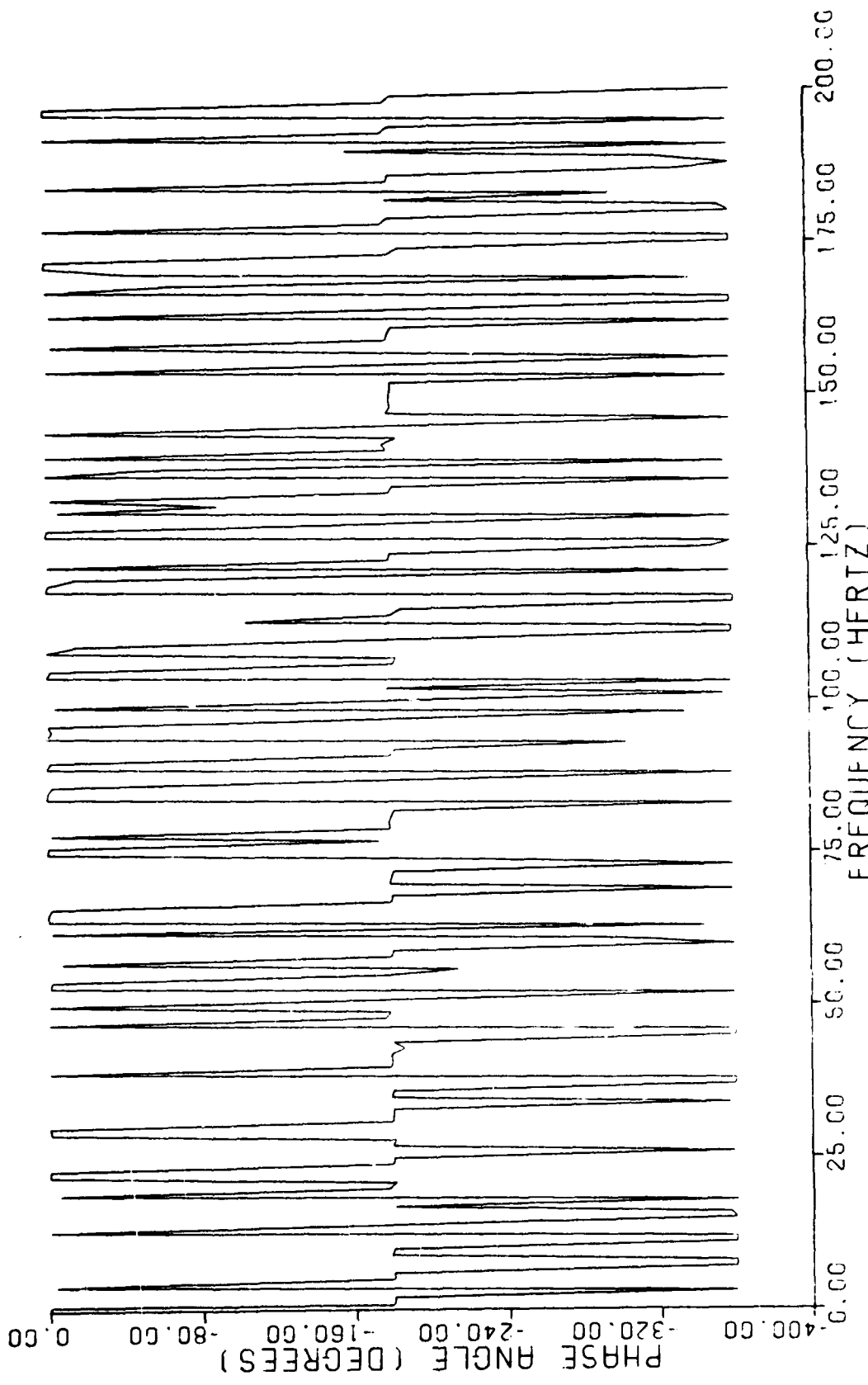


Fig. 42: ASTF Case 1

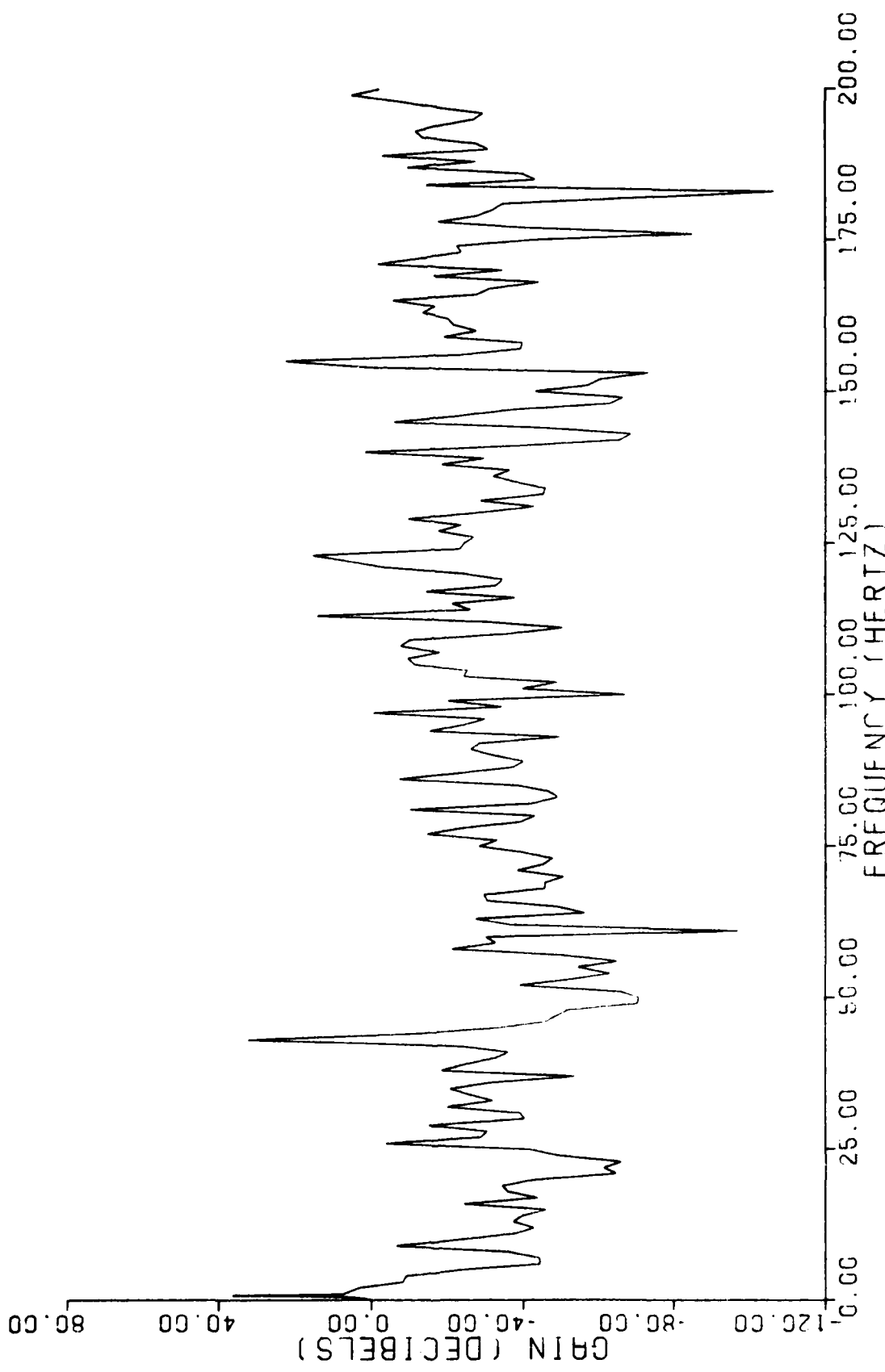


Fig. 43: ASTF Case 2

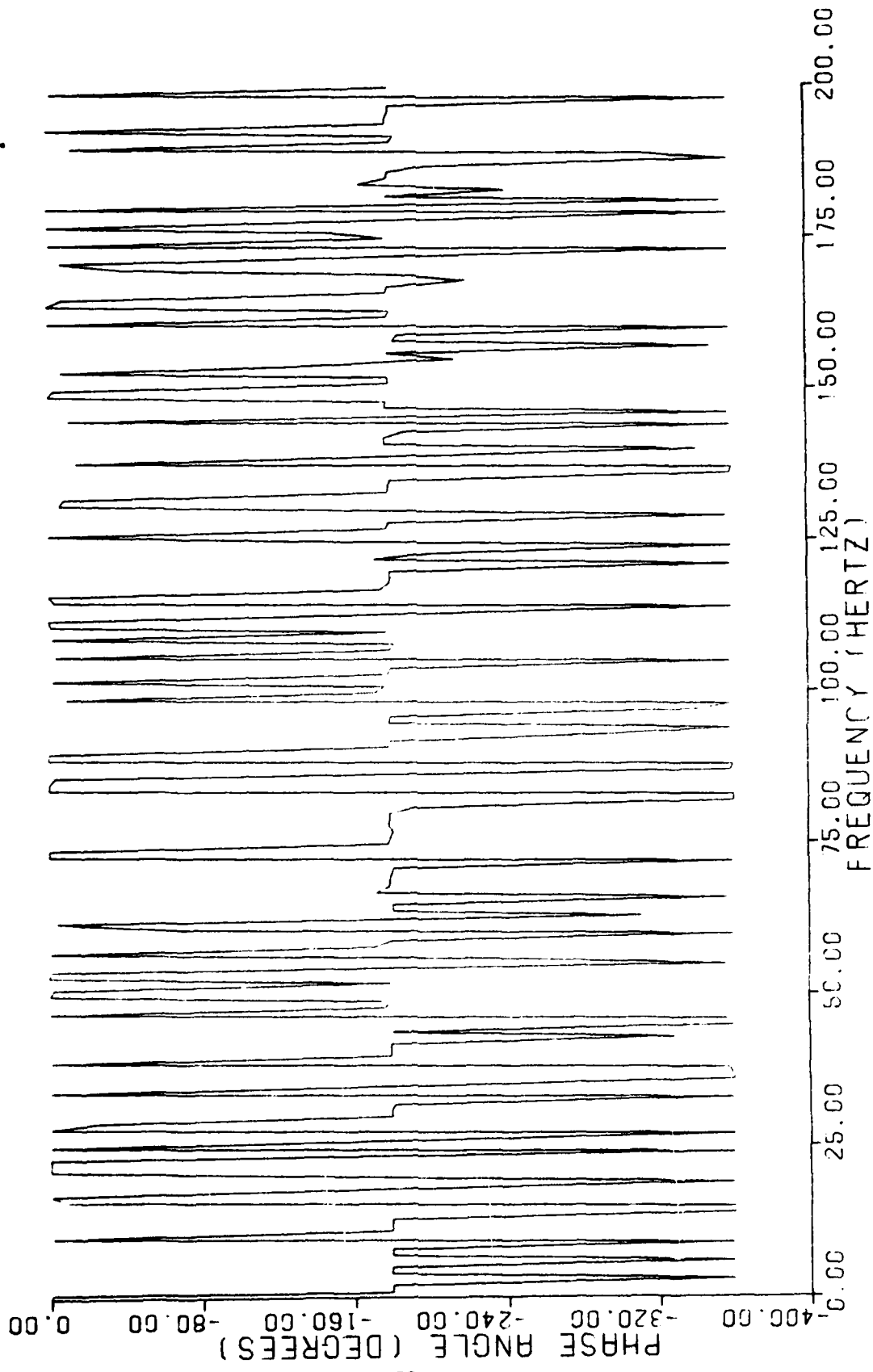


Fig. 44: ASTF Case 2

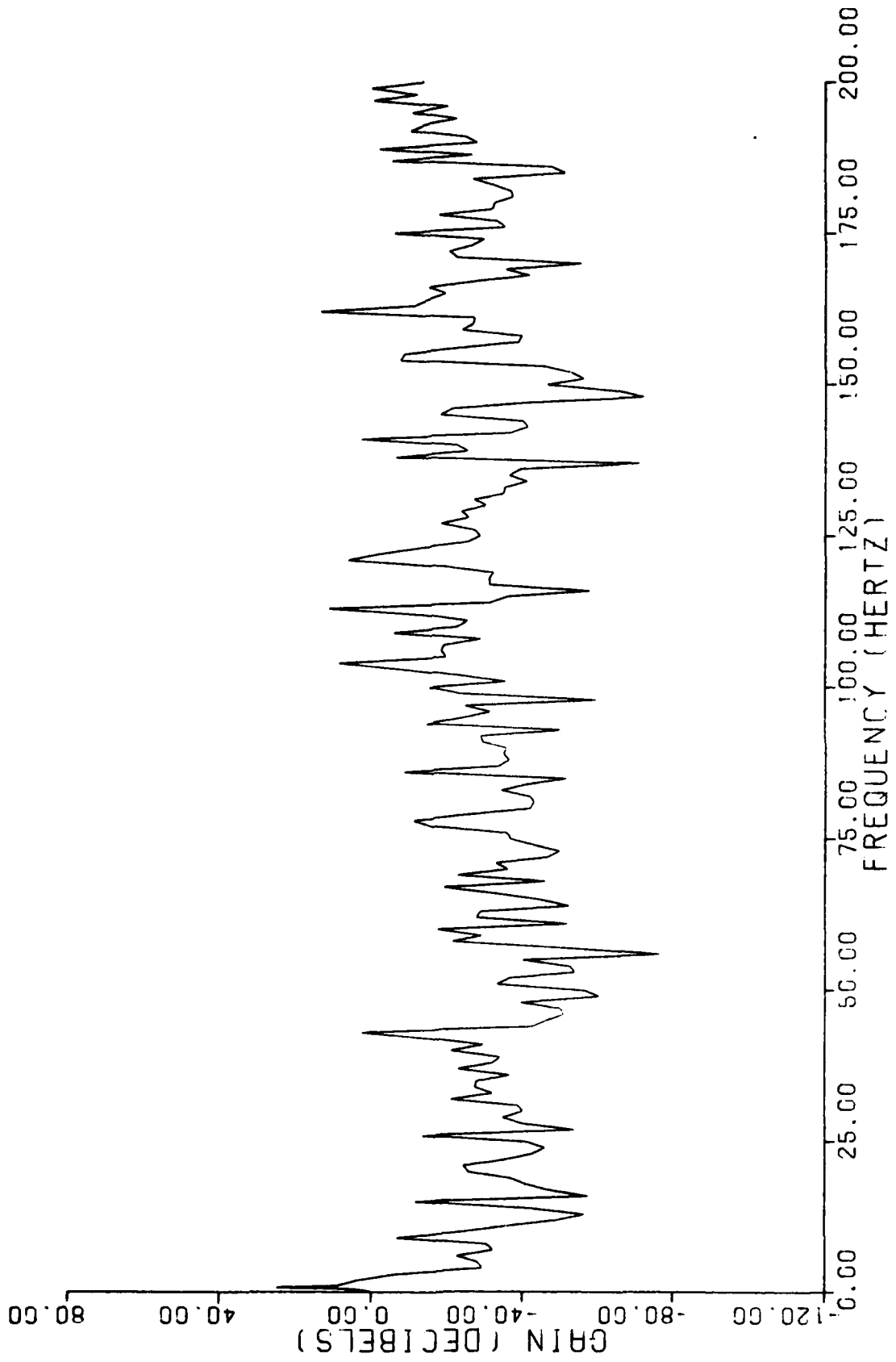


Fig. 45: ASTF Case 3

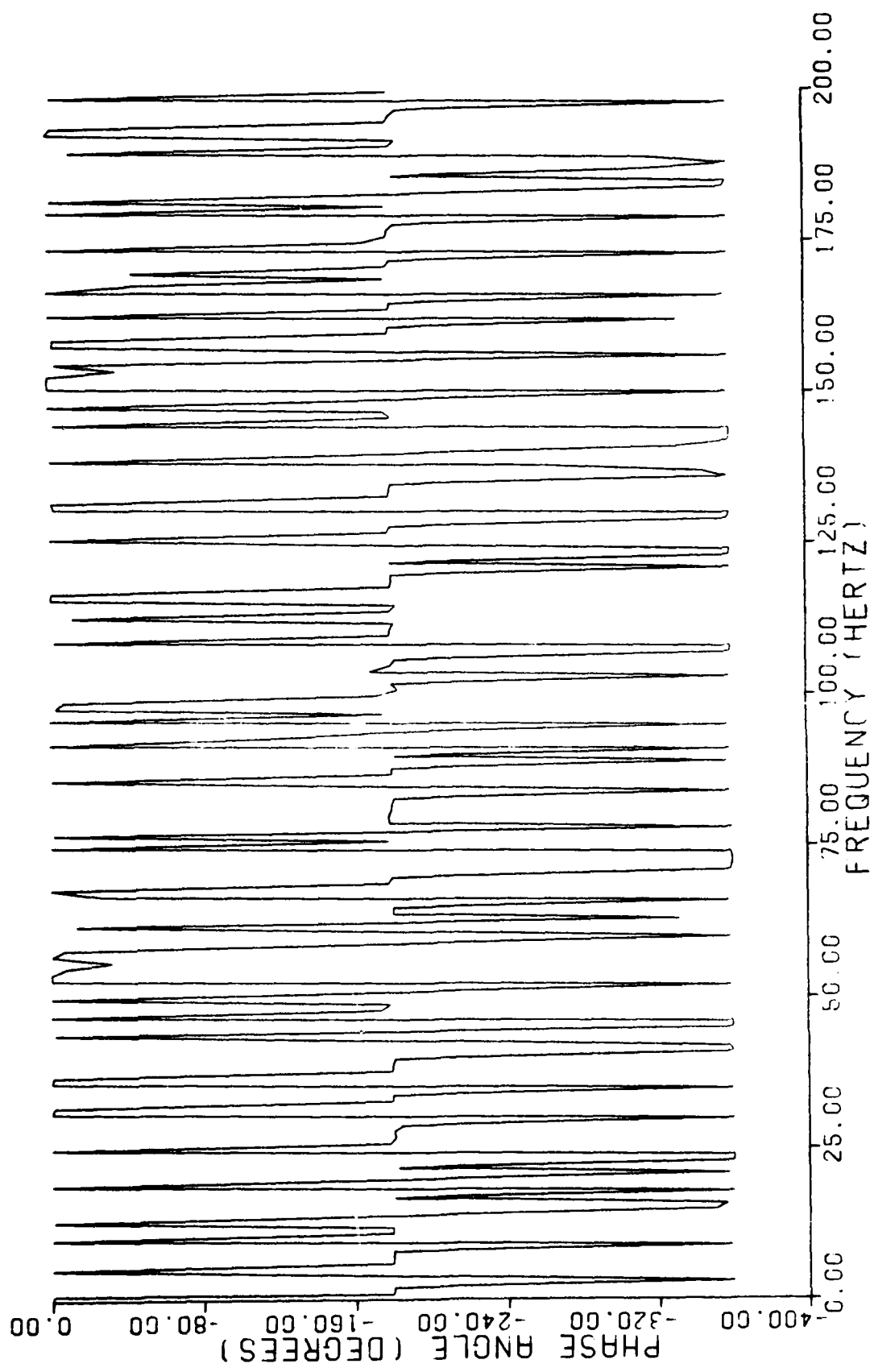


Fig. 46: ASTF Case 3

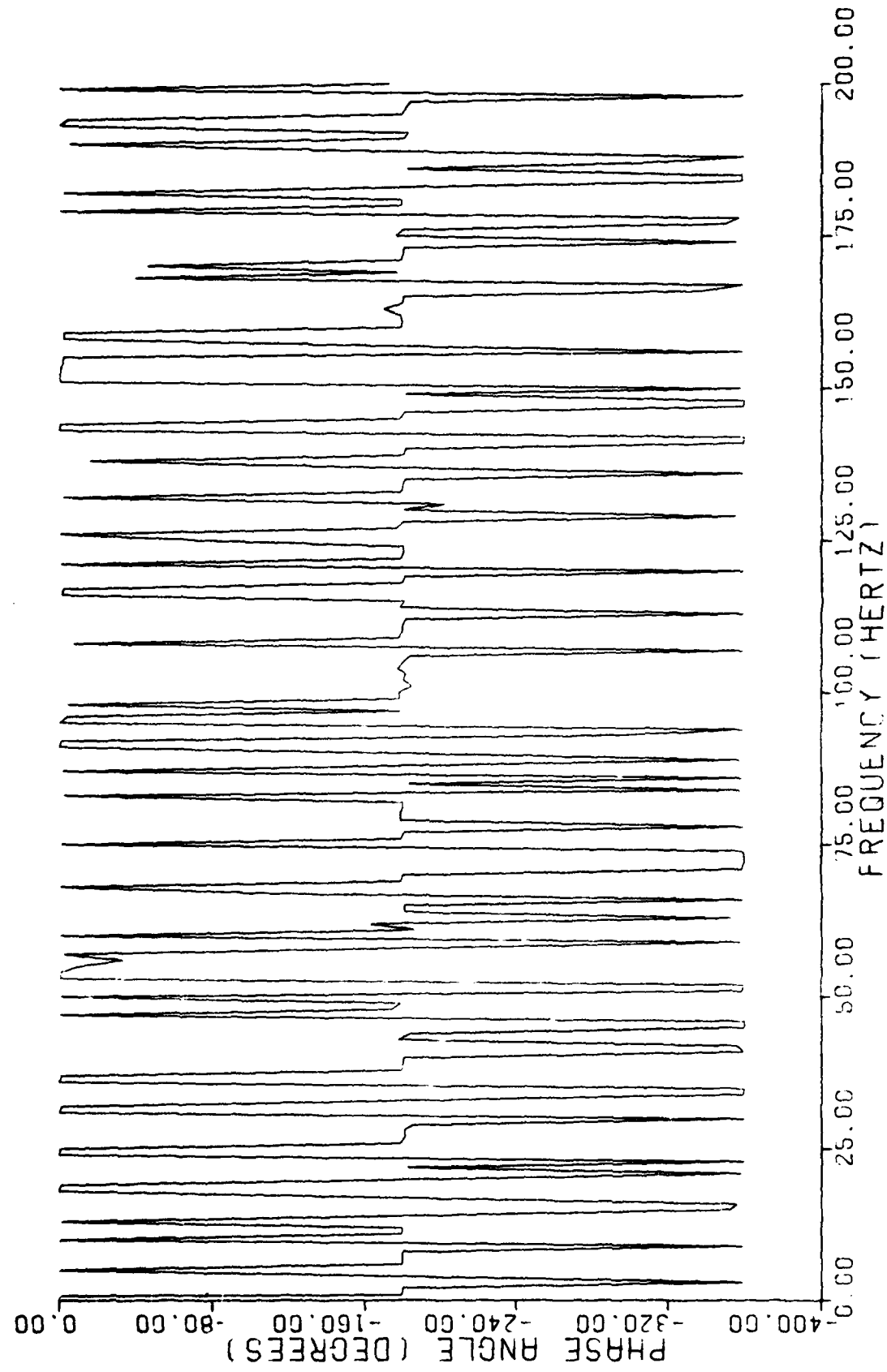


Fig. 48: ASTF Case 4

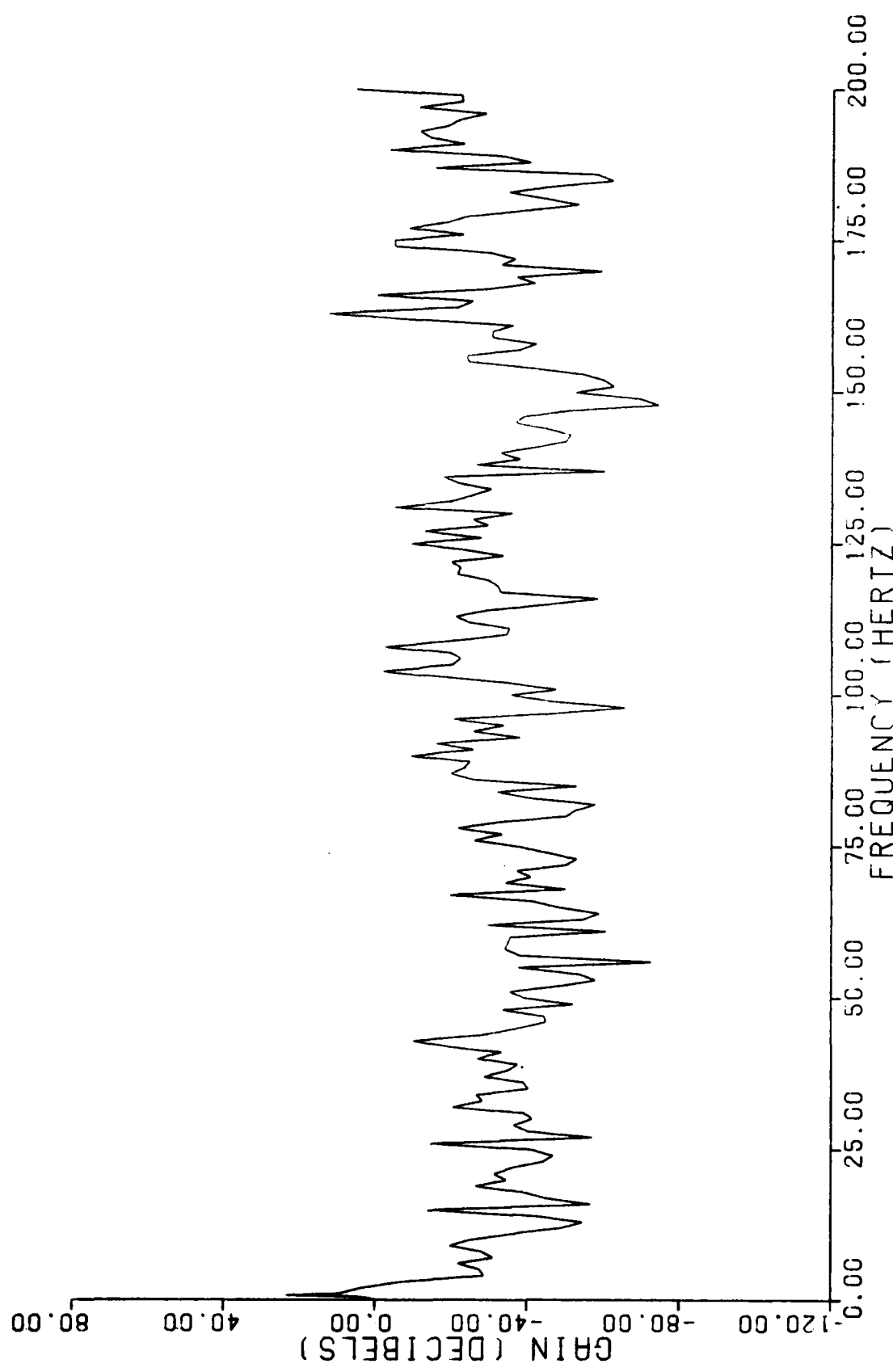


Fig. 49: ASTF Case 5

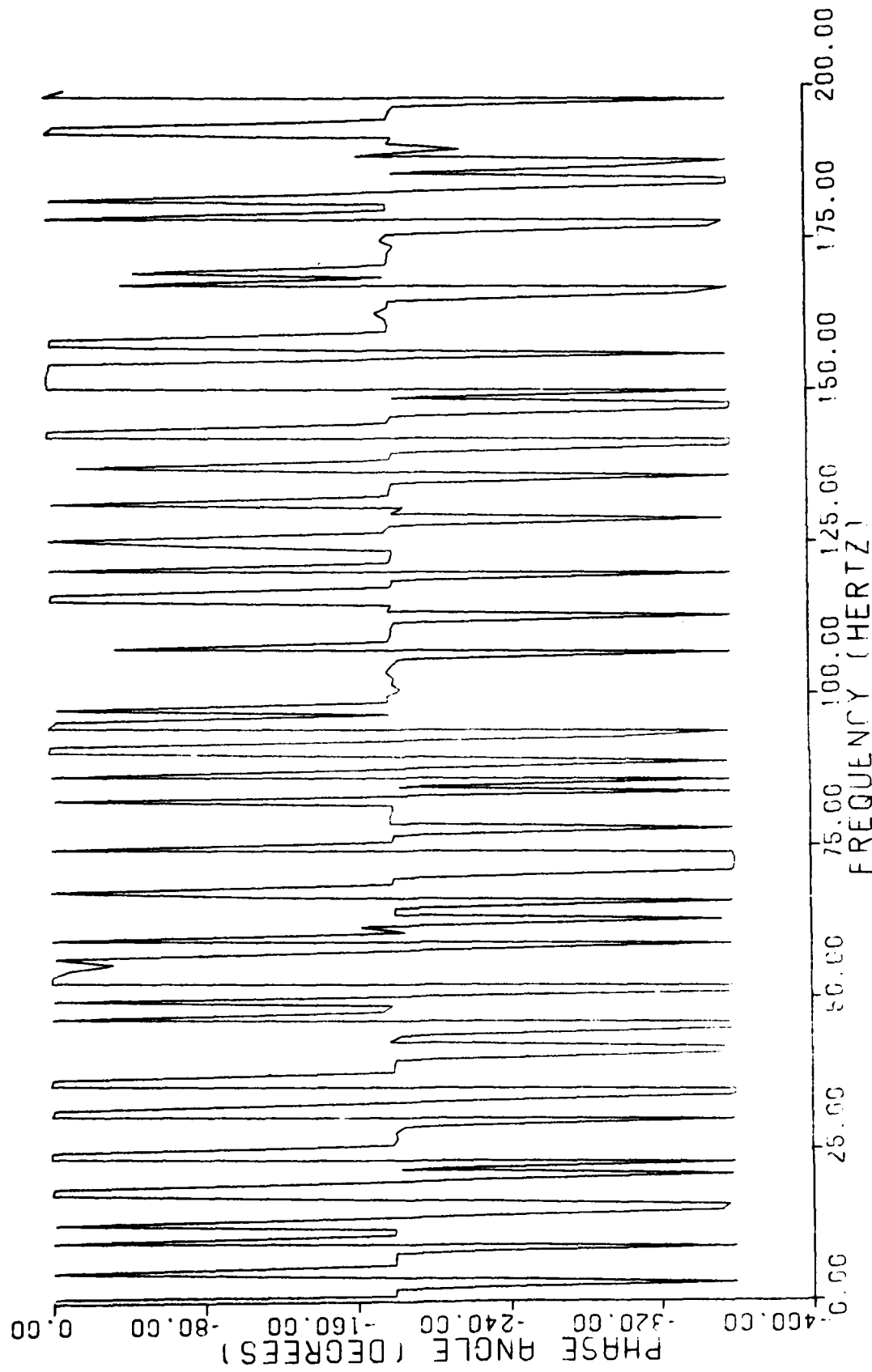


Fig. 50: ASTF Case 5

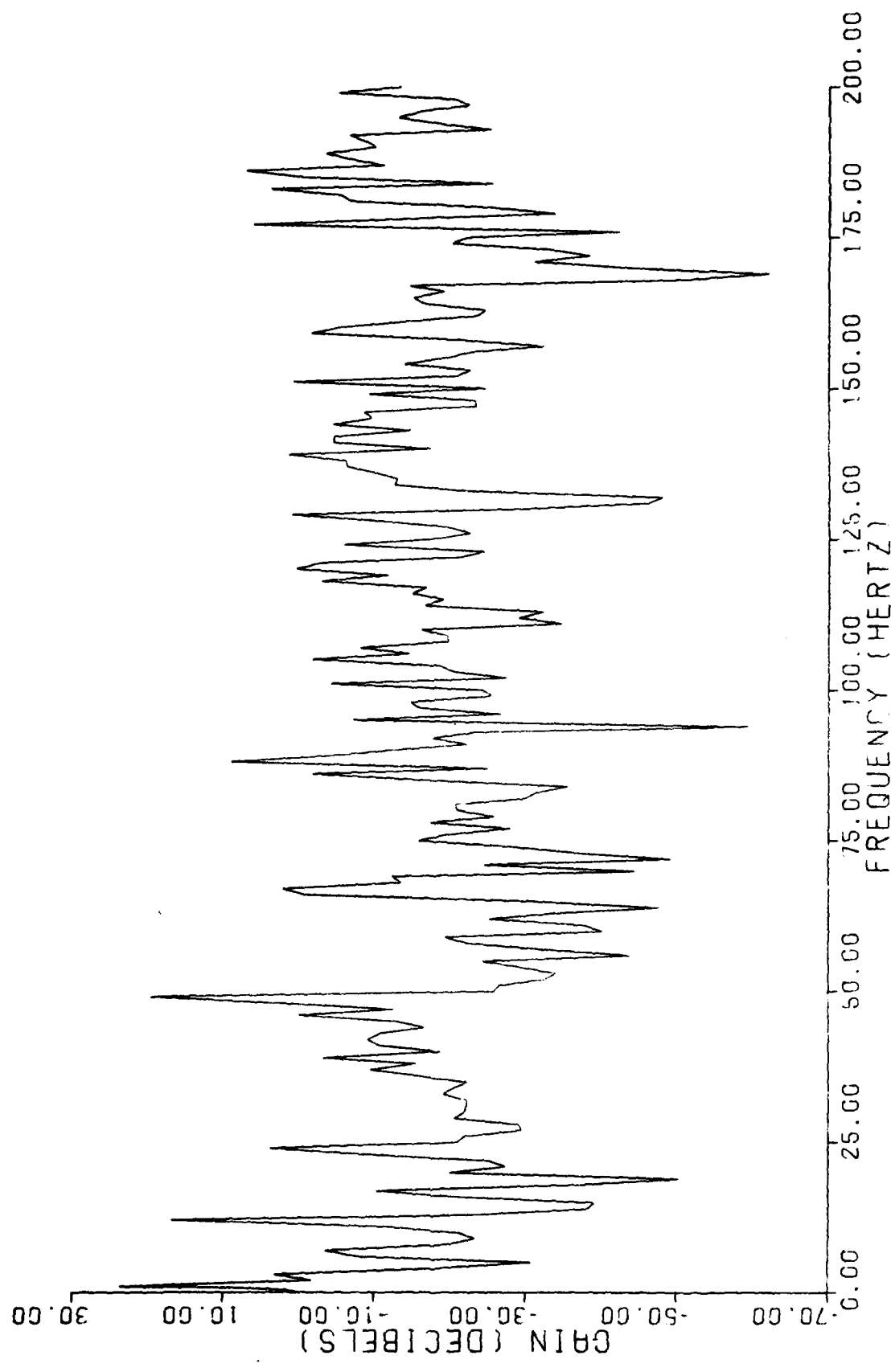


Fig. 51: ASTP Case 6

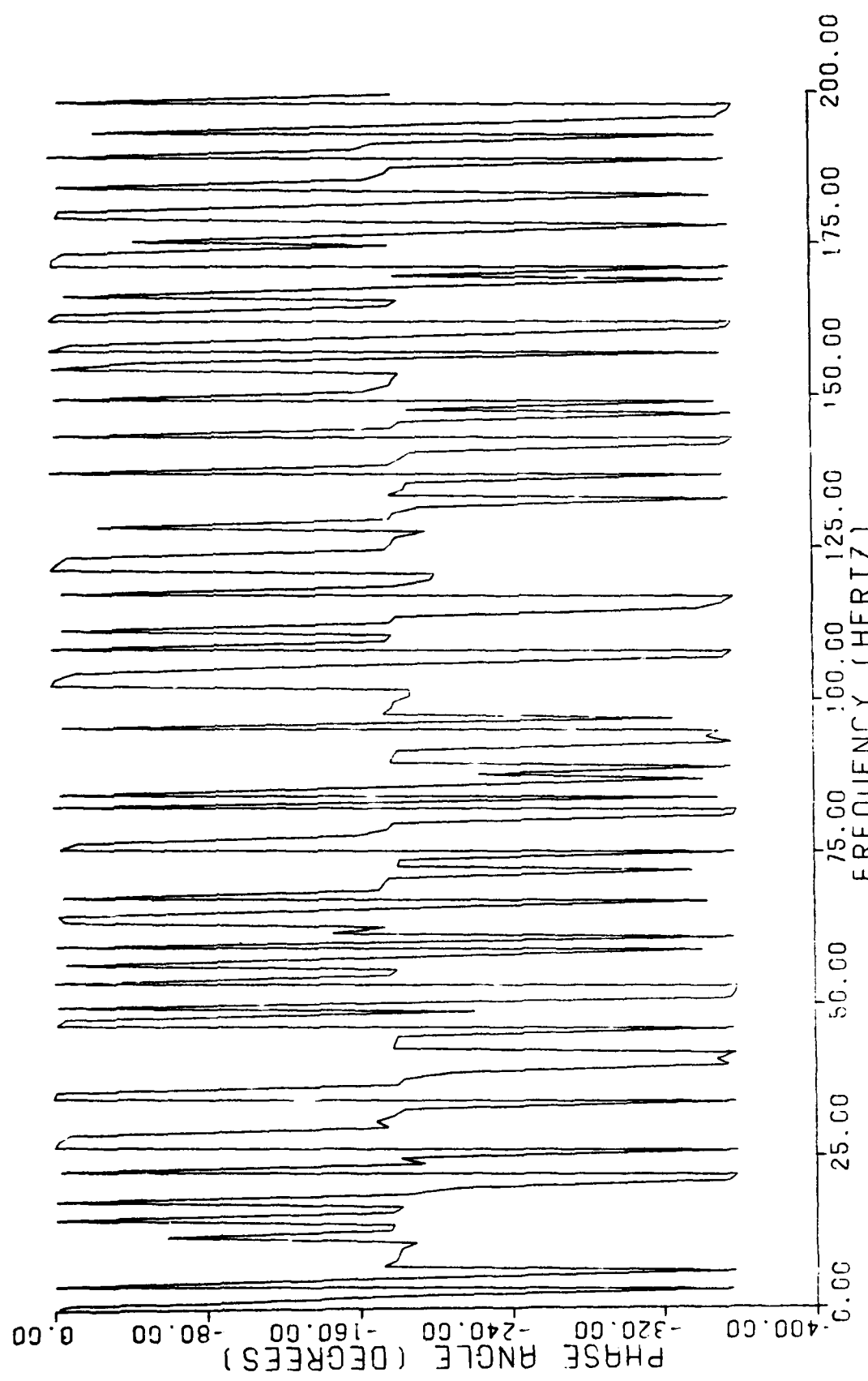


Fig. 52: ASTF Case 6

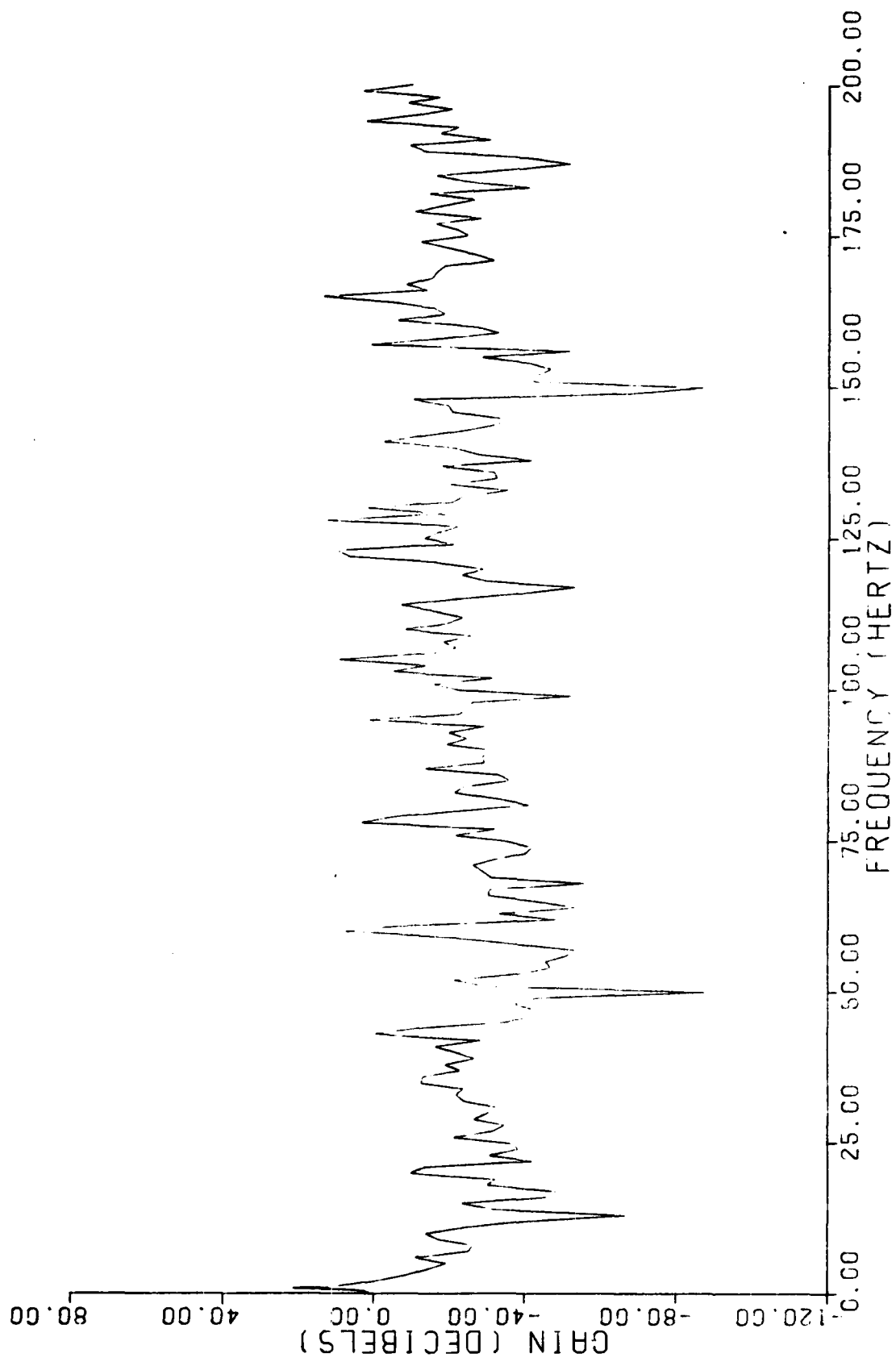


Fig. 53: ASTP Case 7

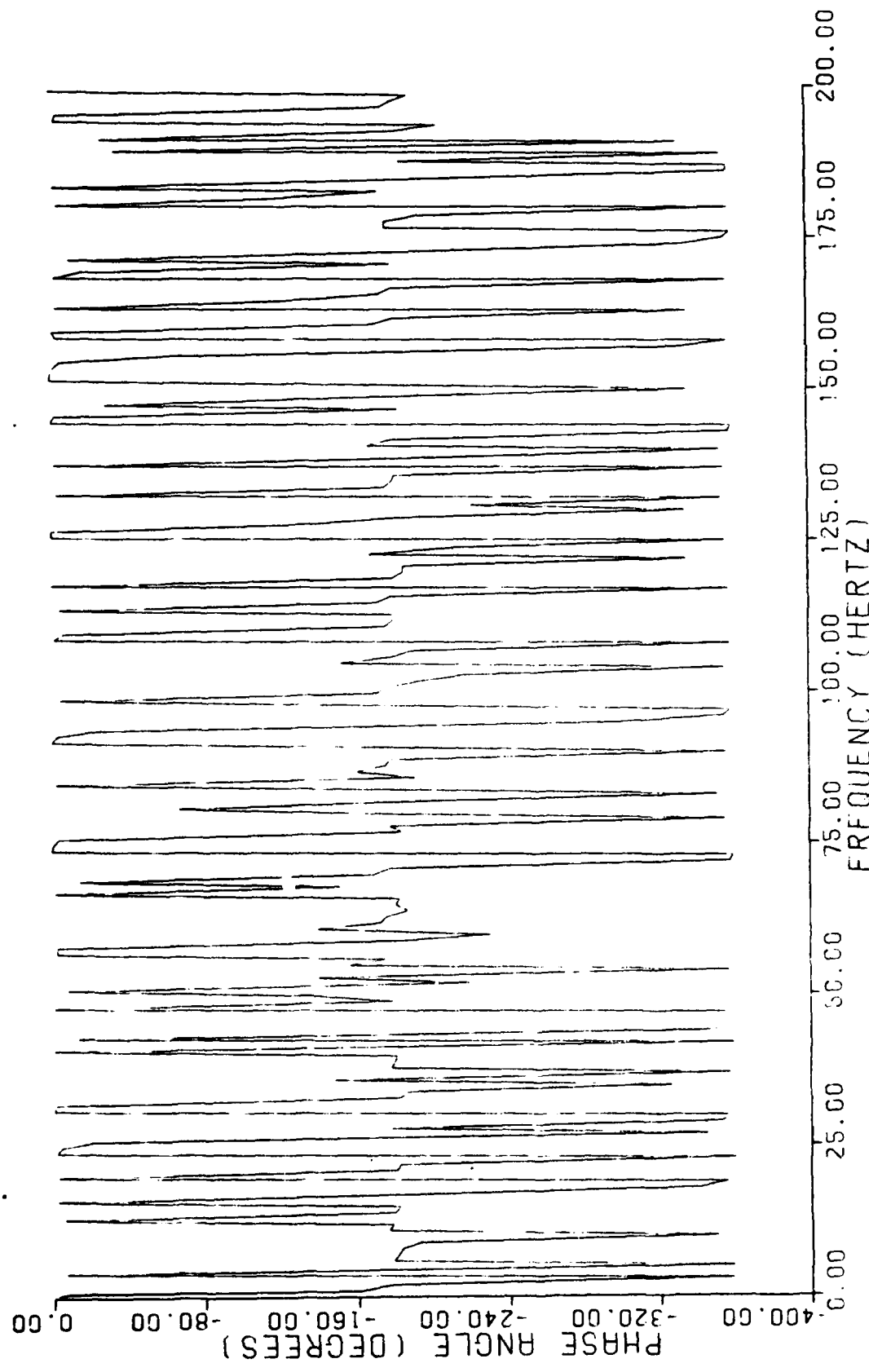


Fig. 54: ASTF Case 7

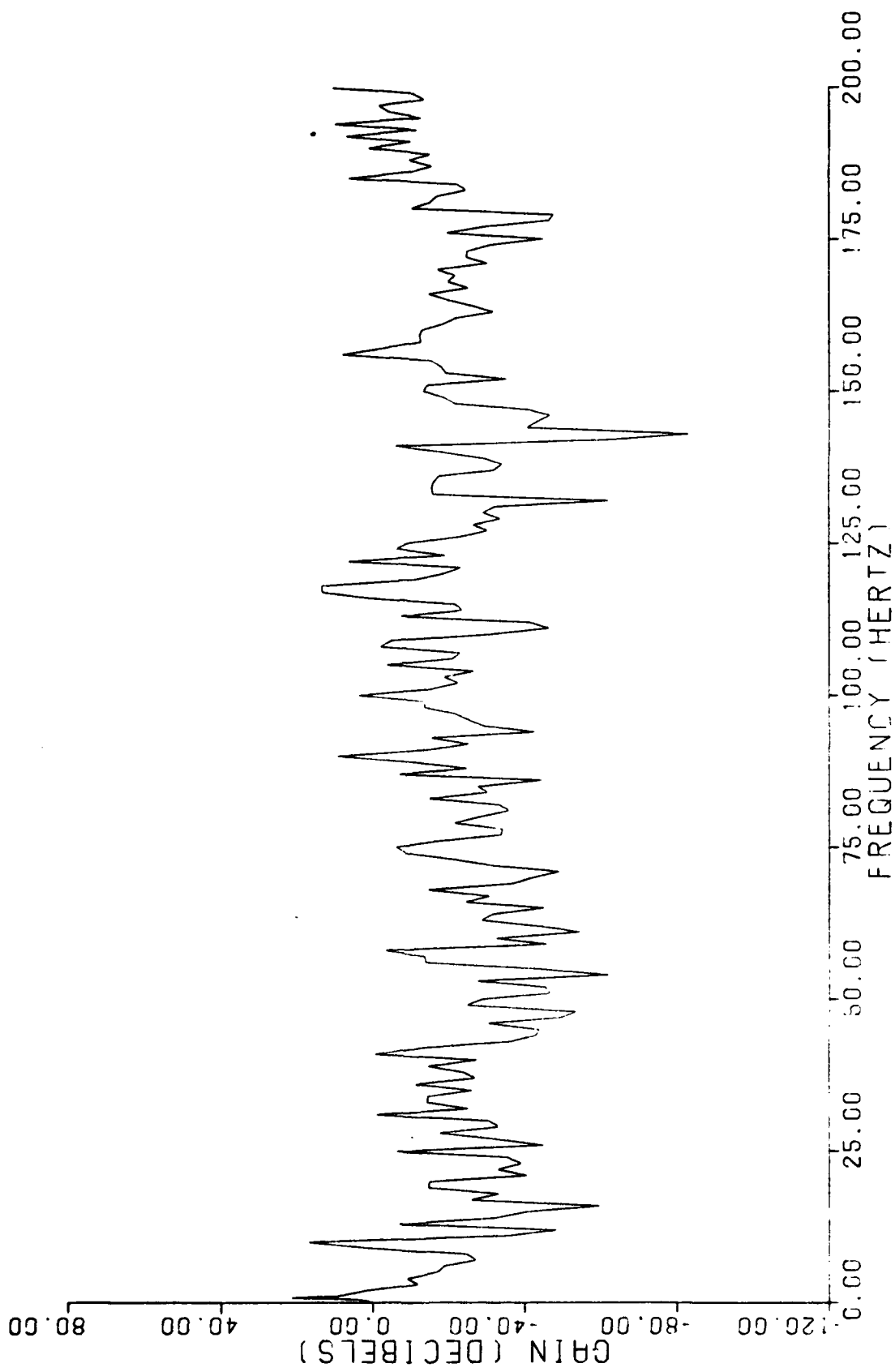


Fig. 55: ASTF Case 8

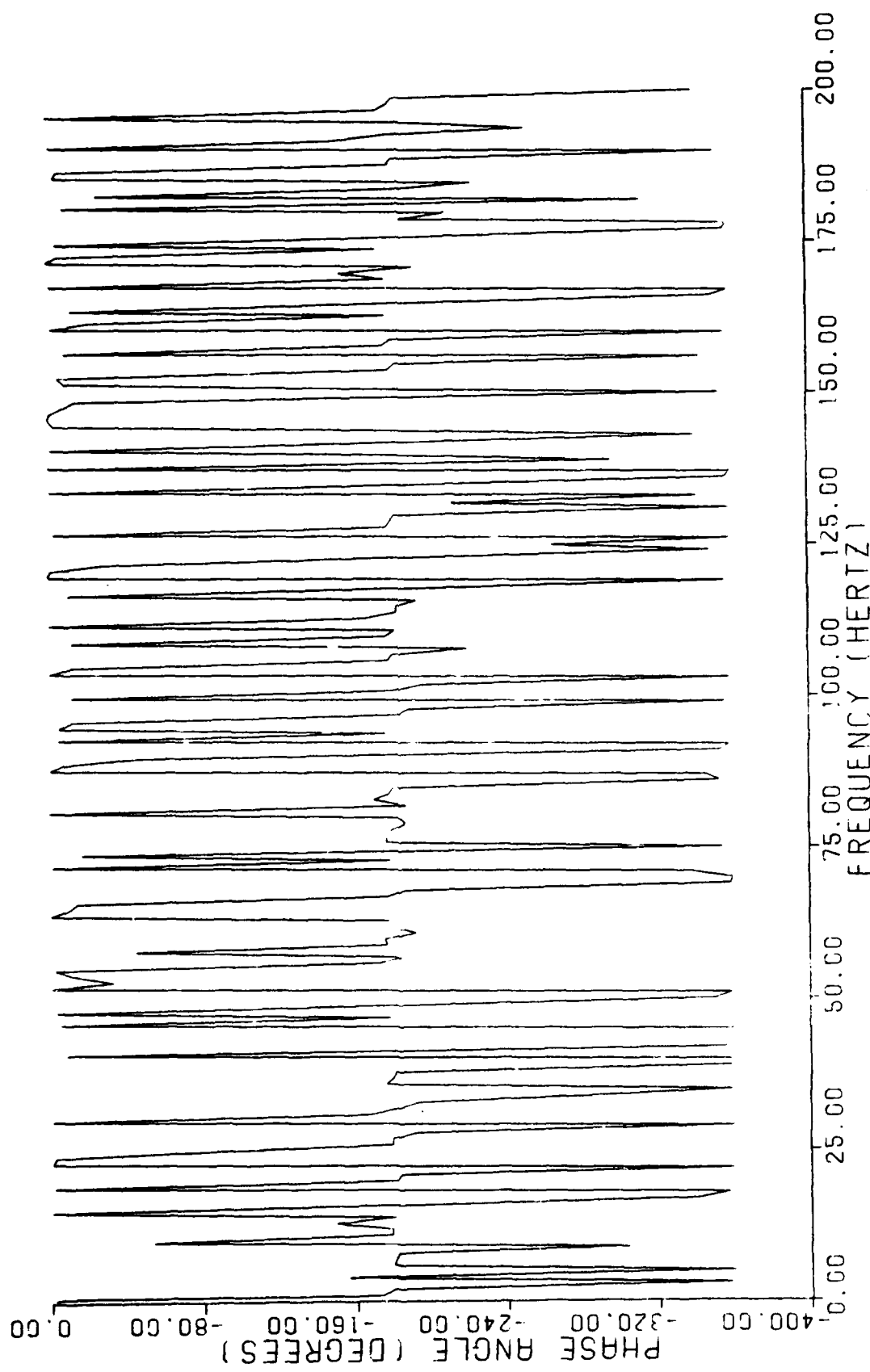


Fig. 56: ASTB Case 8

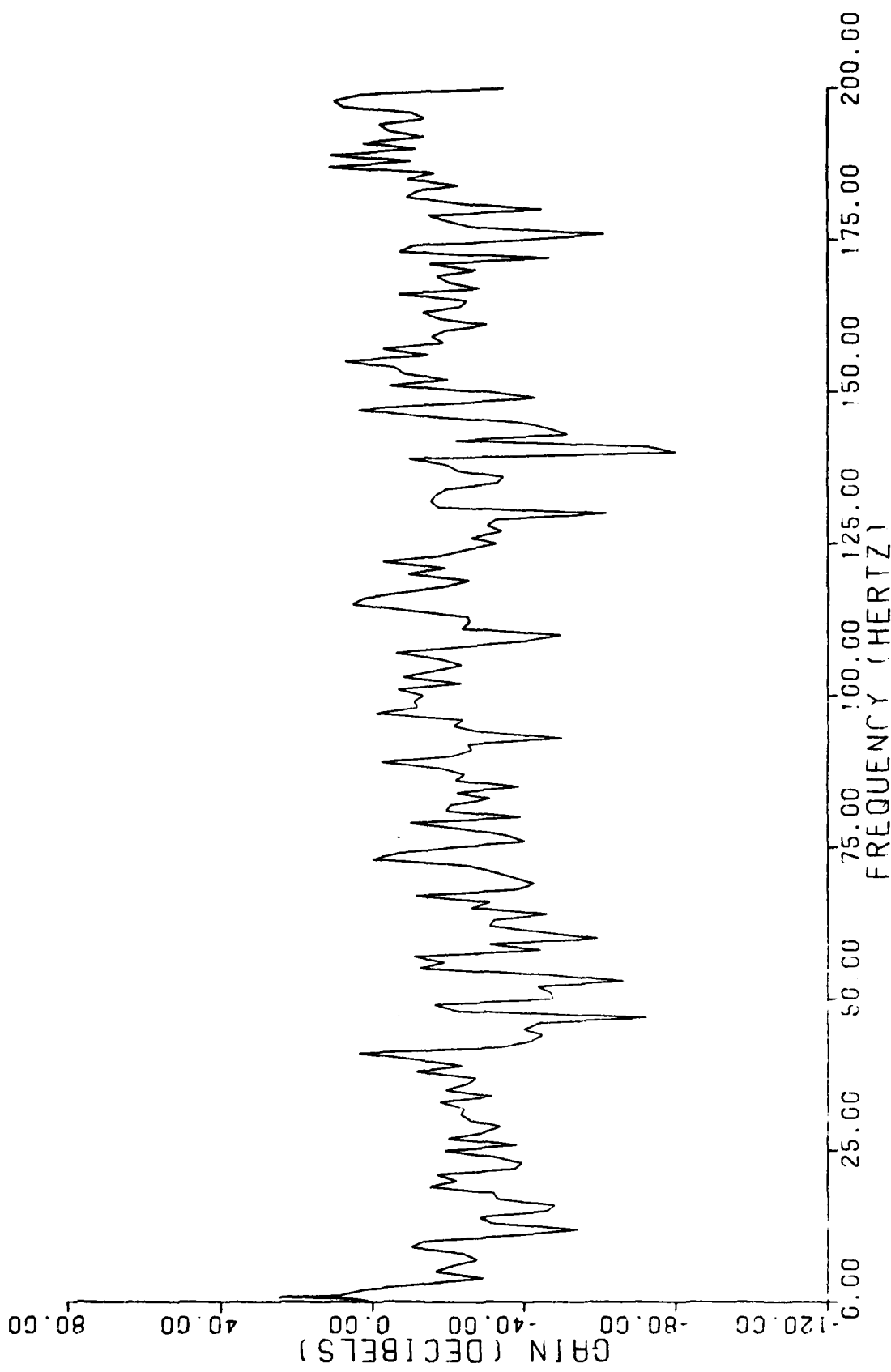


Fig. 57: ASTF Case 9

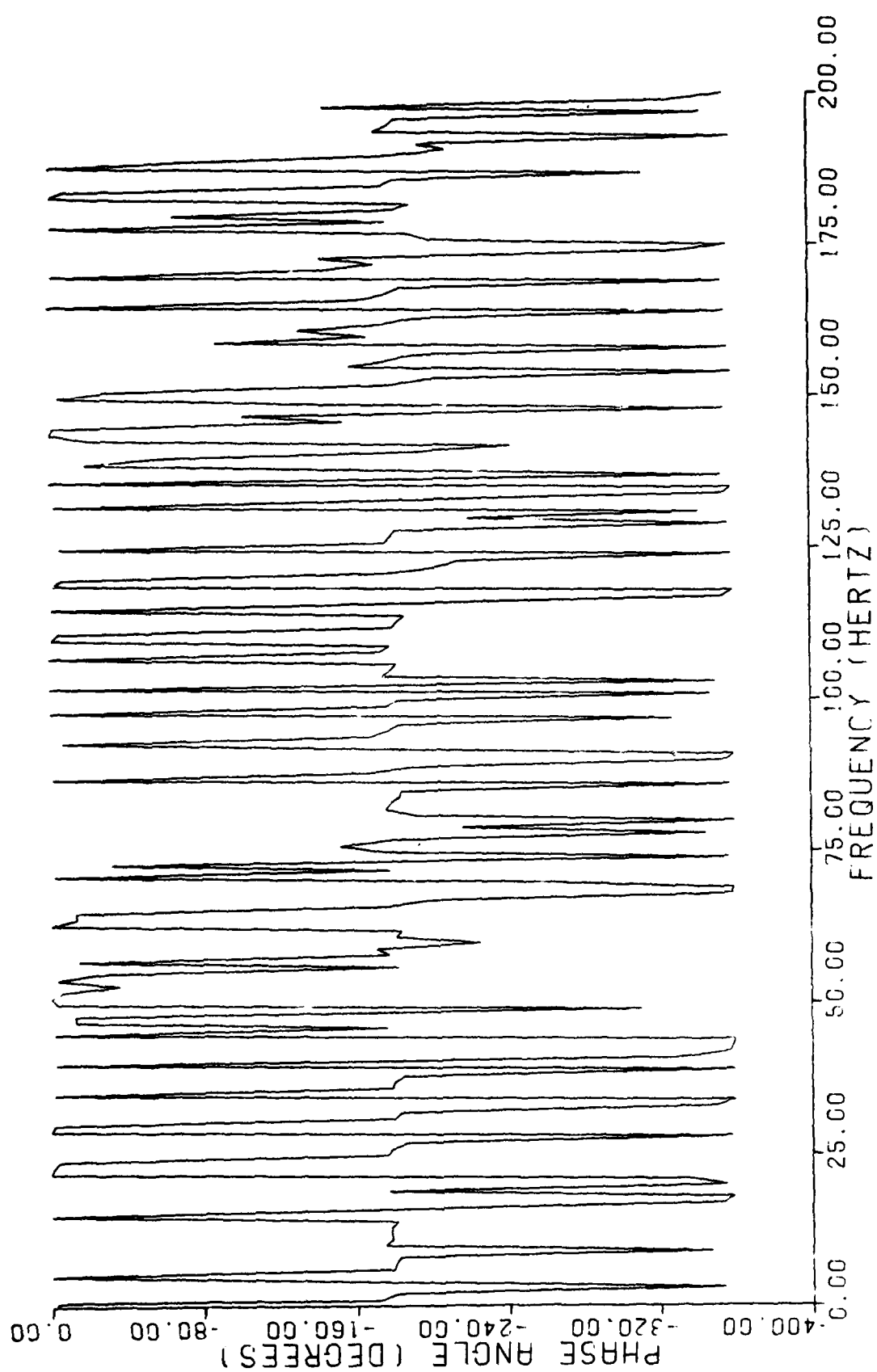


Fig. 58: ASTP Case 9

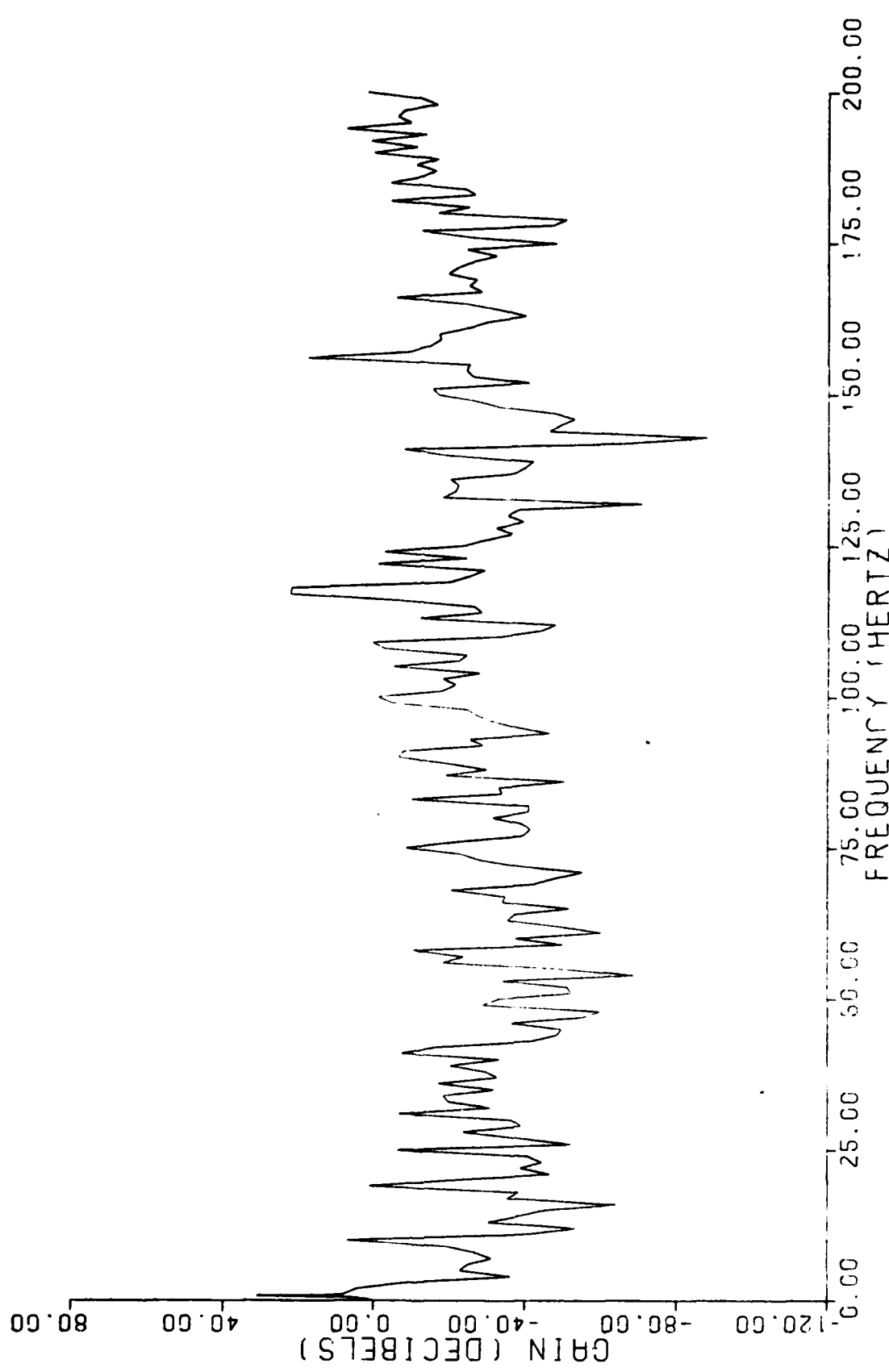


Fig. 59: ASTF Case 10

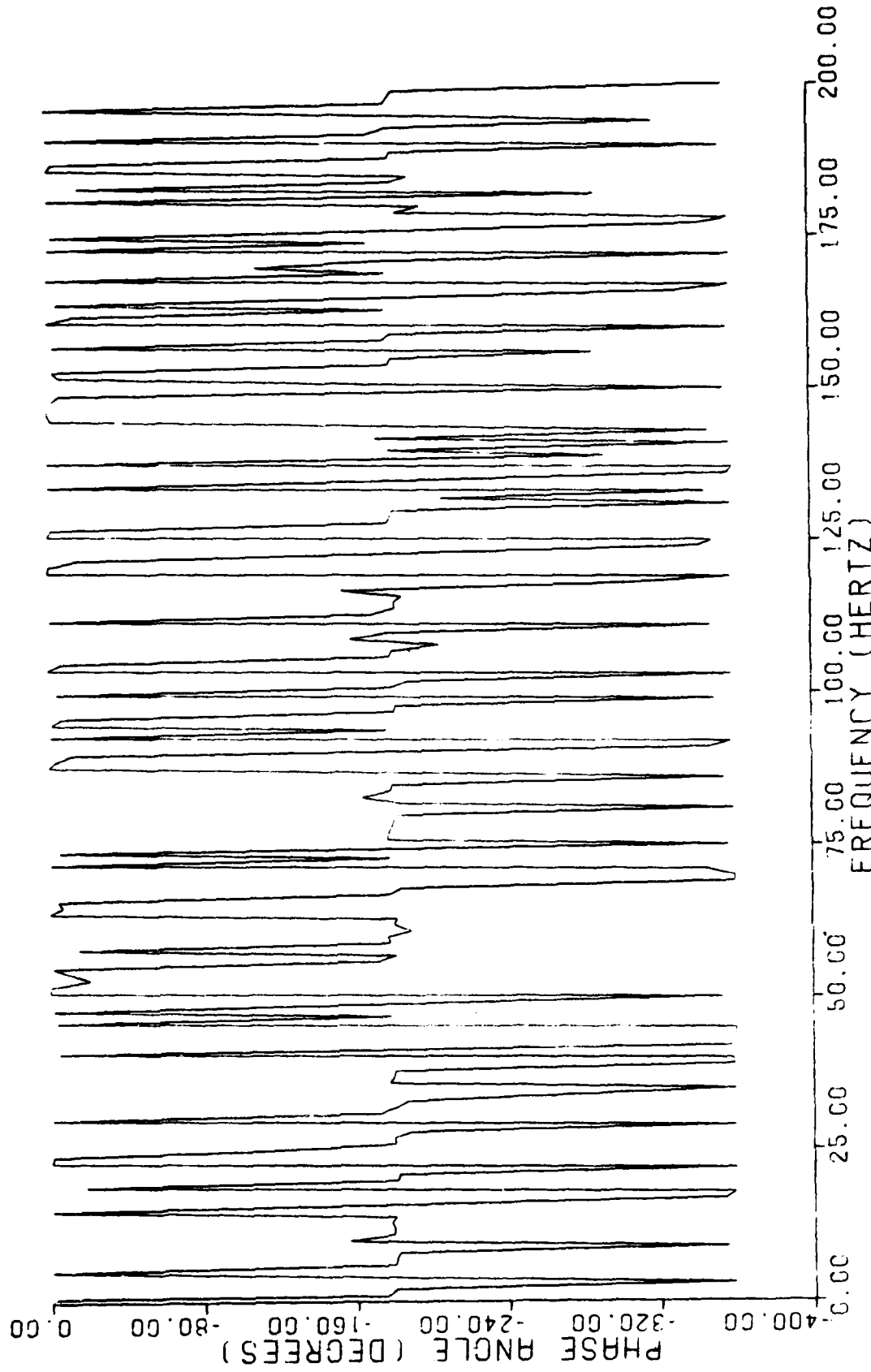


Fig. 60: ASTF Case 10

VIII. Conclusions

1. For blocked lines, the computer program gives results which agree quite well with experimental data obtained on the physical model. The gains agree within ± 5 dB over the range 20-200 Hz.

2. For open lines, using the steady-state resistance as the end impedance, the theory matches the general shape and gain values of the experimental data. With the exception of case 6, the data match within ± 5 dB.

3. In both blocked and open line cases, the theory predicts phase shift within $\pm 10\%$. Most values are much better, within $\pm 2\%$.

4. In general, mean flow in the lines reduced the gain somewhat less upstream of the venturi than at the end of the lines. This was due to the lower end impedance in the cases with flow.

5. The data verify that the theory can be used to accurately predict frequency response on large, complicated systems of lines. The theory is applicable to the ASTF ducting below 100 Hz because the wavelengths below that frequency are larger than the radius of the largest ASTF duct.

6. The cases run on ASTF show very little change in mean gain with frequency. The fundamental frequency occurs at 0.8-1.0 Hz, depending on temperature, at peak gain values of 21-36 dB. The bandwidth of this peak is very narrow (3 Hz). The complex ASTF system, with its multitude of flow paths and valves, is unlikely to see a sustained signal at a single frequency, but is more likely to see a variety of frequencies which will be constantly changing. Thus, due to the narrow bandwidth of the fundamental and the unlikeliness of a sustained signal at a single, constant frequency the ASTF air supply investigated is unlikely to experience a resonant condition.

7. FOD screens have very little effect on ASTF results, and the blocked cases show the general trends of the cases with flow.

IX. Recommendations

1. The new dual-beam oscilloscopes are excellent tools for measuring phase, but some means of filtering out the high frequency noise due to turbulence needs to be found; perhaps a low-pass filter could be used.
2. For experiments run on the ASTF scale model, a method of creating stronger signals must be developed. The pneumatic driver signals were too weak at most frequencies, and signals below 10 Hz were small and non-sinusoidal.
3. Automating the data acquisition process would allow much more data to be taken in the given time.
4. An investigation of the frequency range 0 to 20 Hz needs to be made to determine the accuracy of the theoretical results in this range.
5. More computer runs need to be made on the ASTF configuration to investigate the 0 to 10 Hz spectrum more closely, and to take into account more ASTF flow conditions. The lines in other parts of the ASTF system should be added to the program, accounting for a variety of open and closed valves, and including ducting up to the compressors and turboexpanders.

6. More experimental data are needed on the output
of the butterfly valves to determine if they generate
significant disturbances.

Bibliography

1. Brown, F. T. "The Transient Response of Fluid Lines," Journal of Basic Engineering, Trans. ASME, 84: 547-533 (December 1962).
2. Franke, M. E., J. T. Karam, Jr., and F. C. Lymburner. "Experimental Frequency Response of Fluidic Transmission Lines." Paper presented at the Fourth Cranfield Fluidics Conference: Warwick University, Coventry, England (March 1970).
3. Iberall, A.S. "Attenuation of Oscillatory Pressures in Instrument Lines," Journal of Research, 45: 85-108 (1950).
4. Karam, J. T., Jr. and M. E. Franke. "The Frequency Response of Pneumatic Lines," Journal of Basic Engineering, Trans. ASME, 89: 371-378 (June 1967).
5. Kinsler, Lawrence E., Austin R. Frey, Alan B. Coppens, and James V. Sanders. Fundamentals of Acoustics (Third Edition). New York: John Wiley & Sons, Inc., 1982.
6. Krishnaiyer, R. and T. J. Lechner, Jr. "An Experimental Evaluation of Fluidic Transmission Line Theory," Advances in Fluidics. Edited by F. T. Brown, et al. New York: American Society of Mechanical Engineers, 1967.
7. Malanowski, Alex J. The Dynamic Response of Fluidic Networks. MS Thesis. School of Engineering, Air Force Institute of Technology (AU), Wright-Patterson AFB OH, March 1971.
8. Martin, P. S. Temperature Effects on the Dynamic Characteristics of Blocked Cascaded Pneumatic Transmission Lines. MS Thesis. School of Engineering, Air Force Institute of Technology (AU), Wright-Patterson AFB OH, March 1970.
9. Miller, R. N. Dynamic Characteristics of Blocked, Concentric, Cascaded Pneumatic Transmission Lines. MS Thesis. School of Engineering, Air Force Institute of Technology (AU), Wright-Patterson AFB OH, March 1968.

10. Nichols, N. B. "The Linear Properties of Pneumatic Transmission Lines," Transactions of the Instrument Society of America, 1: 5-14 (January 1962).
11. Wilda, R. W. Pneumatic Line Dynamics. MS Thesis. School of Engineering, Air Force Institute of Technology, Wright-Patterson AFB OH, May 1967.

Appendix A
Computer Program

Modifications to Program as Used by Malanowski

The program of Malanowski was modified to accept more series and parallel lines corresponding to the schematics in Figs. 61-66. This was achieved by renumbering the lines and calculating input impedances for each line looking downstream, using the standard code strings and changing the indexing numbers. The gain and phase across each line in the flow path were then calculated, again using the standard code strings and changing the indexing numbers. The gains and phases from P_{end} to P_{input} and P_{vent} to P_{input} were then calculated by multiplying individual line gains and adding individual line phase angles. The phase angles were adjusted to fit the range 0 to -360 deg by adding or subtracting multiples of 360 deg.

For blocked lines, the mean line pressure was used for the pressure in each line. For open lines the line pressure was included in the data field with line diameters and lengths. The calcomp plotter routine reading sequence was changed. Plots of gain and phase at the end of the line and gain and phase upstream of the venturi are generated.

Computer Program Data Reading Sequence

Program

1. Read ICAS: Reads the control variable which decides whether or not plotter routine is to be used.
2. Read PL: Read the mean line pressure for use in blocked line cases only.
3. Read TF, PG, AMV, RE, GAM, SIG:
TF is the line temperature ($^{\circ}$ F).
PG is the atmosphere pressure (psig).
AMU is the viscosity/in ($\frac{in^2}{sec - ^{\circ}R}$).
GAM is the ratio of specific heats.
SIG is the square root of the Prandtl number.
4. Read N, NLINE:
N is the number of lines.
NLINE is the end configuration (open or blocked).
5. Read DI(I), AD(I): Used only in blocked line cases where:
DI(I) is the line diameter.
AD(I) is the line length.
6. Read DI(I), AD(I), P(I): Used only in open line cases, where:
DI(I) and AD(I) are the same as above.
P(I) is the line pressure in each line.

Calcomp Plotter Routine

7. Read CASE(1): Reads the case number (experiment identification number).

8. Read NPTS, LSMB1, LSMB3:

NPTS is the number of experimental data points to be input.

LSMB1 is the plotter symbol to be used for the results upstream of the venturi.

LSMB3 is the plotter symbol to be used for the results at the end of the line.

9. Read FREQ, PS, PR3, PR1, PHS3, PHS1, FACT, PHR3, PHR1:

FREQ is the experimental frequency.

PS is the RMS voltage output of the input signal transducer.

PR3 is the RMS voltage output of the transducer at the end of the line.

PR1 is the RMS voltage output of the transducer upstream of the venturi.

PHS3 is the "DELAY TIME MULT (DTM) dial reading where the input signal crosses the zero axis on the oscilloscope measuring phase at the end of the line.

PHS1 is the DTM dial reading where the input signal crosses the zero axis on the oscilloscope measuring phase upstream of the venturi.

FACT is the "TIME/DIV or DLYTIME" dial reading in milliseconds/centimeter on both oscilloscopes (both scopes must be on the same setting).

PHR3 is the DTM dial reading where the signal at the end of the line crosses the zero axis on the appropriate scope.

PHR1 is the DTM dial reading where the signal upstream of the venturi crosses the zero axis on the appropriate scope.

```

PROGRAM TOS(INPUT,OLPUT,PLST,TAPES=INUT,TAPE9=PLOT,TAPE6=CUTPUT,
+TAPE7)

C TRANSMISSION LINE STUDY/Z-IN METHOD WITH BRANCH SHORT OUTPUT
DIMENSION DRT1(220),DBT3(221),DI(221),AD(220),AP(220),CV(220),
10MT(221),CNA(221),GMA(220),AMU(221),FN(220),RN(220),GN(221),
2ALN(221),CM(220),AN(220),BTM(221),AMC(220),AZRN(220),BZRN(220),
3AZIN(220),BZI(220),DC(220),DG(220),CD(220),P(220),PHO(220),
+ANU(221),CA(220),BTCA(220),CME(220),RTP(220),GP(220),BETA(220),
5AZOT(220),BZOT(220),REY(220),Q(220),BET(220),OMGP1(100)
DIMENSION DB1(220),DB3(220),CM6X(220),PHASE1(220),PHASE3(220),
+PH1(220),FH3(220),CASE(220),CHF3(100)
DATA F/3.141592E/
DATA TPI/6.2831-53/

*****+
C THIS PROGRAM IS FOR 13 INPUTS ONLY
CALL PLCTS(1,C,F)
*****+
*
1 READ(7,*)ECAS
11 READ(7,*)PL
READ(7,*)TF,P6,AMU,FE,GAM,SIG
READ(7,*)N,ALINE
WRITE(6,200)PL,TF,PG
2:5 FORMAT(11HCONDITIONS:,EX,BHL3 INPLT,5X,PHASE= ,F5.3,2X,
+HT= ,F4.1,2X,EHFBAR= ,F5.2)
WRITE(6,200)
2.6 FORMAT(11HBLOCKED END)
C *****
C AL IS THE LINE LENGTH
C DI IS THE LINE DIAMETER
C A ONE FOR ALINE INDICATES THE LINE IS OPEN AND ANY OTHER
C NUMBER INDICATES A BLOCKED END.
C *****
C
DC 33 I=1,N
IF (ALINE.EQ.1) GO TO 21
P(I)=FL
READ(7,*)DI(I),AD(I)
GO TO 393
21 READ(7,*)CI(I),AD(I),P(I)
398 CONTINUE
IND=1
ME=
DC 23 I=1,N
PR=P(I)*FG
TBR=TF*461.
RH0(I)=PR/(PE*TBR)
AMU(I)=AMU/PHC(I)
CAG(I)=GRT*(PR*GAM/PHC(I))
AR(I)=DI(I)*CI(I)/4.
CV(I)=(1.-P(I)*AMU(I))/AR(I)
DMT(I)=CV(I)/(SIG*SIG)
CNA(I)=(d.-P(I)*AMU)/(AR(I)*AR(I))
Q(I)=.665*DI(I)*DI(I)*SQR(P(I)/RH0(I))
23 CONTINUE
Q(11)=Q(70)*RH0(70)/RH0(11)
Q(17)=Q(11)*RH0(11)/RH0(17)
DC 24 I=13,50
Q(I)=Q(I-1)*RH0(I-1)/RH0(I)
24 CONTINUE
Q(52)=Q(51)*RH0(50)/RH0(52)
DC 25 I=53,64
Q(I)=Q(I-1)*RH0(I-1)/RH0(I)

```

```

25    CONTINUE
      GM1=.5*(GAM-1.)
      DO 26 I=1,N
      REY(I)=(4.*PHC(I)+Q(I))/(PI+DI(I)*AMU)
      PBR=PL(I)*FG
      TEMF=GM1/(GAM+FBF)
      GMK(I)=TEMP*AP(I)
      AGM(I)=AR(I)/(GAM+PBR)
      GTCA(I)=2.2E+CA(I)
      FA(I)=GTCA(I)/AC(I)
      NST=9
      DW=.1
      Y=1.
      DO 40 J=1,NST
      M=M+1
      Y=Y+DW
      W=TPI*Y
      DO 27 I=1,N
      APG=.5-SQRT(W/CV(I))
      RN(I)=CNA(I)*(3.75+APG*(.375/(4.+ARG)))
      DO 28 I=1,N
      DC(I)=-.25+SQRT(W/CMT(I))+.125*SQRT(CMT(I)/W)
      DG(I)=SQRT(W/CMT(I))-1.25*SQRT(CMT(I)/W)
      DD(I)=DC(I)*DC(I)+DG(I)*CG(I)
      GL(I)=W*(GAM-1.)*AGM(I)*CG(I)/DD(I)
      DO 29 I=1,N
      APG=.5-SQRT(CV(I)/W)
      ALN(I)=RH3(I)*(1.+APG*(15.+CV(I)/(W=64.)))/AR(I)
      DO 30 I=1,N
      CV(I)=AGM(I)*(1.+((GAM-1.)*DC(I)/DD(I)))
      TEMP=-W*W
      C CALCULATES ALPHA AND BETA (PROPAGATION OPERATOR)
      DO 31 I=1,N
      TEM1=RN(I)*GN(I)+TEMP*ALN(I)*CN(I)
      TEM2=W*(RN(I)*CN(I)+GN(I)*ALN(I))
      CALL RTCMF(ARG1,ARG2,TEM1,TEM2)
      AN(I)=ARG1
      BTM(I)=ARG2
      31  ANC(I)=TPI/BTM(I)
      C CALCULATES CHARACTERISTIC IMPEDANCE
      DO 32 I=1,N
      TEM1=W*ALN(I)
      TEM2=W*CN(I)
      TEM3=RN(I)
      TEM4=GN(I)
      CALL CPDMF(ARG1,ARG2,TEM3,TEM4,TEM2)
      CALL FCMF(BZPNI,BZPAI,ARE1,ARE2)
      AZPN(I)=AZPAI
      32  BZPN(I)=BZPAI
      C CALCULATES Z END/END LINE CONDITION USED HERE
      IF(MLINE.EQ.1) GO TO 100
      AZIN(7)=100000
      GO TO 200
      1000  AZIN(7)=F(7)/Q(7)
      2001  BZIN(7)=0
      DO 3001 I=65,69
      AZIN(I)=1J*100
      3000  BZIN(I)=0
      C CALCULATES Z IN 1 THRU 5
      DO 33 I=1,5
      TEMP=AN(I)*AD(I)
      IF(TEMP.GT.+8.) GO TO 8
      APG1=COSH(TEMP)
      APG2=SINH(TEMP)
      TEM=-HTN(I)*AC(I)
      TEMP=CIS(TEM)

```

```

    TEM3=ARG2+TEMP
    TEMP=SIN(TEM5)
    TEM2=ARG2+TEMP
    TEM4=ARG1+TEMP
    CALL CMPOV(ARG1,ARG2,TEM1,TEM2,TEM3,TEM4)
    TEM1=AZR4(I)
    TEM2=BZR4(I)
    CALL C4PMF(TEM3,TEM4,TEM1,TEM2,ARG1,ARG2)
    AZIN(I)=TEM3
  33 BZIN(I)=TEM4
  C CALCULATES Z IN 6 THRU 11
    DO 39 I=6,11
    TEM1=AZR4(I)
    TEM2=BZR4(I)
    TEM3=AZIN(I+59)
    TEM4=BZIN(I+59)
    TEM5=AV(I)
    TEM6=AD(I)
    TEM7=BTN(I)
    CALL CALZIN(AARG,BARG,TEM1,TEM2,TEM3,TEM4,TEM5,TEM6,TEM7)
    AZIN(I)=AARG
  34 BZIN(I)=BARG
  C CALCULATES Z IN 12 THRU 16
    DO 35 I=12,16
    TEM1=AZR4(I)
    TEM2=BZR4(I)
    TEM3=AZIN(I-11)
    TEM4=BZIN(I-11)
    TEM5=AV(I)
    TEM6=AD(I)
    TEM7=BTN(I)
    CALL CALZIN(AARG,BARG,TEM1,TEM2,TEM3,TEM4,TEM5,TEM6,TEM7)
    AZIN(I)=AARG
  35 BZIN(I)=BARG
  C CALCULATES RECEIVING Z FOR LINE 17
    TEM1=AZIN(11)
    TEM2=BZIN(11)
    TEM3=AZIN(12)
    TEM4=BZIN(12)
    CALL ZEBRA(AZCTI,BZCTI,TEM1,TEM2,TEM3,TEM4)
    AZOTI(17)=AZCTI
    BZOTI(17)=BZCTI
  C CALCULATES Z IN 17 INCLUDING R-TRANSDUCER
    TEM1=AZPN(17)
    TEM2=BZPN(17)
    TEM3=AV(17)
    TEM4=AD(17)
    TEM5=BTN(17)
    CALL CALZIN(AZINI,BZINI,TEM1,TEM2,AZOTI,BZOTI,TEM3,TEM4,TEM5)
    AZIN(17)=AZINI
    BZIN(17)=BZINI
  C CALCULATES Z IN 18 AND 19
    DO 36 I=18,19
    TEM1=AZR4(I)
    TEM2=BZR4(I)
    TEM3=AZIN(I-1)
    TEM4=BZIN(I-1)
    TEM5=AV(I)
    TEM6=AD(I)
    TEM7=BTN(I)
    CALL CALZIN(AZINI,BZINI,TEM1,TEM2,TEM3,TEM4,TEM5,TEM6,TEM7)
    AZIN(I)=AZINI
  36 BZIN(I)=BZINI
  C CALCULATES RECEIVING Z FOR LINE 20
    TEM1=AZIN(I)

```

```

TEM2=BZIN(19)
TEM3=AZIN(13)
TEM4=BZIN(13)
CALL ZEBRA(AZOTI,BZCTI,TEM1,TEM2,TEM3,TEM4)
AZOT(21)=AZCTI
BZOT(21)=BZOTI
C CALCULATES Z IN FOR LINE 20 INCLUDING R-TRANSDUCER
TEM1=AZR(N(21))
TEM2=BZPN(21)
TEM3=AN(21)
TEM4=AD(21)
TEM5=ETN(21)
CALL CALZIN(AZINI,BZINI,TEM1,TEM2,AZOTI,BZOTI,TEM3,TEM4,TEM5)
AZIN(21)=AZINI
BZIN(21)=BZINI
C CALCULATES Z IN 21 THRU 41
DO 37 I=21,41
TEM1=AZR(N(I))
TEM2=BZRN(I)
TEM3=AZIN(I-1)
TEM4=BZIN(I-1)
TEM5=AN(I)
TEM6=AD(I)
TEM7=BTN(I)
CALL CALZIN(AZINI,BZINI,TEM1,TEM2,TEM3,TEM4,TEM5,TEM6,TEM7)
AZIN(I)=AZINI
37 BZIN(I)=BZINI
C CALCULATES RECEIVING Z FOR LINE 42
TEM1=AZIN(41)
TEM2=BZIN(41)
TEM3=AZIN(14)
TEM4=BZIN(14)
CALL ZEBRA(AZOTI,BZCTI,TEM1,TEM2,TEM3,TEM4)
AZOT(42)=AZCTI
BZOT(42)=BZCTI
C CALCULATES Z IN FOR LINE 42 INCLUDING R-TRANSDUCER
TEM1=AZR(N(42))
TEM2=BZRN(42)
TEM3=AN(42)
TEM4=AD(42)
TEM5=BTN(42)
CALL CALZIN(AZINI,BZINI,TEM1,TEM2,AZOTI,BZOTI,TEM3,TEM4,TEM5)
AZIN(42)=AZINI
BZIN(42)=BZINI
C CALCULATES Z IN 43 THRU 48
DO 39 I=43,48
TEM1=AZR(N(I))
TEM2=BZRN(I)
TEM3=AZIN(I-1)
TEM4=BZIN(I-1)
TEM5=AN(I)
TEM6=AD(I)
TEM7=BTN(I)
CALL CALZIN(AZINI,BZINI,TEM1,TEM2,TEM3,TEM4,TEM5,TEM6,TEM7)
AZIN(I)=AZINI
39 BZIN(I)=BZINI
C CALCULATES RECEIVING Z FOR LINE 49
TEM1=AZIN(49)
TEM2=BZIN(49)
TEM3=AZIN(1)
TEM4=BZIN(1)
TEM5=AZIN(1)
TEM6=BZIN(1)
CALL ZEBRA(AZOTI,BZOTI,TEM1,TEM2,TEM3,TEM4,TEM5,TEM6)
AZOT(49)=AZCTI

```

```

C CALCULATES Z IN FOR LINE 49 INCLUDING R-BRANCHES
TEM1=AZRN(49)
TEM2=BZRN(49)
TEM3=AN(49)
TEM4=AD(49)
TEM5=BTA(49)
CALL CALZIR(AZINI,BZINI,TEM1,TEM2,AZOTI,BZCTI,TEM3,TEM4,TEM5)
AZIN(49)=AZINI
BZIN(49)=BZINI
C CALCULATES Z IN 50
TEM1=AZRN(50)
TEM2=BZRN(50)
TEM3=AZIN(49)
TEM4=BZIN(49)
TEM5=AN(50)
TEM6=AD(50)
TEM7=BTA(50)
CALL CALZIR(AZINI,BZINI,TEM1,TEM2,TEM3,TEM4,TEM5,TEM6,TEM7)
AZIN(50)=AZINI
BZIN(50)=BZINI
C CALCULATES Z IN 51 AND 52
DO 39 I=51,52
TEM1=AZRN(I)
TEM2=BZRN(I)
TEM3=AZIN(I-44)
TEM4=BZIN(I-44)
TEM5=AN(I)
TEM6=AD(I)
TEM7=BTA(I)
CALL CALZIR(AZINI,BZINI,TEM1,TEM2,TEM3,TEM4,TEM5,TEM6,TEM7)
AZIN(I)=AZINI
39 BZIN(I)=BZINI
C CALCULATES RECEIVING Z FOR LINE 53
I=53
TEM1=AZIN(I-38)
TEM2=BZIN(I-38)
TEM3=AZIN(I-2)
TEM4=BZIN(I-2)
CALL ZEBRA(AZOTI,BZCTI,TEM1,TEM2,TEM3,TEM4)
AZOTC(I)=AZCTI
BZOTC(I)=BZCTI
C CALCULATES Z IN 53 INCLUDING R-TRANSDUCER
TEM1=AZRN(I)
TEM2=BZRN(I)
TEM3=AN(I)
TEM4=AD(I)
TEM5=BTA(I)
CALL CALZIR(AZINI,BZINI,TEM1,TEM2,AZCTI,BZOTI,TEM3,TEM4,TEM5)
AZIN(I)=AZINI
BZTAC(I)=BZINI
C CALCULATES Z IN 54 AND 55
DO 70 I=54,55
TEM1=AZRN(I)
TEM2=PZRN(I)
TEM3=BZIN(I-1)
TEM4=BZIN(I-1)
TEM5=AN(I)
TEM6=AD(I)
TEM7=BTA(I)
CALL CALZIR(AZINI,BZINI,TEM1,TEM2,TEM3,TEM4,TEM5,TEM6,TEM7)
AZIN(I)=AZINI
70 BZIN(I)=BZINI
C CALCULATES Z IN 56
I=56
TEM8=AN(I)*AD(I)
A9G1=ECSH(TEM8)

```

```

    ARG0=SINH(TEMP)
    TEM5=BT4(I)*AD(I)
    TEMF=CCS(TEM5)
    TEM1=ARG1+TEMP
    TEM3=ARG2+TEMP
    TEMP=SIN(TEM5)
    TEM2=ARG2+TEMP
    TEM4=ARG1+TEMP
    CALL CVPDV(ARG1,ARG2,TEM1,TEM2,TEM3,TEM4)
    TEM1=AZRN(I)
    TEM2=BZPN(I)
    CALL CVPME(TEM3,TEM4,TEM1,TEM2,ARG1,ARG2)
    AZIN(I)=TEM3
    BZIN(I)=TEM4
C CALCULATES Z IN 57
    TEM1=AZPN(I)
    TEM2=BZPN(I)
    TEM3=AZIN(I-1)
    TEM4=BZIN(I-1)
    TEM5=AN(I)
    TEM6=AD(I)
    TEM7=BT4(I)
    CALL CALZIN(AARG,BARG,TEM1,TEM2,TEM3,TEM4,TEM5,TEM6,TEM7)
    AZIN(I)=AARG
    BZIN(I)=BARG
C CALCULATES RECEIVING Z FOR LINE 58
    TEM1=AZIN(58)
    TEM2=BZIN(58)
    TEM3=AZIN(57)
    TEM4=BZIN(57)
    CALL ZEPACKAZCTI,BZCTI,TEM1,TEM2,TEM3,TEM4)
    AZOT(58)=AZCTI
    BZOT(58)=BZCTI
C CALCULATES Z IN 59 INCLUDING P-BRANCH
    TEM1=AZRN(59)
    TEM2=BZRN(59)
    TEM3=AN(59)
    TEM4=AD(59)
    TEM5=BTN(59)
    CALL CALZIN(AZINI,BZINI,TEM1,TEM2,AZOTI,BZCTI,TEM3,TEM4,TEM5)
    AZIN(59)=AZINI
    BZIN(59)=BZCTI
C CALCULATES RECEIVING Z FOR LINE 60
    TEM1=AZIN(60)
    TEM2=BZIN(60)
    TEM3=AZIN(60)
    TEM4=BZIN(60)
    CALL ZEPACKAZCTI,BZCTI,TEM1,TEM2,TEM3,TEM4)
    AZOT(60)=AZCTI
    BZOT(60)=BZCTI
C CALCULATES Z IN 60 INCLUDING R-TRANSDUCER
    TEM1=AZRN(60)
    TEM2=BZRN(60)
    TEM3=AN(60)
    TEM4=AD(60)
    TEM5=BTN(60)
    CALL CALZIN(AZINI,BZINI,TEM1,TEM2,AZOTI,BZCTI,TEM3,TEM4,TEM5)
    AZIN(60)=AZINI
    BZIN(60)=BZCTI
C CALCULATES RECEIVING Z FOR LINE 61
    TEM1=AZIN(61)
    TEM2=BZIN(61)
    TEM3=AZIN(61)
    TEM4=BZIN(61)
    .. CALL ZEPACKAZCTI,BZCTI,TEM1,TEM2,TEM3,TEM4)

```

```

AZOT(61)=AZCTI
BZOT(61)=BZCTI
C CALCULATES Z IN 61 INCLUDING R-BRANCH
TEM1=AZPN(61)
TEM2=BZPN(61)
TEM3=AN(61)
TEM4=AD(61)
TEM5=BTN(61)
CALL CALZIN(AZINI,BZINI,TEM1,TEM2,AZCTI+BZOTI,TEM3,TEM4,TEM5)
AZIN(61)=AZINI
BZIN(61)=BZINI
C CALCULATES RECEIVING Z FOR LINE 59
TEM1=AZIN(61)
TEM2=BZIN(61)
TEM3=AZIN(59)
TEM4=BZIN(59)
CALL ZEBRA(AZOTT,BZCTI,TEM1,TEM2,TEM3,TEM4)
AZOT(59)=AZCTI
BZOT(59)=BZCTI
C CALCULATES Z IN 59 INCLUDING R-BRANCH
TEM1=AZPN(59)
TEM2=BZPN(59)
TEM3=AN(59)
TEM4=AD(59)
TEM5=BTN(59)
CALL CALZIN(AZINI,BZINI,TEM1,TEM2,AZCTI+BZOTI,TEM3,TEM4,TEM5)
AZIN(59)=AZINI
BZIN(59)=BZINI
C CALCULATES RECEIVING Z FOR LINE 62
TEM1=AZIN(59)
TEM2=BZIN(59)
TEM3=AZIN(59)
TEM4=BZIN(59)
CALL ZFHRA(AZOTI,BZCTI,TEM1,TEM2,TEM3,TEM4)
AZOT(62)=AZCTI
BZOT(62)=BZCTI
C CALCULATES Z IN 62 INCLUDING R-BRANCH
TEM1=AZPN(62)
TEM2=BZPN(62)
TEM3=AN(62)
TEM4=AD(62)
TEM5=BTN(62)
CALL CALZIN(AZINI,BZINI,TEM1,TEM2,AZCTI+BZOTI,TEM3,TEM4,TEM5)
AZIN(62)=AZINI
BZIN(62)=BZINI
C CALCULATES Z IN 63 AND 64
DO 41 I=63,64
TEM1=AZPN(I)
TEM2=BZPN(I)
TEM3=AZIN(I-1)
TEM4=BZIN(I-1)
TEM5=AN(I)
TEM6=AD(I)
TEM7=BTN(I)
CALL CALZIN(AZINI,BZINI,TEM1,TEM2,TEM3,TEM4,TEM5,TEM6,TEM7)
AZIN(I)=AZINI
BZIN(I)=BZINI
41
C CALCULATES F11/F17 INCLUDING R-TRANSDUCER
I=17
TFMP=RTN(I)*AD(I)
CSRI1=COS(TFMP)
SRI1=SIN(TFMP)
TFMP=AN(I)*AD(I)
APG1=CCOSH(TFMP)
APG2=SHIN(TFMP)
TEM1=APG1*CSRI1

```

```

TEM2=ARG2+CABII
AZOTI=AZOT(I)
BZOTI=BZOT(I)
AZINI=AZINI(I)
BZINI=BZINI(I)
CALL CMPOV(TEM7,TEMP,AZOTI,BZOTI,AZINI,BZINI)
CALL CMFNF(TEM3,TEM4,TEM7,TEM8,TEM1,TEM.)
TEM5=ARG2+CABII
TEM6=ARG1+CABII
TEM7=AZEN(I)
TEM10=HZRN(I)
CALL CMPOV(TEM7,TEMP,AZOTI,BZOTI,TEM9,TEM10)
CALL CMFNF(TEM1,TEM2,TEM7,TEM8,TEM5,TEM6)
TEM1=TEM3-TEM1
TEM2=TEM4-TEM2
TEM3=TEM1+TEM2+TEM2
BETAC(I)=ATAN2(TEM2,TEM1)
RET(I)=(15./PI)*BETAC(I)
RTD(I-4)=SOFT(TEMP)
GFC(I-5)=2.*ALOG10(RTF(I-6))
C CALCULATES P17/P18,F1P/F19
DC 42 I=18,19
TEMP=RTA(I)+AD(I)
CCRII=COS(TEMP)
SNTII=SIN(TEMP)
TEMP=AN(I)+AD(I)
ARG1=COSH(TEMP)
ARG2=SINH(TEMP)
TEM1=ARG1+CABII
TEM2=ARG2+CABII
AZINI1=AZINI(I-1)
BZINI1=BZINI(I-1)
AZINI=AZINI(I)
BZINI=BZINI(I)
CALL CMPOV(TEM7,TEMP,AZINI1,BZINI1,AZINI,BZINI)
CALL CMFNF(TEM3,TEM4,TEM7,TEM8,TEM1,TEM2)
TEM5=ARG2+CABII
TEM6=ARG1+CABII
TEM7=AZRN(I)
TEM10=HZRN(I)
CALL CMPOV(TEM7,TEM8,AZINI1,BZINI1,TEM9,TEM10)
CALL CMFNF(TEM1,TEM2,TEM7,TEM8,TEM5,TEM6)
TEM1=TEM3-TEM1
TEM2=TEM4-TEM2
TEM3=TEM1+TEM2+TEM2
BETAC(I)=ATAN2(TEM2,TEM1)
RET(I)=(15./PI)*BETAC(I)
RTD(I-1)=SOFT(TEMP)
42 GFC(-1)=2.*ALOG10(RTF(I-1))
C CALCULATES F19/F20 INCLUDING R-TRANSDUCER
TEM
TEMP=RTA(I)+AD(I)
CCRII=COS(TEMP)
SNTII=SIN(TEMP)
TEMP=AN(I)+AD(I)
ARG1=COSH(TEMP)
ARG2=SINH(TEMP)
TEM1=ARG1+CABII
TEM2=ARG2+CABII
AZOTI=AZOT(I)
BZOTI=BZOT(I)
AZINI=AZINI(I)
BZINI=BZINI(I)
CALL CMPOV(TEM7,TEM8,AZOTI,BZOTI,AZINI,BZINI)
CALL CMFNF(TEM3,TEM4,TEM7,TEM8,TEM1,TEM2)
TEM5=ARG2+CABII

```

```

TEM5=ARG1*CSBII
TEM9=AZRN(I)
TEM10=PZRN(I)
CALL CMPDV(TEM7,TEM8,AZOTI,BZOTI,TEM9,TEM10)
CALL CPMF(TEM1,TEM2,TEM7,TEM8,TEM5,TEM6)
TEM1=TEM3-TEM1
TEM2=TEM4-TEM2
TEMP=TEM1+TEM1+TEM2+TEM2
BETAC(I)=ATAN2(TEM2,TEMP)
BET(I)=(180./PI)*BETAC(I)
RTP(I-1)=SOFT(TEMF)
GPI(I-1)=20.+ALOGIC(RTP(I-1))
C CALCULATES P20/P21 THRU P40/P41
DC 43 I=21,41
TEMF=BTN(I)*ADC(I)
CSR11=COS(TEMP)
SNBII=SIN(TEMP)
TEMF=AN(I)*ADC(I)
ARG1=CCSH(TEMP)
ARG2=SHINH(TEMP)
TEM1=ARG1*CSR11
TEM2=ARG2*SNBII
AZINI1=AZIN(I-1)
BZINI1=BZIN(I-1)
AZINI=AZIN(I)
BZINI=PZIN(I)
CALL CMPDV(TEM7,TEM8,AZINI1,BZINI1,AZINI,BZINI)
CALL CPMF(TEM3,TEM4,TEM7,TEM8,TEM1,TEM2)
TEM5=ARG2*CSR11
TEM6=ARG1*SNBII
TEMP=AZRN(I)
TEM10=BZRN(I)
CALL CMPDV(TEM7,TEM8,AZINI1,BZINI1,TEM9,TEM10)
CALL CPMF(TEM1,TEM2,TEM7,TEM8,TEM5,TEM6)
TEM1=TEM3-TEM1
TEM2=TEM4-TEM2
TEMP=TEM1+TEM1+TEM2+TEM2
BETAC(I)=ATAN2(TEM2,TEMP)
BET(I)=(180./PI)*BETAC(I)
RTP(I-1)=SOFT(TEMP)
GPI(I-1)=20.+ALOGIC(RTP(I-1))
C CALCULATES P41/F42 INCLUDING R-TRANSDUCER
I=42
TEMF=BTN(I)*ADC(I)
CSR11=COS(TEMP)
SNBII=SIN(TEMP)
TEMP=AN(I)*ADC(I)
ARG1=CCSH(TEMP)
ARG2=SHINH(TEMP)
TEM1=ARG1*CSR11
TEM2=ARG2*SNBII
AZOTI=AZOT(I)
BZOTI=BZOT(I)
AZINI=AZIN(I)
BZINI=PZIN(I)
CALL CMPDV(TEM7,TEM8,AZOTI,BZOTI,AZINI,BZINI)
CALL CPMF(TEM3,TEM4,TEM7,TEM8,TEM1,TEM2)
TEM5=ARG2*CSR11
TEM6=ARG1*SNBII
TEMP=AZRN(I)
TEM10=BZRN(I)
CALL CMPDV(TEM7,TEM8,AZOTI,BZOTI,TEM9,TEM10)
CALL CPMF(TEM1,TEM2,TEM7,TEM8,TEM5,TEM6)
TEM1=TEM3-TEM1
TEM2=TEM4-TEM2
TEMP=TEM1+TEM1+TEM2+TEM2

```

```

BETAC(I)=ATAN2(TEM2,TEM1)
BET(I)=(180./PI)*BETAC(I)
RTP(I-1)=SOFT(TEMP)
GP(I-1)=20.*ALOG10(RTP(I-1))
C CALCULATES P42/P43 THRL P47/P48
DC 44 I=43,46
TEMP=R*NC(I)*AC(I)
CSRI1=CCS(TEMP)
SNRI1=SIN(TEMP)
TEMP=AN(I)*AD(I)
ARG1=CCSH(TEMP)
ARG2=SINH(TEMP)
TEM1=ARG1*CSRI1
TEM2=ARG2*SNRI1
AZINI1=AZIN(I-1)
HZINI1=PZIN(I-1)
AZIN1=AZIN(I)
HZIN1=PZIN(I)
BZIN1=BZIN(I)
CALL CMPDV(TEM7,TEM3,AZINI1,BZINI1,AZINI,HZINI)
CALL CPMF(TEM3,TEM4,TEM7,TEMA,TEM1,TEM2)
TEM5=ARG2*CSRI1
TEM6=ARG1*SNRI1
TEM9=A744(I)
TEM10=BZRN(I)
CALL CMPDV(TEM7,TEMP,AZINI1,BZINI1,TEM9,TEM10)
CALL CPMF(TEM1,TEM2,TEM7,TEM8,TEM5,TEM6)
TEM1=TEM3-TEM1
TEM2=TEM4-TEM2
TEM=TEM1+TEM2+TEM2
BETAC(I)=ATAN2(TEM2,TEM1)
HFT(I)=(180./PI)*BETAC(I)
RTP(I-1)=SOFT(TEMP)
GP(I-1)=20.*ALOG10(RTP(I-1))
C CALCULATES P48/P49 INCLUDING R-BRANCHES
I=49
TEMP=BTN(I)*AD(I)
CSRI1=COS(TEMP)
SNRI1=SIN(TEMP)
TEMP=AN(I)*AD(I)
ARG1=CCSH(TEMP)
ARG2=SINH(TEMP)
TEM1=ARG1*CSRI1
TEM2=ARG2*SNRI1
AZOTI=AZOT(I)
HZOTI=BZOT(I)
AZINI=AZIN(I)
HZINI=PZIN(I)
CALL CMPDV(TEM7,TEM6,AZOTI,BZOTI,AZINI,BZINI)
CALL CPMF(TEM3,TEM4,TEM7,TEMA,TEM1,TEM2)
TEM5=ARG2*CSRI1
TEM6=ARG1*SNRI1
TEM9=BZRN(I)
TEM10=BZRN(I)
CALL CMPDV(TEM7,TEM8,AZOTI,BZOTI,TEM9,TEM10)
CALL CPMF(TEM1,TEM2,TEM7,TEM8,TEM5,TEM6)
TEM1=TEM3-TEM1
TEM2=TEM4-TEM2
TEM=TEM1+TEM2+TEM2
BETAC(I)=ATAN2(TEM2,TEM1)
BET(I)=(180./PI)*BETAC(I)
RTP(I-1)=SOFT(TEMP)
GP(I-1)=20.*ALOG10(RTP(I-1))
C CALCULATES P49/P50
I=51
TEMP=BTN(I)*AD(I)
CSHT1=COS(TEMP)

```

```

SINII1=SIN(TEMP)
TEMP=AN(I)*AD(I)
ARG1=COSH(TEMP)
ARG2=SINH(TEMP)
TEM1=ARG1*CSEII1
TEM2=ARG2*SSEII1
AZINI1=AZIN(I-1)
BZINI1=BZIN(I-1)
AZINI=AZIN(I)
BZINI=BZIN(I)
CALL CMPOV(TEM7,TEMP,AZINI1,BZINI1,AZINI,BZINI)
CALL CMPPMF(TEM3,TEM4,TEM7,TEMP,TEM1,TEM2)
TEM5=ARG2*CSEII1
TEM6=ARG1*SSEII1
TEM7=AZRNC(I)
TEM10=BZRNC(I)
CALL CMPOV(TEM7,TEM1,AZINI1,BZINI1,TEM9,TEM10)
CALL CMPPMF(TEM1,TEM2,TEM7,TEM8,TEM5,TEM6)
TEM1=TEM3-TEM1
TEM2=TEM4-TEM2
TEM3=TEM1+TEM2+TEM2
BETA(I)=ATAN2(TEM2,TEM1)
RET(I)=(19./PI)*BETA(I)
RTP(I-1)=SOPT(TEMP)
GPI(I-1)=25.*ALOG10(RTP(I-1))
C CALCULATES P50/F62 INCLUDING R-BRANCH
I=52
TEMP=RTNC(I)*AD(I)
CSRI1=COS(TEMP)
SSEII1=SIN(TEMP)
TEMF=AN(I)*AD(I)
ARG1=CCOSH(TEMP)
ARG2=CSINH(TEMP)
TEM1=ARG1*CSEII1
TEM2=ARG2*SSEII1
AZOTI=AZOT(I)
BZOTI=BZOT(I)
AZINI=AZIN(I)
BZINI=BZIN(I)
CALL CMPOV(TEM7,TEMP,AZOTI,BZOTI,AZINI,BZINI)
CALL CMPPMF(TEM3,TEM4,TEM7,TEMP,TEM1,TEM2)
TEM5=ARG2*CSEII1
TEM6=ARG1*SSEII1
TEM7=AZRNC(I)
TEM10=BZRNC(I)
CALL CMPOV(TEM7,TEMP,AZOTI,BZOTI,TEM9,TEM10)
CALL CMPPMF(TEM1,TEM2,TEM7,TEMP,TEM5,TEM6)
TEM1=TEM3-TEM1
TEM2=TEM4-TEM2
TEM3=TEM1+TEM2+TEM2
BETA(I)=ATAN2(TEM2,TEM1)
RET(I)=(19./PI)*BETA(I)
RTP(I-1)=CGFT(TEMP)
GPI(I-1)=2.*ALOG10(RTP(I-1))
C CALCULATES P62/F63 AND P63/P64
DC 45 I=53,F4
TEMF=RTNC(I)*AD(I)
CSRI1=COS(TEMP)
SSEII1=SIN(TEMP)
TEMF=AN(I)*AD(I)
ARG1=CCOSH(TEMP)
ARG2=CSINH(TEMP)
TEM1=ARG1*CSEII1
TEM2=ARG2*SSEII1
AZINI1=AZIN(I-1)
BZINI1=BZIN(I-1)

```

```

AZINI=AZINI(I)
BZINI=BZINI(I)
CALL CMPOV(TEM7,TEM8,AZINI1,BZINI1,AZINI,BZINI)
CALL CMPMF(TEM3,TEM4,TEM7,TEM8,TEM1,TEM2)
TEM5=ALFG2*CSR11
TEM6=ALFG1*CSR11
TEM3=AZPN(I)
TEM10=BZPN(I)
CALL CMPOV(TEM7,TEM8,AZINI1,BZINI1,TEM9,TEM10)
CALL CMPMF(TEM1,TEM2,TEM7,TEM8,TEM9,TEM6)
TEM1=TEM3-TEM1
TEM2=TEM4-TEM2
TEMF=TEM1*TEM1+TEM2*TEM2
RETA(I)=ATAN2(TEM2,TEM1)
RET(I)=(1P .-/PI)*RETA(I)
PTP(I-1)=SQRT(TEMF)
45 GP(I-1)=2E.+ ALOG1((PTP(I-1)))
C CALCULATES GAIN 41/E3
RTPT1=1
DC 46 I=41,EE
46 RTPT1=RTPT1+RTP(I)
RTPT1=FTPT1+RTP(62)+RTP(63)
GPT1=2E.+ALCG1*(FTPT1)
C CALCULATES GAIN 19/E3
RTPT2=1
DC 47 I=19,EE
47 RTPT2=RTPT2+RTP(I)
RTPT2=FTPT2+RTPT1
GET2=2E.+ALCG10(FTPT2)
C CALCULATES GAIN 11/E3
RTPT3=RTPT2+RTP(16)+RTP(17)+RTP(11)
GPT3=2E.+ALCG10(FTPT3)
C CALCULATES PHASE ANGLE 42/64
BETA1R=1
DC 48 I=42,EE
48 BETA1R=BETAIR+RETA(I)
DC 49 I=62,EE
49 BETA1R=BETAIR+RETA(I)
C CALCULATES PHASE ANGLE 21/64
BETA2R=1
DC 51 I=21,EE
50 BETA2R=RETA2R+RETA(I)
BETA2R=BETA1R+BETA1R
BETA2D=(180./PI)*BETA2R
C CALCULATES PHASE ANGLE 17/64
BETA3R=1
DC 51 I=17,EE
51 BETA3R=RETA3R+RETA(I)
BETA3R=BETA3R+BETA2R
52 IF(BETA3R>LE.C.) GO TO 53
BETA3R=RETA3R-TPI
GO TO 52
53 IF(BETA3R<GE.-TPI) GO TO 54
BETA3R=RETA3R+TPI
GO TO 53
54 BETA3D=(180./PI)*BETA3R
55 IF(BETA1R>LE.C.) GO TO 56
BETA1R=BETA1R-TPI
GO TO 53
56 IF(BETA1R>GE.-TPI) GO TO 57
BETA1R=BETA1R+TPI
GO TO 56
57 BETA1D=(180./PI)*BETA1R
58 WRITE(6,701)Y,GET1,PETA1D,GPT3,BETA3D
591 FORMAT(2X,FG.3,2X,F11.4,2X,F11.4,2X,F11.4,2X,F11.4)
      ORT1(N)=GPT1

```

```

DAT(1)=GP1
OMG(1)=V
PHASE1(1)=BETA1D
PHASE3(1)=BETA3D
CONTINUE
GO TO (85,611),IND
85 Y=1.
DM=1.
NST=200
IND=2
GO TO 40

C
C ***** THIS SECTION IS FOR THE CALCCMP PLOTTER. ONE SET OF
C EXPERIMENTAL DATA MUST BE INCLUDED WITH EACH RUN.
C
C NPTS IS THE NUMBER OF EXPERIMENTAL POINTS TO BE INPUT.
C LSMB1 IS THE PLOTTER SYMBOL TO BE USED FOR GP1 AND PHT1.
C LSMB3 IS THE PLOTTER SYMBOL TO BE USED FOR GP3 AND PHT3.
C SEE A CALCCMP PLOTTER USERS MANUAL FOR DESCRIPTION.
C FREQ,PG,PR3,PF1,PH33,PHS1,FACT,FMR3, AND PHR1 ARE THE INPUT
C EXPERIMENTAL VALUES.
C FREQ IS THE MEASURED FREQUENCY.
C PG IS THE MEASURED INPUT DYNAMIC PRESSURE.
C PR3 IS THE MEASURED DYNAMIC PRESSURE AT THE END OF THE LINE.
C PR1 IS THE MEASURED DYNAMIC PRESSURE UPSTREAM OF VENTURI.
C PH33 IS THE DIAL READING ON THE CSCILLOSCOPE WHERE THE
C INPUT SIGNAL CROSSES THE ZERO AXIS ON THE SCOPE MEAS-
C USING THE SIGNAL AT THE END OF THE LINE.
C PHS1 IS THE DIAL READING ON THE CSCILLOSCOPE WHERE THE
C INPUT SIGNAL CROSSES THE ZERO AXIS ON THE SCOPE MEAS-
C USING THE SIGNAL UPSTREAM OF THE VENTURI.
C FACT IS THE MULTIPLYING FACTOR ON THE CSCILLOSCOPE IN
C MILLISECONDS/CENTIMETER.
C PHR3 AND PHF1 ARE THE DIAL READINGS ON THE CSCILLOSCOPES
C WHERE THE SIGNAL AT THE END OF THE LINE AND UPSTREAM OF
C THE VENTURI (RESPECTIVELY) CROSS THE ZERO AXIS ON THE
C APPROPRIATE SCOPE.
C THE PROGRAM THEN FINDS (PH33-PH31) AND MULTIPLIES THIS
C DIFFERENCE TIMES THE FACTOR TO GET THE PHASE SHIFT IN
C MILLISECONDS.
C
C*****611 IF(ICAT>502,502,61)
C10 CALL SCALE(DRT1,5.,%,1)
CALL SCALE(DRT3,5.,%,1)
OMG(M+1)=0.
OMG(M+2)=25.
CALL AXIS(.000,.17HFREQUENCY (HFRTZ),-17.8..0.,OMG(M+1),OMG(M+2))
CALL AXIS(.000.15HGAIN (DECIBELS),15.5..90.,DRT3(M+1),
+DRT3(M+2))
CALL LINE(OMG,DRT3,%,1,0.0)
FORMAT(EN,1A2)
READ(5,204)CASE(1)
READ(5,*)NPTS,LSMB1,LSMB3
WRITE(6,203)CASE(1)
FORMAT(EN,1A2)
WRITE(6,217)
207 EOBMAIS7X,AHEFLQ,5X,5HGAIN1,7X,6MPHASE1,7X,5HGATNZ,8X,6MPHASE3

```

```

J=2
L=0
DO 69 I=1,NPTS
READ(5,*)FREQ,PS,PR3,PR1,PHS3,PHS1,FACT,PHR3,PHR1
PHT1=(PHS1-FHR1)*FACT+FREQ*W*.36
PHT3=(PHS3-FHR3)*FACT+FREQ*W*.36
GP1=20.*ALG10(PR1/PS)
GP3=20.*ALG10(PR3/PS)
WETTE(S,2)*FREQ,GP1,PHT1,GP3,PHT3
209 FORMAT(2X,5F12.5)
DR1(I)=GP1
DR3(I)=GP3
OMGX(I)=FREQ
IF(PHT3.EQ.0) GO TO 66
J=J+1
PH1(J)=PHT1
OMGF1(J)=FREQ
JMAX=J
66 IF(PHT1.EQ.0) GO TO 69
L=L+1
PH1(L)=PHT1
OMGF1(L)=FREQ
LMAX=L
6 CONTINUE
OMGX(NPTS+1)=CMG(M+1)
DR1(NPTS+1)=DRT1(M+1)
DR3(NPTS+1)=DRT3(M+1)
OMGX(NPTS+2)=CMG(M+2)
DR1(NPTS+2)=DRT1(M+2)
DR3(NPTS+2)=DRT3(M+2)
CALL LINE(CMGX,DB3,APTS+1,-1,LSMB3)
CALL PLOT(15.0,0,-3)
CALL SCALE(PHASE1,5.,M,1)
CALL SCALE(PHASE3,5.,M,1)
CALL AXIS(0.,0.,17HFREQUENCY (HERTZ),-17,8.,0.,CMG(M+1),OMG(M+2))
CALL AXIS(0.,0.,21HFASE ANGLE (DEGREES),21,5.,90.,PHASE3(M+1),
+PHASE3(M+2))
CALL LINE(CMG,PHASE3,M,1,0,3)
OMGF1(LMAX+1)=CMG(M+1)
OMGF1(LMAX+2)=CMG(M+2)
OMGF3(JMAX+1)=CMG(M+1)
OMGF3(JMAX+2)=CMG(M+2)
PH1(LMAX+1)=PHASE1(M+1)
PH3(JMAX+1)=PHASE3(M+1)
PH1(LMAX+2)=PHASE1(M+2)
PH3(JMAX+2)=PHASE3(M+2)
CALL LINE(CMG,PHASE3,JMAX,1,-1,LSMB3)
1003 CALL PLOT(15.0,0,-3)
CALL AXIS(0.,0.,17HFREQUENCY (HERTZ),-17,8.,0.,OMG(M+1),OMG(M+2))
CALL AXIS(0.,0.,15HGAIN (DECIBELS),15,5.,90.,DRT1(M+1),
+DRT1(M+2))
CALL LINE(CMG,DRT1,M,1,0,4)
CALL LINE(CMGX,DB1,APTS+1,-1,LSMB1)
CALL PLOT(15.0,0,-3)
CALL AXIS(0.,0.,17HFREQUENCY (HERTZ),-17,8.,0.,OMG(M+1),OMG(M+2))
CALL AXIS(0.,0.,21HFASE ANGLE (DEGREES),21,5.,90.,PHASE1(M+1),
+PHASE1(M+2))
CALL LINE(CMG,PHASE1,M,1,0,3)
CALL LINE(CMGF1,PH1,LMAX+1,-1,LSMB1)
CALL PLOT(15.0,0,-3)
*****  

*****  

*****  

C
501 CALL PLOTE
502 STOP

```

```

      EPD
C CALCULATES ROOT OF A COMPLEX NUMBER
SUBROUTINE FCMP(X,Y,A,B)
CALL ANGL(TEMP,A,B)
TEMP=.5*TEMP
Y=A+A*B
X=SGRT(Y)
X=SGRT(X)
Y=X*SIN(TEMP)
X=X*COS(TEMP)
RETURN
END
C MULTIPLIES TWO COMPLEX NUMBERS
SUBROUTINE CMPLX(X,Y,A1,A2,B1,B2)
X=A1*B1-A2*B2
Y=A1*B2+A2*B1
RETURN
END
C FINDS THE QUOTIENT OF TWO COMPLEX NUMBERS
SUBROUTINE CMPOV(C1,C2,A1,A2,B1,B2)
TEMP=B1*B1+B2*B2
C1=A1*B1+A2*B2
C1=C1/TEMP
C2=B1*A2-A1*B2
C2=C2/TEMP
RETURN
END
      SUBROUTINE HSIN(X)
A=EXP(X)
B=EXP(-X)
A=A-B
ARG=.5*A
RETURN
END
      SUBROUTINE HCOS(X)
A=EXP(X)
B=EXP(-X)
A=A+B
ARG=.5*A
RETURN
END
      SUBROUTINE ANGL(C,A,B)
DATA PI/3.1415926/
C=ABS(H/A)
C=ATAN(C)
IF (A.GT.0.) GO TO 5
IA=1
GO TO 7
5 IA=2
7 IF (B.GT.0.) GO TO 10
IB=2
GO TO 15
10 IB=0
15 IA=IA+IB+1
GO TO (35,37,25,20)+IA
20 C=C-PI
GO TO 35
25 C=-C
GO TO 35
30 C=PI-C
35 RETURN
END

```

```

SUBROUTINE CALZIN(AZIN1,BZIN1,AZRN1,BZRN1,AZIN2,BZIN2,AN1,D11,
1RTY1)
TEMP=AN1+D11
CALL HCCSX(ARG1,TEMP)
CALL HSINX(ARG2,TEMP)
TENV=RTY1+D11
CSBI1=COS(TENV)
SNBI1=SIN(TENV)
ZR=1.
CALL CMPMF(TEM1,TEM2,AZIN2,BZIN2,ARG1,ZR)
CALL CMPMF(TEM3,TEM4,AZRN1,BZRN1,ARG2,ZR)
CALL CMPMF(TEM5,TEM6,AZIN2,BZIN2,ARG2,ZR)
CALL CMPMF(TEM7,TEM8,AZRN1,BZRN1,ARG1,ZR)
A1=TEM1+TEM3
B1=TEM2+TEM4
A2=TEM5+TEM7
R2=TEM6+TEM8
CALL CMFMF(TEM1,TEM2,A1,B1,CSBI1,ZR)
CALL CMFMF(TEM3,TEM4,A2,R2,CSBI1,ZR)
CALL CMFMF(TEM5,TEM6,A1,B1,ZR,SNBI1)
CALL CMFMF(TEM7,TEM8,A2,R2,ZR,SNBI1)
TEM3=TEM3+TEM1
TEM4=TEM4+TEM2
TEM7=TEM7+TEM5
TEM8=TEM8+TEM6
CALL CMPDV(TEM1,TEM2,TEM3,TEM4,TEM7,TEM8)
CALL CMPMP(AZIN1,BZIN1,TEM1,TEM2,AZRN1,BZRN1)
RETURN
END

```

```

SUBROUTINE ZERFA(C1,C2,A1,A2,B1,B2)
D1=1.
D2=J.
CALL CMPOV(ARG1,ARG2,C1,D2,A1,A2)
CALL CMPOV(ARG2,ARG4,D1,D2,B1,B2)
ARG1=ARG1+ARG3
ARG2=ARG2+ARG4
CALL CMPOV(C1,C2,D1,D2,ARG1,ARG2)
RETURN
END

```

```

C CALCULATES Z FOR 3 LINES COMING INTO 1
SUBROUTINE ZERFA3(D1,D2,A1,A2,B1,B2,C1,C2)
E1=1
E2=J
CALL CMPOV(ARG1,ARG2,E1,E2,A1,A2)
CALL CMPOV(ARG3,ARG4,E1,E2,B1,B2)
CALL CMPOV(ARG5,ARG6,E1,E2,C1,C2)
ARG1=ARG1+ARG3+ARG5
ARG2=ARG2+ARG4+ARG6
CALL CMPOV(D1,D2,E1,E2,ARG1,ARG2)
RETURN
END

```

Appendix B

Complete Line Dimensions

Figures 61-63 are schematics of the experimental model with the signal input at lines 1, 2, and 3, respectively. The model lines entered in the computer program were numbered according to these schematics. The line diameters and lengths for each case are given in Tables IV-XI.

Figures 64-66 are schematics of the ASTF lines with signals input at legs 1, 2, and 3, respectively. The ASTF lines entered in the computer program were numbered according to these schematics. The line diameters and lengths are given in Tables XII-XVII.

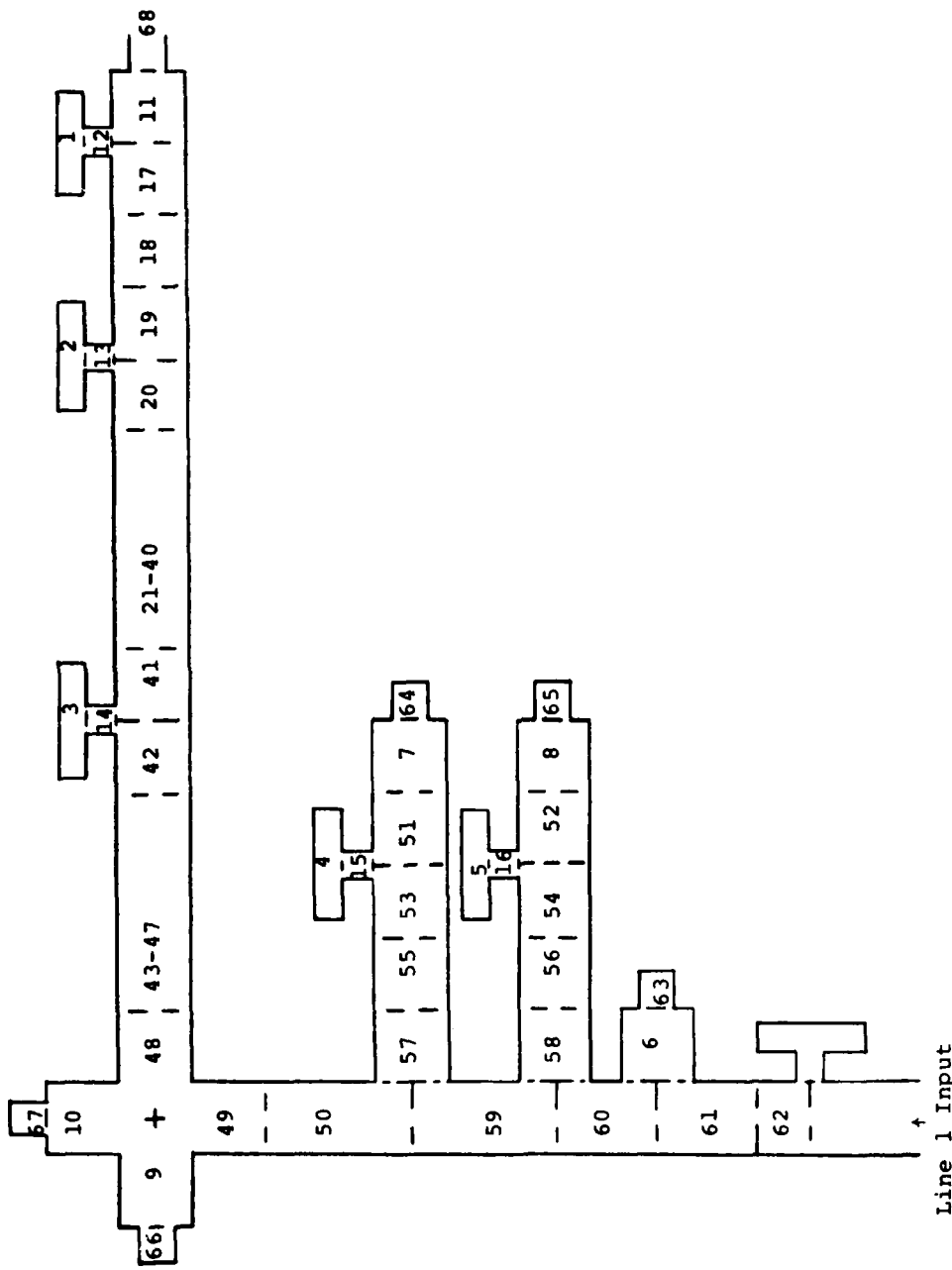


Fig. 61: Schematic of Lines with Input at Line 1

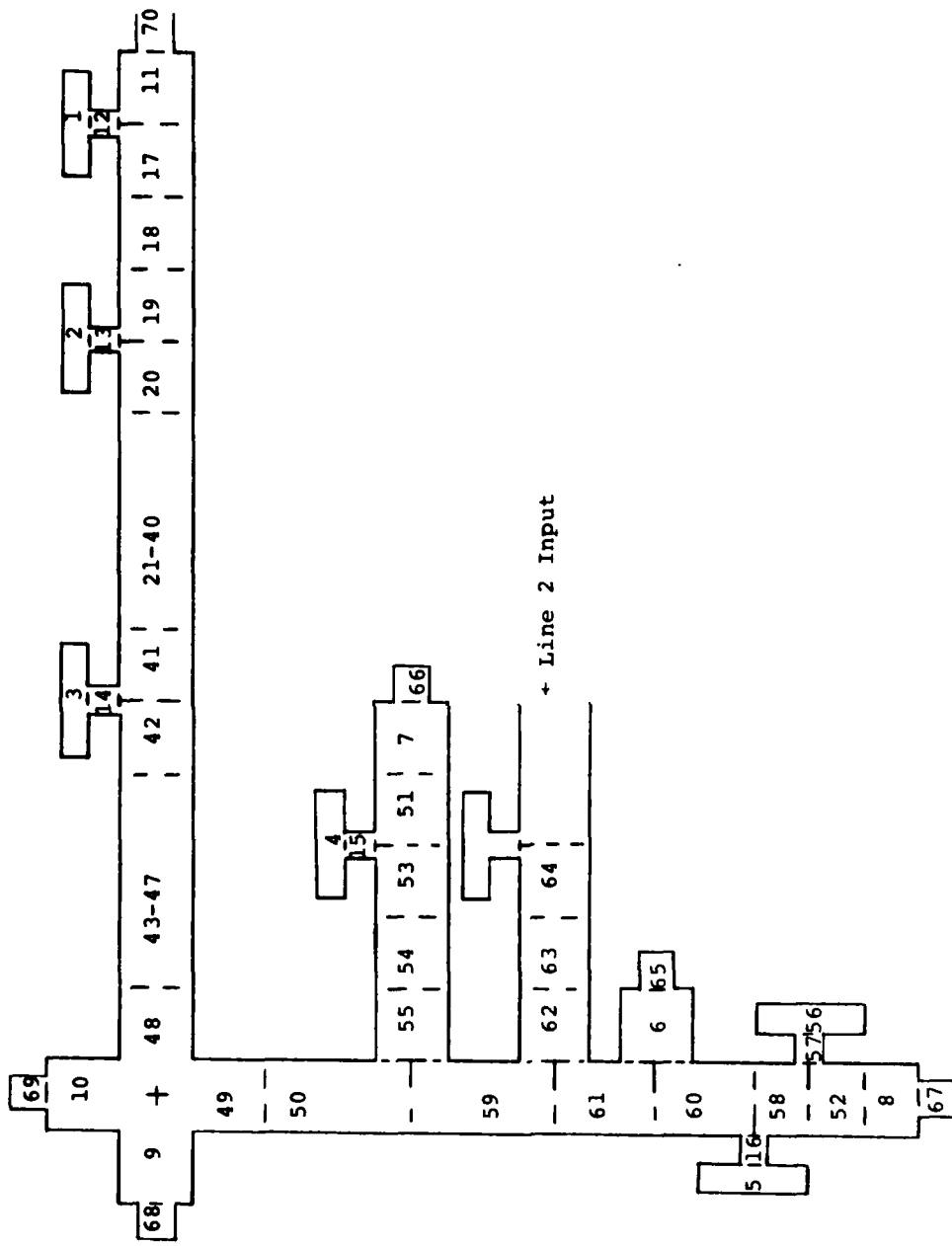


Fig. 62: Schematic of Lines with Input at Line 2

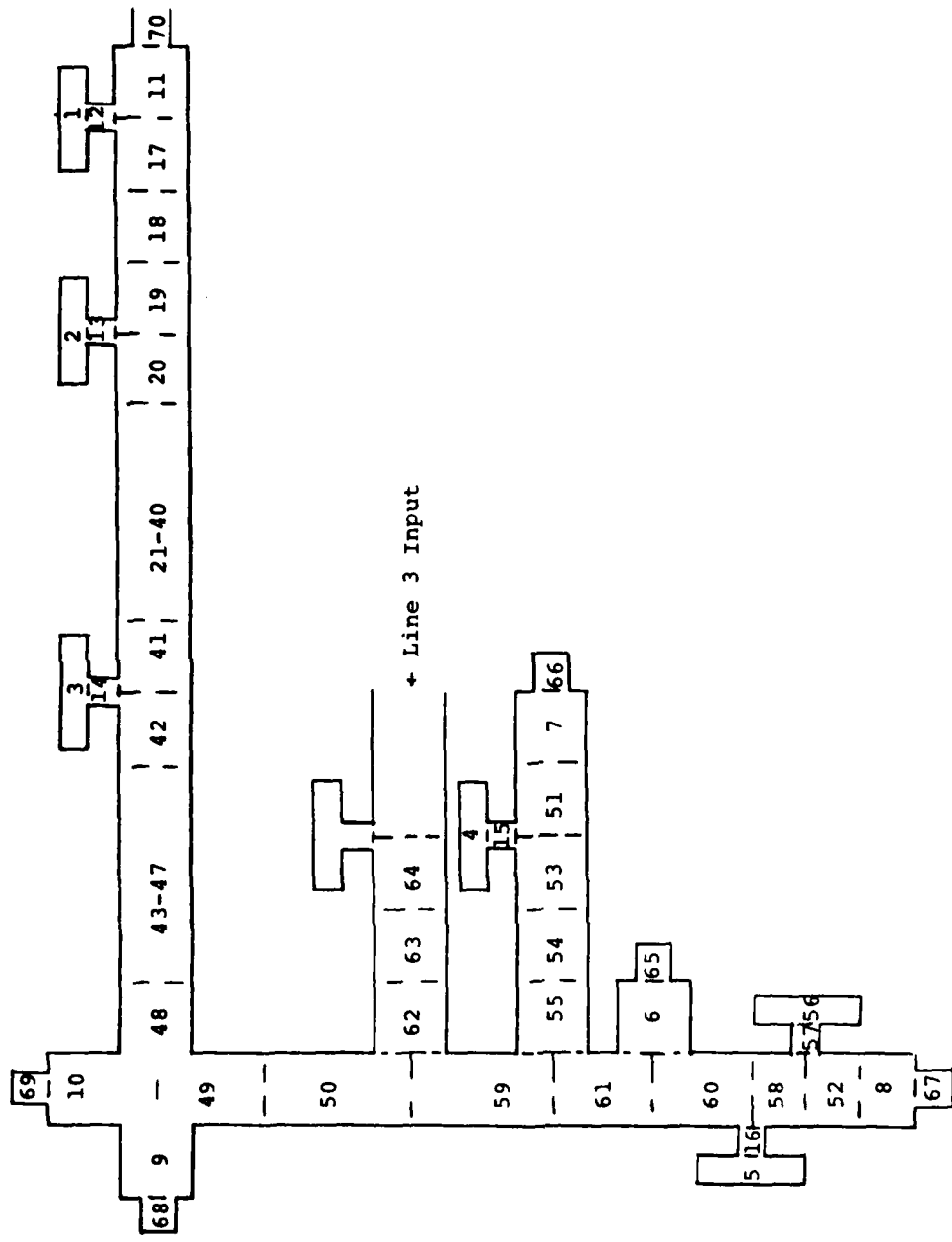


Fig. 63: Schematic of Lines with Input at Line 3

Table IV

Case 1

Line	Diameter in.	Length in.	Line	Diameter in.	Length in.
1	0.375	0.020	35	1.117	0.0001
2	0.375	0.020	36	1.117	0.0001
3	0.375	0.020	37	1.117	0.0001
4	0.375	0.020	38	1.117	0.0001
5	0.375	0.020	39	1.117	0.0001
6	0.750	102.0	40	0.093	0.715
7	0.938	0.250	41	1.117	0.381
8	0.938	0.313	42	1.117	151.5
9	0.189	532.50	43	0.696	53.25
10	0.818	103.50	44	1.117	151.5
11	1.117	0.024	45	0.622	53.25
12	0.052	0.024	46	0.622	53.25
13	0.052	0.024	47	0.622	53.25
14	0.052	0.024	48	0.622	53.25
15	0.052	0.024	49	0.818	96.0
16	0.052	0.024	50	0.818	96.0
17	1.117	198.0	51	0.818	4.375
18	0.696	0.063	52	0.818	4.375
19	1.117	198.0	53	0.818	1.50
20	1.117	0.620	54	0.818	1.50
21	1.117	37.283	55	0.622	41.25
22	1.117	0.0001	56	0.622	41.25
23	1.117	0.0001	57	0.622	41.25
24	1.117	0.0001	58	0.622	41.25
25	1.117	0.0001	59	0.818	108.0
26	1.117	0.0001	60	0.818	132.0
27	1.117	0.0001	61	0.818	90.0
28	1.117	0.0001	62	0.818	0.0001
29	1.117	0.0001	63	0.0001	0.0001
30	1.117	0.0001	64	0.0001	0.0001
31	1.117	0.0001	65	0.0001	0.0001
32	1.117	0.0001	66	0.0001	0.0001
33	1.117	0.0001	67	0.001	0.0001
34	1.117	0.0001	68	0.0000	0.0000

Table V

Case 2

Line	Diameter in.	Length in.	Line	Diameter in.	Length in.
1	0.375	0.020	36	1.117	0.0001
2	0.375	0.020	37	1.117	0.0001
3	0.375	0.020	38	1.117	0.0001
4	0.375	0.020	39	1.117	0.0001
5	0.375	0.020	40	0.093	0.715
6	0.750	102.0	41	1.117	0.381
7	0.938	0.313	42	1.117	49.45
8	0.938	0.625	43	0.696	0.063
9	0.189	532.50	44	1.117	151.5
10	0.818	103.50	45	0.622	53.25
11	1.117	0.024	46	0.622	53.25
12	0.052	0.024	47	0.622	53.25
13	0.052	0.024	48	0.622	53.25
14	0.052	0.024	49	0.818	96.0
15	0.052	0.024	50	0.818	96.0
16	0.052	0.024	51	0.818	4.375
17	1.117	198.0	52	0.818	1.652
18	0.696	0.063	53	0.818	1.50
19	1.117	198.0	54	0.622	41.25
20	1.117	0.620	55	0.622	41.25
21	1.117	37.283	56	0.352	0.063
22	1.117	0.0001	57	0.093	0.625
23	1.117	0.0001	58	0.818	1.750
24	1.117	0.0001	59	0.818	108.0
25	1.117	0.0001	60	0.818	90.0
26	1.117	0.0001	61	0.818	132.0
27	1.117	0.0001	62	0.622	41.25
28	1.117	0.0001	63	0.622	41.25
29	1.117	0.0001	64	0.818	1.50
30	1.117	0.0001	65	0.0001	0.0001
31	1.117	0.0001	66	0.0001	0.0001
32	1.117	0.0001	67	0.0001	0.0001
33	1.117	0.0001	68	0.0001	0.0001
34	1.117	0.0001	69	0.0001	0.0001
35	1.117	0.0001	70	0.0000	0.0000

Table VI

Case 3

Line	Diameter in.	Length in.	Line	Diameter in.	Length in.
1	0.375	0.020	36	1.117	0.0001
2	0.375	0.020	37	1.117	0.0001
3	0.375	0.020	38	1.117	0.0001
4	0.375	0.020	39	1.117	0.0001
5	0.375	0.020	40	0.093	0.715
6	0.750	102.0	41	1.117	0.381
7	0.938	0.250	42	1.117	49.45
8	0.938	0.625	43	0.696	0.063
9	0.189	532.50	44	1.117	151.5
10	0.818	103.50	45	0.622	53.25
11	1.117	0.024	46	0.622	53.25
12	0.052	0.024	47	0.622	53.25
13	0.052	0.024	48	0.622	53.25
14	0.052	0.024	49	0.818	96.0
15	0.052	0.024	50	0.818	96.0
16	0.052	0.024	51	0.818	4.375
17	1.117	198.0	52	0.818	1.652
18	0.696	0.063	53	0.818	1.50
19	1.117	198.0	54	0.622	41.25
20	1.117	0.620	55	0.622	41.25
21	1.117	37.283	56	0.352	0.063
22	1.117	0.0001	57	0.093	0.625
23	1.117	0.0001	58	0.818	1.750
24	1.117	0.0001	59	0.818	108.0
25	1.117	0.0001	60	0.818	90.0
26	1.117	0.0001	61	0.818	132.0
27	1.117	0.0001	62	0.622	41.25
28	1.117	0.0001	63	0.622	41.25
29	1.117	0.0001	64	0.818	1.50
30	1.117	0.0001	65	0.0001	0.0001
31	1.117	0.0001	66	0.0001	0.0001
32	1.117	0.0001	67	0.0001	0.0001
33	1.117	0.0001	68	0.0001	0.0001
34	1.117	0.0001	69	0.0001	0.0001
35	1.117	0.0001	70	0.0000	0.0000

Table VII

Case 4

Line	Diameter in.	Length in.	Line	Diameter in.	Length in.
1	0.375	0.020	36	0.203	1.907
2	0.375	0.020	37	0.203	1.907
3	0.375	0.020	38	0.203	1.907
4	0.375	0.020	39	0.203	1.907
5	0.375	0.020	40	0.203	1.912
6	0.750	102.0	41	1.117	0.425
7	0.938	0.250	42	1.117	49.45
8	0.938	0.625	43	0.696	0.063
9	0.189	532.50	44	1.117	151.5
10	0.818	103.50	45	0.622	53.25
11	1.117	0.024	46	0.622	53.25
12	0.052	0.024	47	0.622	53.25
13	0.052	0.024	48	0.622	53.25
14	0.052	0.024	49	0.818	96.0
15	0.052	0.024	50	0.818	96.0
16	0.052	0.024	51	0.818	4.375
17	1.117	198.0	52	0.818	1.652
18	0.696	0.063	53	0.818	1.50
19	1.117	198.0	54	0.622	41.25
20	1.117	0.425	55	0.622	41.25
21	0.203	1.907	56	0.352	0.063
22	0.203	1.907	57	0.093	0.625
23	0.203	1.907	58	0.818	1.750
24	0.203	1.907	59	0.818	108.0
25	0.203	1.907	60	0.818	90.0
26	0.203	1.907	61	0.818	132.0
27	0.203	1.907	62	0.622	41.25
28	0.203	1.907	63	0.622	41.25
29	0.203	1.907	64	0.818	1.50
30	0.203	1.907	65	0.0001	0.0001
31	0.203	1.907	66	0.0001	0.0001
32	0.203	1.907	67	0.0001	0.0001
33	0.203	1.907	68	0.0001	0.0001
34	0.203	1.907	69	0.0001	0.0001
35	0.203	1.907	70	0.0000	0.0000

Table VIII

Case 6

Line	Diameter in.	Length in.	Line	Diameter in.	Length in.
1	0.375	0.020	36	1.117	0.0001
2	0.375	0.020	37	1.117	0.0001
3	0.375	0.020	38	1.117	0.0001
4	0.375	0.020	39	1.117	0.0001
5	0.375	0.020	40	0.093	0.715
6	0.750	102.0	41	1.117	0.381
7	0.938	0.250	42	1.117	49.45
8	0.938	0.625	43	0.696	0.063
9	0.189	532.50	44	1.117	151.5
10	0.818	103.50	45	0.622	53.25
11	1.117	0.024	46	0.622	53.25
12	0.052	0.024	47	0.622	53.25
13	0.052	0.024	48	0.622	53.25
14	0.052	0.024	49	0.818	96.0
15	0.052	0.024	50	0.818	96.0
16	0.052	0.024	51	0.818	4.375
17	1.117	198.0	52	0.818	1.652
18	0.696	0.063	53	0.818	1.50
19	1.117	198.0	54	0.622	41.25
20	1.117	0.620	55	0.622	41.25
21	1.117	37.283	56	0.352	0.063
22	1.117	0.0001	57	0.093	0.625
23	1.117	0.0001	58	0.818	1.750
24	1.117	0.0001	59	0.818	108.0
25	1.117	0.0001	60	0.818	90.0
26	1.117	0.0001	61	0.818	132.0
27	1.117	0.0001	62	0.622	41.25
28	1.117	0.0001	63	0.622	41.25
29	1.117	0.0001	64	0.818	1.50
30	1.117	0.0001	65	0.0001	0.0001
31	1.117	0.0001	66	0.0001	0.0001
32	1.117	0.0001	67	0.0001	0.0001
33	1.117	0.0001	68	0.0001	0.0001
34	1.117	0.0001	69	0.0001	0.0001
35	1.117	0.0001	70	0.120	0.672

Table IX

Case 7

Line	Diameter in.	Length in.	Line	Diameter in.	Length in.
1	0.375	0.020	36	1.117	0.0001
2	0.375	0.020	37	1.117	0.0001
3	0.375	0.020	38	1.117	0.0001
4	0.375	0.020	39	1.117	0.0001
5	0.375	0.020	40	0.203	0.715
6	0.750	102.0	41	1.117	0.381
7	0.938	0.250	42	1.117	49.45
8	0.938	0.625	43	0.696	0.063
9	0.189	532.50	44	1.117	151.5
10	0.818	103.50	45	0.622	53.25
11	1.117	0.024	46	0.622	53.25
12	0.052	0.024	47	0.622	53.25
13	0.052	0.024	48	0.622	53.25
14	0.052	0.024	49	0.818	96.0
15	0.052	0.024	50	0.818	96.0
16	0.052	0.024	51	0.818	4.375
17	1.117	198.0	52	0.818	1.652
18	0.696	0.063	53	0.818	1.50
19	1.117	198.0	54	0.622	41.25
20	1.117	0.620	55	0.622	41.25
21	1.117	37.283	56	0.352	0.063
22	1.117	0.0001	57	0.093	0.625
23	1.117	0.0001	58	0.818	1.750
24	1.117	0.0001	59	0.818	108.0
25	1.117	0.0001	60	0.818	90.0
26	1.117	0.0001	61	0.818	132.0
27	1.117	0.0001	62	0.622	41.25
28	1.117	0.0001	63	0.622	41.25
29	1.117	0.0001	64	0.818	1.50
30	1.117	0.0001	65	0.0001	0.0001
31	1.117	0.0001	66	0.0001	0.0001
32	1.117	0.0001	67	0.0001	0.0001
33	1.117	0.0001	68	0.0001	0.0001
34	1.117	0.0001	69	0.0001	0.0001
35	1.117	0.0001	70	0.0000	0.0000

Table X

Case 8

Line	Diameter in.	Length in.	Line	Diameter in.	Length in.
1	0.375	0.020	36	1.117	0.0001
2	0.375	0.020	37	1.117	0.0001
3	0.375	0.020	38	1.117	0.0001
4	0.375	0.020	39	1.117	0.0001
5	0.375	0.020	40	0.203	0.715
6	0.750	102.0	41	1.117	0.381
7	0.938	0.250	42	1.117	49.45
8	0.938	0.625	43	0.696	0.063
9	0.189	532.50	44	1.117	151.5
10	0.818	103.50	45	0.622	53.25
11	1.117	0.024	46	0.622	53.25
12	0.052	0.024	47	0.622	53.25
13	0.052	0.024	48	0.622	53.25
14	0.052	0.024	49	0.818	96.0
15	0.052	0.024	50	0.818	96.0
16	0.052	0.024	51	0.818	4.375
17	1.117	198.0	52	0.818	1.652
18	0.696	0.063	53	0.818	1.50
19	1.117	198.0	54	0.622	41.25
20	1.117	0.620	55	0.622	41.25
21	1.117	37.283	56	0.352	0.063
22	1.117	0.0001	57	0.093	0.625
23	1.117	0.0001	58	0.818	1.750
24	1.117	0.0001	59	0.818	108.0
25	1.117	0.0001	60	0.818	90.0
26	1.117	0.0001	61	0.818	132.0
27	1.117	0.0001	62	0.622	41.25
28	1.117	0.0001	63	0.622	41.25
29	1.117	0.0001	64	0.818	1.50
30	1.117	0.0001	65	0.0001	0.0001
31	1.117	0.0001	66	0.0001	0.0001
32	1.117	0.0001	67	0.0001	0.0001
33	1.117	0.0001	68	0.0001	0.0001
34	1.117	0.0001	69	0.0001	0.0001
35	1.117	0.0001	70	0.120	0.672

Table XI

Case 9

Line	Diameter in.	Length in.	Line	Diameter in.	Length in.
1	0.375	0.020	36	1.117	0.0001
2	0.375	0.020	37	1.117	0.0001
3	0.375	0.020	38	1.117	0.0001
4	0.375	0.020	39	1.117	0.0001
5	0.375	0.020	40	0.203	0.715
6	0.750	102.0	41	1.117	0.381
7	0.938	0.250	42	1.117	49.45
8	0.938	0.625	43	0.696	0.063
9	0.189	532.50	44	1.117	151.5
10	0.818	103.50	45	0.622	53.25
11	1.117	0.024	46	0.622	53.25
12	0.052	0.024	47	0.622	53.25
13	0.052	0.024	48	0.622	53.25
14	0.052	0.024	49	0.818	96.0
15	0.052	0.024	50	0.818	96.0
16	0.052	0.024	51	0.818	4.375
17	1.117	198.0	52	0.818	1.652
18	0.696	0.063	53	0.818	1.50
19	1.117	198.0	54	0.622	41.25
20	1.117	0.620	55	0.622	41.25
21	1.117	37.283	56	0.352	0.063
22	1.117	0.0001	57	0.093	0.625
23	1.117	0.0001	58	0.818	1.750
24	1.117	0.0001	59	0.818	108.0
25	1.117	0.0001	60	0.818	90.0
26	1.117	0.0001	61	0.818	132.0
27	1.117	0.0001	62	0.622	41.25
28	1.117	0.0001	63	0.622	41.25
29	1.117	0.0001	64	0.818	1.50
30	1.117	0.0001	65	0.0001	0.0001
31	1.117	0.0001	66	0.0001	0.0001
32	1.117	0.0001	67	0.0001	0.0001
33	1.117	0.0001	68	0.0001	0.0001
34	1.117	0.0001	69	0.0001	0.0001
35	1.117	0.0001	70	0.043	0.672

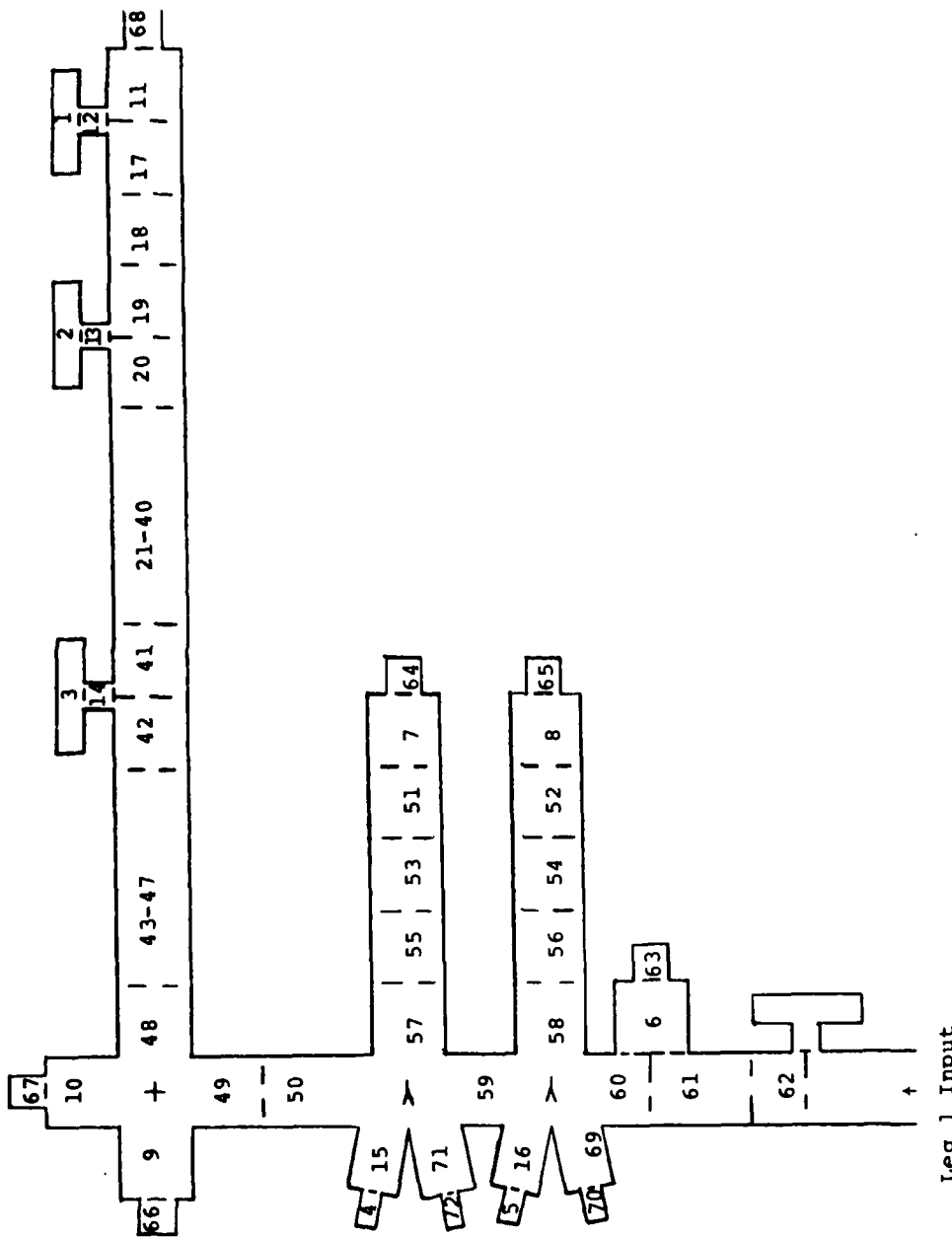


Fig. 64: Schematic of ASTF Lines with Leg 1 Input

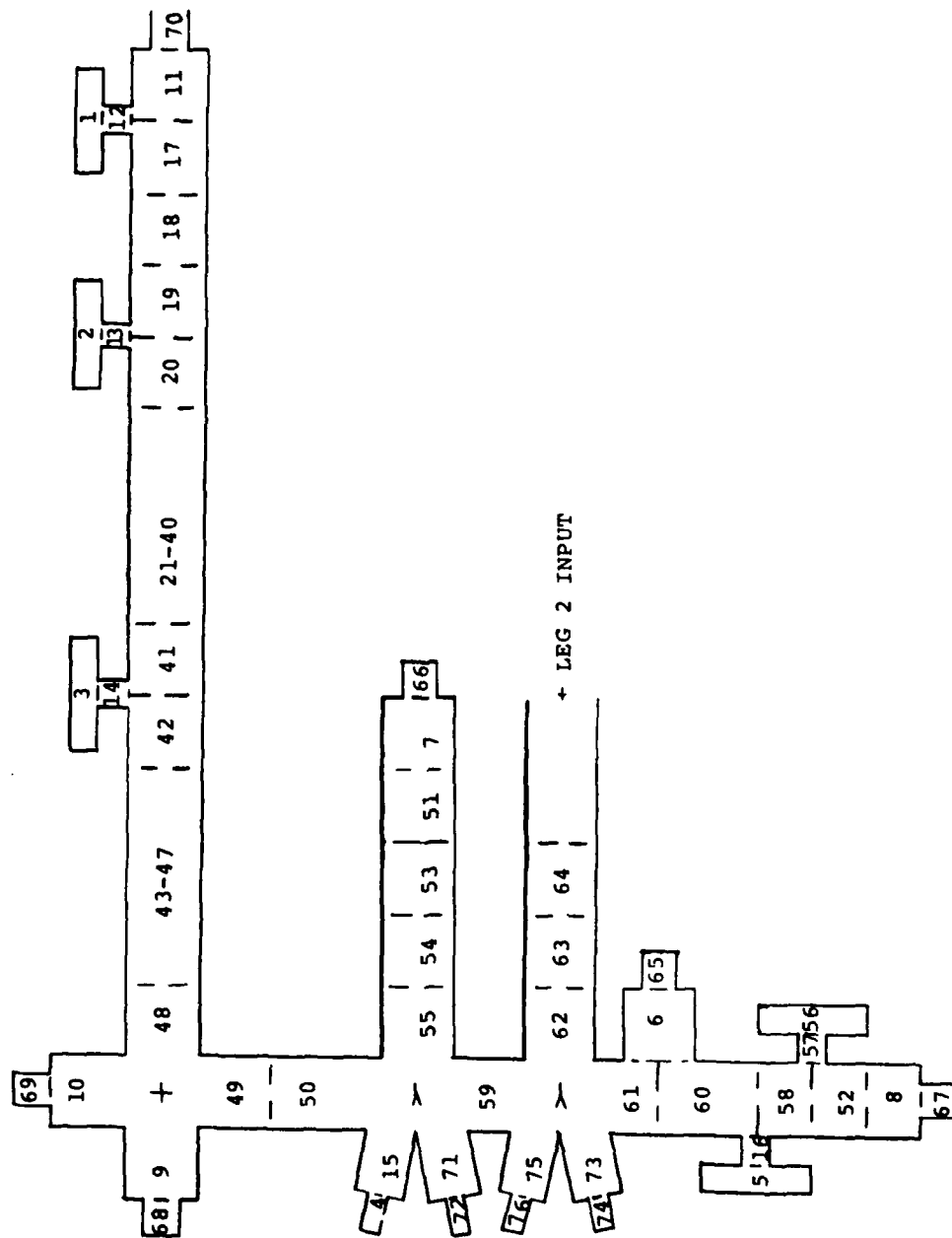
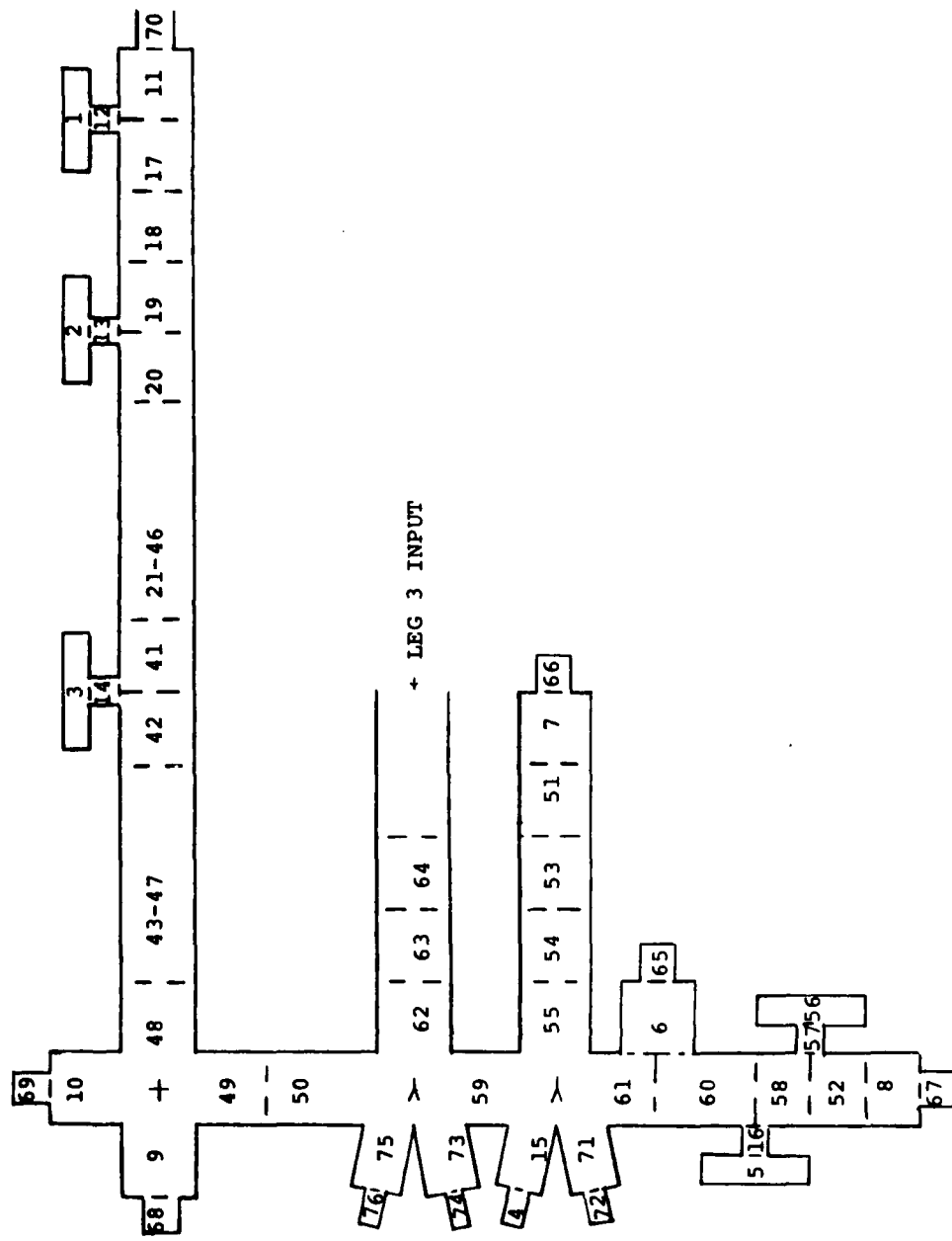


Fig. 65: Schematic of ASTF Lines with Leg 2 Input



B-16

Fig. 66: Schematic of ASTF Lines with Leg 3 Input

Table XII
ASTF Case 1

Line	Diameter in.	Length in.	Line	Diameter in.	Length in.
1	0.0001	0.0001	37	51.34	3.59
2	0.0001	0.0001	38	54.84	3.59
3	0.0001	0.0001	39	65.46	3.59
4	0.0001	0.0001	40	76.92	3.59
5	0.0001	0.0001	41	95.82	3.59
6	180	180	42	264	158
7	108	84	43	258.67	24
8	108	84	44	264	52
9	72	1065	45	228	102
10	180	207	46	156	102
11	264	0.0001	47	120	213
12	0.0001	0.0001	48	120	213
13	0.0001	0.0001	49	180	192
14	0.0001	0.0001	50	180	192
15	48	65	51	108	84
16	48	54	52	108	84
17	264	462	53	108	0.0001
18	258.67	24	54	108	0.0001
19	264	306	55	108	0.0001
20	78.57	3.59	56	108	0.0001
21	70.38	3.59	57	108	0.0001
22	64.65	3.59	58	108	0.0001
23	59.73	3.59	59	180	216
24	55.65	3.59	60	180	264
25	52.38	3.59	61	156	102
26	49.11	3.59	62	156	102
27	48.27	3.59	63	0.0001	0.0001
28	47.56	3.59	64	0.0001	0.0001
29	45.84	3.59	65	0.0001	0.0001
30	45.00	3.59	66	0.0001	0.0001
31	45.00	3.59	67	0.0001	0.0001
32	45.00	3.59	68	0.0000	0.0000
33	45.00	3.59	69	30	54
34	45.00	3.59	70	0.0001	0.0001
35	45.84	3.59	71	24	61
36	47.46	3.59	72	0.0001	0.0001

Table XIII
ASTF Case 2

Line	Diameter in.	Length in.	Line	Diameter in.	Length in.
1	0.0001	0.0001	39	65.46	3.59
2	0.0001	0.0001	40	76.92	3.59
3	0.0001	0.0001	41	95.82	3.59
4	0.0001	0.0001	42	264	158
5	0.0001	0.0001	43	258.67	24
6	180	180	44	264	52
7	108	84	45	228	102
8	0.0001	0.0001	46	156	102
9	72	1065	47	120	213
10	180	207	48	120	213
11	264	0.0001	49	180	192
12	0.0001	0.0001	50	180	192
13	0.0001	0.0001	51	108	84
14	0.0001	0.0001	52	0.0001	0.0001
15	48	65	53	108	0.0001
16	0.0001	0.0001	54	108	0.0001
17	264	462	55	108	0.0001
18	258.67	24	56	0.0001	0.0001
19	264	306	57	0.0001	0.0001
20	78.57	3.59	58	0.0001	0.0001
21	70.38	3.59	59	180	216
22	64.65	3.59	60	156	204
23	59.73	3.59	61	180	264
24	55.65	3.59	62	108	56
25	52.38	3.59	63	108	56
26	49.11	3.59	64	108	56
27	48.27	3.59	65	0.0001	0.0001
28	47.56	3.59	66	0.0001	0.0001
29	45.84	3.59	67	0.0001	0.0001
30	45.00	3.59	68	0.0001	0.0001
31	45.00	3.59	69	0.0001	0.0001
32	45.00	3.59	70	0.0000	0.0000
33	45.00	3.59	71	24	61
34	45.00	3.59	72	0.0001	0.0001
35	45.84	3.59	73	30	54
36	47.84	3.59	74	0.0001	0.0001
37	51.34	3.59	75	48	54
38	54.84	3.59	76	0.0001	0.0001

Table XIV

ASTF Case 3

Line	Diameter in.	Length in.	Line	Diameter in.	Length in.
1	0.0001	0.0001	39	65.46	3.59
2	0.0001	0.0001	40	76.92	3.59
3	0.0001	0.0001	41	95.82	3.59
4	0.0001	0.0001	42	264	158
5	0.0001	0.0001	43	258.67	24
6	180	180	44	264	52
7	108	84	45	228	102
8	0.0001	0.0001	46	156	102
9	72	1065	47	120	213
10	180	207	48	120	213
11	264	0.0001	49	180	192
12	0.0001	0.0001	50	180	192
13	0.0001	0.0001	51	108	84
14	0.0001	0.0001	52	0.0001	0.0001
15	48	54	53	108	0.0001
16	0.0001	0.0001	54	108	0.0001
17	264	462	55	108	0.0001
18	258.67	24	56	0.0001	0.0001
19	264	306	57	0.0001	0.0001
20	78.57	3.59	58	0.0001	0.0001
21	70.38	3.59	59	180	216
22	64.65	3.59	60	156	204
23	59.73	3.59	61	180	264
24	55.65	3.59	62	108	56
25	52.38	3.59	63	108	56
26	49.11	3.59	64	108	56
27	48.27	3.59	65	0.0001	0.0001
28	47.56	3.59	66	0.0001	0.0001
29	45.84	3.59	67	0.0001	0.0001
30	45.00	3.59	68	0.0001	0.0001
31	45.00	3.59	69	0.0001	0.0001
32	45.00	3.59	70	0.0000	0.0000
33	45.00	3.59	71	30	54
34	45.00	3.59	72	0.0001	0.0001
35	45.84	3.59	73	24	61
36	47.84	3.59	74	0.0001	0.0001
37	51.34	3.59	75	48	65
38	54.84	3.59	76	0.0001	0.0001

Table XV
ASTF Case 4

Line	Diameter in.	Length in.	Line	Diameter in.	Length in.
1	0.0001	0.0001	39	65.46	3.59
2	0.0001	0.0001	40	76.92	3.59
3	0.0001	0.0001	41	95.82	3.59
4	0.0001	0.0001	42	264	158
5	0.0001	0.0001	43	190.37	24
6	180	180	44	264	52
7	108	84	45	228	102
8	0.0001	0.0001	46	156	102
9	72	1065	47	120	213
10	180	207	48	120	213
11	264	0.0001	49	180	192
12	0.0001	0.0001	50	180	192
13	0.0001	0.0001	51	108	84
14	0.0001	0.0001	52	0.0001	0.0001
15	48	54	53	108	0.0001
16	0.0001	0.0001	54	108	0.0001
17	264	462	55	108	0.0001
18	190.37	24	56	0.0001	0.0001
19	264	306	57	0.0001	0.0001
20	78.57	3.59	58	0.0001	0.0001
21	70.38	3.59	59	180	216
22	64.65	3.59	60	156	204
23	59.73	3.59	61	180	264
24	55.65	3.59	62	108	56
25	52.38	3.59	63	108	56
26	49.11	3.59	64	108	56
27	48.27	3.59	65	0.0001	0.0001
28	47.56	3.59	66	0.0001	0.0001
29	45.84	3.59	67	0.0001	0.0001
30	45.00	3.59	68	0.0001	0.0001
31	45.00	3.59	69	0.0001	0.0001
32	45.00	3.59	70	0.0000	0.0000
33	45.00	3.59	71	30	54
34	45.00	3.59	72	0.0001	0.0001
35	45.84	3.59	73	24	61
36	47.84	3.59	74	0.0001	0.0001
37	51.34	3.59	75	48	65
38	54.84	3.59	76	0.0001	0.0001

Table XVI
ASTF Case 5

Line	Diameter in.	Length in.	Line	Diameter in.	Length in.
1	0.0001	0.0001	39	65.46	3.59
2	0.0001	0.0001	40	76.92	3.59
3	0.0001	0.0001	41	95.82	3.59
4	0.0001	0.0001	42	264	158
5	0.0001	0.0001	43	190.37	24
6	180	180	44	264	52
7	108	84	45	228	102
8	0.0001	0.0001	46	156	102
9	72	1065	47	120	213
10	180	207	48	120	213
11	264	0.0001	49	180	192
12	0.0001	0.0001	50	180	192
13	0.0001	0.0001	51	108	84
14	0.0001	0.0001	52	0.0001	0.0001
15	48	54	53	108	0.0001
16	0.0001	0.0001	54	108	0.0001
17	264	462	55	108	0.0001
18	182.90	24	56	0.0001	0.0001
19	264	306	57	0.0001	0.0001
20	78.57	3.59	58	0.0001	0.0001
21	70.38	3.59	59	180	216
22	64.65	3.59	60	156	204
23	59.73	3.59	61	180	264
24	55.65	3.59	62	108	56
25	52.38	3.59	63	108	56
26	49.11	3.59	64	108	56
27	48.27	3.59	65	0.0001	0.0001
28	47.56	3.59	66	0.0001	0.0001
29	45.84	3.59	67	0.0001	0.0001
30	45.00	3.59	68	0.0001	0.0001
31	45.00	3.59	69	0.0001	0.0001
32	45.00	3.59	70	0.0000	0.0000
33	45.00	3.59	71	30	54
34	45.00	3.59	72	0.0001	0.0001
35	45.84	3.59	73	24	61
36	47.84	3.59	74	0.0001	0.0001
37	51.34	3.59	75	48	65
38	54.84	3.59	76	0.0001	0.0001

Table XVII
ASTF Cases 6-10

Line	Diameter in.	Length in.	Line	Diameter in.	Length in.
1	0.0001	0.0001	39	65.46	3.59
2	0.0001	0.0001	40	76.92	3.59
3	0.0001	0.0001	41	95.82	3.59
4	0.0001	0.0001	42	264	158
5	0.0001	0.0001	43	258.67	24
6	180	180	44	264	52
7	108	84	45	228	102
8	0.0001	0.0001	46	156	102
9	72	1065	47	120	213
10	180	207	48	120	213
11	264	0.0001	49	180	192
12	0.0001	0.0001	50	180	192
13	0.0001	0.0001	51	108	84
14	0.0001	0.0001	52	0.0001	0.0001
15	48	54	53	108	0.0001
16	0.0001	0.0001	54	108	0.0001
17	264	462	55	108	0.0001
18	258.67	24	56	0.0001	0.0001
19	264	306	57	0.0001	0.0001
20	78.57	3.59	58	0.0001	0.0001
21	70.38	3.59	59	180	216
22	64.65	3.59	60	156	204
23	59.73	3.59	61	180	264
24	55.65	3.59	62	108	56
25	52.38	3.59	63	108	56
26	49.11	3.59	64	108	56
27	48.27	3.59	65	0.0001	0.0001
28	47.56	3.59	66	0.0001	0.0001
29	45.84	3.59	67	0.0001	0.0001
30	45.00	3.59	68	0.0001	0.0001
31	45.00	3.59	69	0.0001	0.0001
32	45.00	3.59	70	31	0.0001
33	45.00	3.59	71	30	54
34	45.00	3.59	72	0.0001	0.0001
35	45.84	3.59	73	24	61
36	47.84	3.59	74	0.0001	0.0001
37	51.34	3.59	75	48	65
38	54.84	3.59	76	0.0001	0.0001

Appendix C
Signal Analysis Equipment Specifications

Table XVIII
Signal Analysis Equipment Specifications

Equipment	Manufacturer	Model Number	Serial Numbers	Frequency Range (Hz)
Wave Analyzer	Hewlett-Packard	302A	116, 117, 175	20-50K
Dual-Beam Oscilloscope	Tektronix	7613 (W/7A26 Amp) (W/7B53A Time Base)	B377669 B377675	DC to 20K
Frequency Counter	Computer Measurements Company (CMC)	726C	120366	N/A
Quartz Pressure Transducer	Kistler	701A 7001	65079 128286, 128287	N/A
Charge Amplifier	Kistler	504A 504D	N/A 1487	DC to 150K
Mean Pressure Transducer	Bell & Howell	CEC-1000	9302	N/A
DC Millivoltmeter	DIGITEK	268	704	N/A
DC Power Supply	Hewlett-Packard	6205B	1140A09045	N/A
Pneumatic Signal Generator	Bendix	6625L04360- 22300	N/A	.1 to 1K
Flowmeter	Fischer & Porter	Flowrator B3A25	P5-1037/21	N/A

Vita

Mark Landon Ross was born [REDACTED] [REDACTED]

[REDACTED] He graduated from [REDACTED] in Kennett, Missouri in 1975 and was appointed to the United States Air Force Academy. He graduated from the Academy in 1979, receiving the degree of Bachelor of Science in Engineering Mechanics.

Ross was first assigned to the 6510th Test Wing, Air Force Flight Test Center, Edwards AFB, California in July 1979. He worked as a flight test instrumentation engineer until a unit reorganization in 1980 assigned him with the Instrumentation Division to the 6520th Test Group at Edwards. He was assigned to the School of Engineering, Air Force Institute of Technology, in June 1982.

Permanent Address: [REDACTED] [REDACTED]
[REDACTED]

UNCLASSIFIED

SECURITY CLASSIFICATION OF THIS PAGE

The dynamic response of a scale model of the Aeropropulsion Systems Test Facility (ASTF) air supply ducting was determined experimentally over a frequency range from 20-200 Hz. Blocked lines with no flow and orifice terminated lines with a mean flow were used. The experiments examined the effects of signal input on three different lines and of using different size venturis. Gain and phase were measured upstream of the venturi and at the end of the line.

The experimental results were compared with the results of a computer program based on Nichols' theory as modified by Krishnaiyer and Lechner. With few exceptions, the gains were predicted within ± 5 dB, and phase angles within $\pm 10\%$. This agreement between theory and experiment verified that the theory can be applied successfully to large, complex systems and that the computer program was running properly.

The verified program was then applied to the full-scale ASTF air supply and results analyzed. The ASTF results show higher gains at low frequencies and no reduction in the average gain with frequency. This was as expected for the large ASTF ducting, which ranges from 4.22 ft in diameter.

UNCLASSIFIED

SECURITY CLASSIFICATION OF THIS PAGE

UNCLASSIFIED

SECURITY CLASSIFICATION OF THIS PAGE

REPORT DOCUMENTATION PAGE

1. REPORT SECURITY CLASSIFICATION UNCLASSIFIED		1b. RESTRICTIVE MARKINGS	
2a. SECURITY CLASSIFICATION AUTHORITY		3. DISTRIBUTION/AVAILABILITY OF REPORT Approved for public release; distribution unlimited	
2b. DECLASSIFICATION/DOWNGRADING SCHEDULE			
4. PERFORMING ORGANIZATION REPORT NUMBER(S) AFIT/GAE/AA/83-20		5. MONITORING ORGANIZATION REPORT NUMBER(S)	
6a. NAME OF PERFORMING ORGANIZATION School of Engineering	6b. OFFICE SYMBOL (If applicable) AFIT/ENY	7a. NAME OF MONITORING ORGANIZATION	
6c. ADDRESS (City, State and ZIP Code) Air Force Institute of Technology Wright-Patterson AFB, OH 45433		7b. ADDRESS (City, State and ZIP Code)	
8a. NAME OF FUNDING/SPONSORING ORGANIZATION Arnold Engineer- ing Development Center	8b. OFFICE SYMBOL (If applicable) AEDC/AOE	9. PROCUREMENT INSTRUMENT IDENTIFICATION NUMBER	
8c. ADDRESS (City, State and ZIP Code) Arnold Engineering Development Center AEDC/AOE Arnold AFS, TN 37389	10. SOURCE OF FUNDING NOS.		
11. TITLE (Include Security Classification) See Box 19		PROGRAM ELEMENT NO.	PROJECT NO.
12. PERSONAL AUTHOR(S) Mark L. Ross, B.S., Capt., USAF		TASK NO.	WORK UNIT NO.
13a. TYPE OF REPORT MS Thesis	13b. TIME COVERED FROM _____ TO _____	14. DATE OF REPORT (Yr., Mo., Day) 1983 December	
16. SUPPLEMENTARY NOTATION		15. PAGE COUNT 151	
<p style="text-align: center;"><i>By [Signature]</i> LYNN E. WALTERS Dean for Education and Professional Development Air Force Institute of Technology (AFIT)</p> <p style="text-align: right;">3 JAN 1984</p>			
17. COSATI CODES		18. SUBJECT TERMS (Check boxes by Area Code and identify by block number) Aeropropulsion Systems Test Facility (ASTF), Dynamic Response, Fluid Transmission Lines	
19. ABSTRACT (Continue on reverse if necessary and identify by block number)			
<p>Title: DYNAMIC CHARACTERISTICS OF A JET ENGINE TEST FACILITY AIR SUPPLY</p> <p>Thesis Chairman: Dr. Milton E. Franke</p>			
20. DISTRIBUTION/AVAILABILITY OF ABSTRACT		21. ABSTRACT SECURITY CLASSIFICATION	
UNCLASSIFIED/UNLIMITED <input checked="" type="checkbox"/> SAME AS RPT. <input type="checkbox"/> DTIC USERS <input type="checkbox"/>		UNCLASSIFIED	
22a. NAME OF RESPONSIBLE INDIVIDUAL Dr. Milton E. Franke		22b. TELEPHONE NUMBER (Include Area Code) (513)-255-2362	22c. OFFICE SYMBOL AFIT/ENY